**Title**

Studies using Underwater Acoustic Tracking Arrays



**Author**

Snyder, Eric R

**Publication Date**

2024

Peer reviewed|Thesis/dissertation

UNIVERSITY OF CALIFORNIA SAN DIEGO

# Studies using Underwater Acoustic Tracking Arrays

A dissertation submitted in partial satisfaction of the
requirements for the degree Doctor of Philosophy

in

Oceanography

by

Eric R. Snyder

Committee in charge:

John A. Hildebrand, Chair
Simone Baumann-Pickering
Bruce Cornuelle
Kaitlin Frasier
William Hodgkiss
James Nieh
Alba Solsona Berga

2024

The Dissertation of Eric R. Snyder is approved, and it is acceptable in quality and form for publication on microfilm and electronically.

University of California San Diego

2024

DEDICATION

For Emily and Miles

# EPIGRAPH

”Sir Grummore,” he said coyly, ”has observed a phenomenon, by Jove!”
”A phenomenon?”
”A thing,” explained Sir Grummore.
”What sort of thing?” asked the King suspiciously.
”Something you will like.”
”It has four legs,” added the Saracen.
”Is it animal?” asked the King, ”vegetable or mineral?”
”Animal.”
”A pig?” inquired the King, who was beginning to feel they must be driving at something.
”No, no, Pellinore. Not a pig. Get pigs out of your head right away. This thing makes a noise like hounds.”
”Like sixty hounds,” explained Sir Palomides.
”It is a whale!” cried the King.
”No, no, Pellinore. A whale has no legs.”
”But it makes such a noise.”
”Does a whale?”
”My dear fellow, how am I to know?”

-T. H. White, *The Once and Future King*

TABLE OF CONTENTS

Dissertation Approval Page . . . iii

Dedication . . . iv

Epigraph . . . v

Table of Contents . . . vi

List of Figures . . . viii

List of Tables . . . x

Acknowledgements . . . xi

Abstract of the Dissertation . . . xiii

Chapter 1 *Where's Whaledo*: A software toolkit for array localization of animal vocalizations . . . 1

Chapter 2 *Ziphius cavirostris* diving behavior in the Tanner Basin . . . 31
2.1 Introduction . . . 31
2.2 Methods . . . 33
2.2.1 Data Collection and Parameter Calculation . . . 33
2.2.2 Diving Behavior . . . 35
2.2.3 Source level estimation . . . 36
2.3 Results . . . 38
2.4 Discussion . . . 39
2.4.1 Preference for Slope in Foraging . . . 39
2.4.2 Acoustic Diving behaviors . . . 43
2.4.3 Click directionality . . . 44
2.4.4 Future Work . . . 45
2.5 Conclusions . . . 46

Chapter 3 Echoes Across the Gulf: Challenges of long-range localization of broadband sources in the Gulf of Mexico . . . 50
3.1 Introduction . . . 50
3.1.1 Airguns . . . 50
3.1.2 Propagation modeling . . . 51
3.1.3 This contribution . . . 52
3.2 Methods . . . 53
3.2.1 Associating received signals to sources . . . 53
3.2.2 Environmental characterization . . . 55
3.2.3 Propagation modeling between sources and receivers . . . 56

3.3 Results . . . . . . . . . . 64
3.4 Discussion . . . . . . . . . . 65
3.4.1 Comparison of Data and PE model outputs . . . . . . . . . . 66
3.5 Conclusion . . . . . . . . . . 67

Bibliography . . . . . . . . . . 76

LIST OF FIGURES


Figure 1.1. **Time Difference of Arrival.** . . . . . . 7

Figure 1.2. **The *Where's Whaledo* workflow.** . . . . . . 10

Figure 1.3. **The `brushDOA` user interface for editing detections on two 4-channel arrays.** . . . . . . 12

Figure 1.4. **Click-Train Correlation.** . . . . . . 14

Figure 1.5. **Visualization of the DOA intersect localization method.** . . . . . . 17

Figure 1.6. **Study site.** . . . . . . 19

Figure 1.7. ***Zc* track reconstructions with clear source association.** . . . . . . 23

Figure 1.8. ***Zc* tracks with large group sizes.** . . . . . . 29

Figure 1.9. **Reconstructing *Zc* tracks in the presence of false-detections.** . . . . . . 30

Figure 2.1. **Study site in Tanner Basin.** . . . . . . 34

Figure 2.2. **All *Zc* tracks.** . . . . . . 39

Figure 2.3. **Heat map of detection locations.** . . . . . . 40

Figure 2.4. **Detection Angles.** . . . . . . 41

Figure 2.5. **Group Sizes.** . . . . . . 42

Figure 2.6. **Tracks by type.** . . . . . . 42

Figure 2.7. **Track segments for SL calculation.** . . . . . . 43

Figure 2.8. **Source Level vs. Beam Angle**. . . . . . . 47

Figure 2.9. **Source Level vs. 3-D Beam Angle of each track segments**. . . . . . . 48

Figure 2.10. **Source Level vs. Beam Angle of all track segments**. . . . . . . 49

Figure 2.11. **Source Level vs. 3-D Beam Angle of all track segments combined**. . . . . . . 49

Figure 3.1. **Map of ship locations and all sites** . . . . . . 54

Figure 3.2. **Map of ship locations and site MC, and plot of depths at ship locations.** 55

Figure 3.3. **Isovelocity ray plots.** . . . . . . 58

Figure 3.4. **Group and phase speeds for an isovelocity environment.** . . . . . . 58

Figure 3.5. **Munk sound speed profile with sediment layer.** . . . . . . 59

Figure 3.6. **Ray plot for Munk SSP with sediment layer.** . . . . . . 60

Figure 3.7. **Group and phase speeds for a Munk SSP with sediment layer.** . . . . . . 60

Figure 3.8. **A ray reflecting off a sloped bottom.** . . . . . . 61

Figure 3.9. **Ray plot for a sloped bathymetry.** . . . . . . 61

Figure 3.10. **Group and phase speeds for an upward-sloped bathymetry.** . . . . . . 62

Figure 3.11. **Group and phase speeds for a downward-sloped bathymetry.** . . . . . . 62

Figure 3.12. **Dispersion patterns for various sloped bathymetries (isovelocity and perfectly reflecting boundaries).** . . . . . . 62

Figure 3.13. **3-D rays in a wedge.** . . . . . . 63

Figure 3.14. **Receiver 1 waterfall plot sorted by time.** . . . . . . 70

Figure 3.15. **PE Model waterfall plot of ship 1 to receiver MC.** . . . . . . 71

Figure 3.16. **Spectrograms of first shot from ship 1 to MC–PE model and real data.** 72

Figure 3.17. **Spectra of data from ship 1 to MC sorted by range–PE model and real data.** . . . . . . 73

Figure 3.18. **Group speeds vs. launch angles estimated from ray trace on a realistic environment for all source positions of ship 1 to site MC.** . . . . . . 74

Figure 3.19. **Group speed estimates of first arrival, estimated from ray trace, PE, and TDOA inversion for ship 1, site MC.** . . . . . . 75

LIST OF TABLES

Table 2.1. Instrument Locations . . . . . . . . . . 35

Table 2.2. Dive Types . . . . . . . . . . 38

## ACKNOWLEDGEMENTS

I would like to acknowledge Professor John Hildebrand for his support as the chair of my committee. His irreplaceable expertise and guidance have been invaluable. Thank you for the mentorship, guidance, patience, wisdom, and countless hours you dedicated to me and my success.

I would like to acknowledge my committee members: Simone Baumann-Pickering for your remarkable expertise, dedication to the success of your students and mentees, and example of true excellence in science; Bruce Cornuelle for your invaluable support, wealth of knowledge, humor, and kindness. Your teachings have profoundly influenced my work here and will continue to benefit me throughout my career; Kaitlin Frasier for your unwavering support and mentorship, and for always making time to teach me and share ideas; William Hodgkiss for your unparalleled expertise, thoroughness, and support. So much of what I know about signal processing and acoustics stems from your excellent teaching; James Nieh for your kindness and support, and your insightful contributions throughout this thesis; Alba Solsona Berga for your mentorship, hard work, and thorough feedback. Your contributions to this work were indispensable.

I would like to acknowledge my mentor and collaborator Sean Wiggins. Without your hours providing me with education, support, and guidance, none of this would have been possible. I would also like to thank Lauren Baggett for all of her hard work in support of this research and for her ingenuity and enthusiasm for science.

I would like the thank all of my other friends, professors, interns, lab-mates, colleagues, collaborators, everyone in the MBARC labs, the Students with Dependents workgroup, AOS students, the 2017 cohort, Margaret, and everyone else who shared ideas, kindness, and friendship.

Lastly, I would like to thank my family. Mom, Dad, Jenicia, Jayden, Kayli, Stephanie, Dallin, and your spouses and kids: thank you for all of your love and support. David, Ruth, and all the Wassinks: thank you for all the support and for welcoming me into your family.

And most of all, thank you Emily and Miles for being with me on this journey and for sacrificing so much. I love you both.

Chapter 1, in full, is a reprint of the material as it appears in: Snyder, E. R., Solsona-Berga, A., Baumann-Pickering, S., Frasier, K. E., Wiggins, S. M., & Hildebrand, J. A. (2023). Where's Whaledo: A software toolkit for array localization of animal vocalizations. bioRxiv, 2023-08.

ABSTRACT OF THE DISSERTATION

Studies using Underwater Acoustic Tracking Arrays

by

Eric R. Snyder

Doctor of Philosophy in Oceanography

University of California San Diego, 2024

John A. Hildebrand, Chair

The oceans contain a cacophony of sounds from biological, geological, meteorological, and anthropogenic sources. As computational power and data storage capabilities have increased, long-term passive acoustic recordings have been increasingly employed to study the oceans. Multiple hydrophones can be deployed in a site or region to gain more information on the spatial properties of acoustic soundscapes. In this thesis, we use hydrophone arrays to track vocalizing animals and anthropogenic sound sources, and by so doing gain valuable insights into ocean environments.

Chapter 1 introduces *Where's Whaledo*: software toolkit and workflow for efficiently and reliably localizing and tracking groups of vocalizing animals. Methods were developed to

identify and remove false detections in small-aperture direction of arrival estimates, associate detections across widely-spaced instruments using click trains, estimate source locations, and calculate confidence intervals.

Chapter 2 employs *Where's Whaledo* on *Ziphius cavirostris* in the Tanner Basin, demonstrating the toolkit's capabilities by reconstructing the tracks of 143 dives. The localized animals demonstrated a preference for the steeper bathymetry at the study site, as well as a possible preference for swimming in groups of two or more animals. 12 of these tracks were used to estimate the beam pattern of a *Zc* echolocation click.

Chapter 3 demonstrates the challenges and complexities of long-range propagation by examining recordings of five vessels performing a coordinated seismic survey using high-intensity signals from airgun arrays. Using several identifiable patterns in the acoustic data, each arrival in a 110-minute period was associated with its source vessel so changes in dispersion patterns could be observed over time. Both ray trace and parabolic equation models were used to simulate dispersion patterns. Potential causes of differences between the modeled signals and the observed signals are discussed, and recommendations are made for future analyses.

# Chapter 1

# *Where's Whaledo*: A software toolkit for array localization of animal vocalizations


## Abstract

*Where's Whaledo* is a software toolkit that uses a combination of automated processes and user interfaces to greatly accelerate the process of reconstructing animal tracks from arrays of passive acoustic recording devices. Passive acoustic localization is a non-invasive yet powerful way to contribute to species conservation. By tracking animals through their acoustic signals, important information on diving patterns, movement behavior, habitat use, and feeding dynamics can be obtained. This method is useful for helping to understand habitat use, observe behavioral responses to noise, and develop potential mitigation strategies. Animal tracking using passive acoustic localization requires an acoustic array to detect signals of interest, associate detections on various receivers, and estimate the most likely source location by using the time difference of arrival (TDOA) of sounds on multiple receivers. *Where's Whaledo* combines data from two small-aperture volumetric arrays and a variable number of individual receivers. In a case study conducted in the Tanner Basin off Southern California, we demonstrate the effectiveness of *Where's Whaledo* in localizing groups of *Ziphius cavirostris*. We reconstruct the tracks of six individual animals vocalizing concurrently and identify *Ziphius cavirostris* tracks despite being obscured by a large pod of vocalizing dolphins.

# Author summary

Reconstructing the movement of animals from their vocalizations is a powerful method to observe their behavior in situations where visual monitoring is impractical. Arrays of acoustic recording devices can be used to determine the location of vocalizing animals and a series of locations can be linked to form tracks. However, reconstructing tracks requires methods of determining which animal in a group is vocalizing, finding the same vocalization on multiple recording devices, and determining the most likely location of the animal based on the relative times the sound arrived at various recording devices. We have developed a toolkit called *Where's Whaledo* to assist researchers in reconstructing the behavior of these animals using arrays of acoustic recording devices. This toolkit greatly accelerates the process of reconstructing their tracks using a combination of automated processes and user interfaces. We use *Where's Whaledo* to reconstruct the tracks of deep-diving beaked whales (*Zc*). We successfully reconstruct tracks of groups of up to five whales vocalizing concurrently.


# Introduction

Passive acoustic monitoring (PAM) has been increasingly utilized to monitor animals in the wild [16, 108, 90]. The use of arrays of acoustic sensors has further enabled the localization of animal sounds, providing additional avenues of research including the study of behavior and a better understanding of animal population dynamics [77, 14]. Acoustic sensing has advantages over other common methods that are dependent on observers having suitable weather and lighting conditions to carry out visual surveys. PAM provides a method for non-invasive, long-term observations.

Cetaceans in particular are difficult to directly observe, but they produce species-specific vocalizations for both navigation and communication [75, 108]. Arrays of acoustic recording devices can be deployed to collect continuous data for months, providing a non-invasive method for studying cetacean behavior and presence. This method has become essential for studying deep-diving cetacean species, like beaked whales (family *Ziphiidae*), Sperm whales (*Physeter macrocephalus*), Risso's Dolphins (*Grampus griseus*), and pilot whales (genus *Globicephala*), which are pelagic and often spend relatively little time at the surface [12, 99, 103, 4, 9]. PAM has provided valuable insights into their behavior despite their elusiveness [6, 12, 37, 11, 27, 47].

For deep-divers, PAM is emerging as an essential method for studying their population structure and dynamics [63, 46, 88]. This requires *a priori* knowledge of a number of features, like group size, vocalization rates, and acoustic detection ranges and probabilities. While some studies have estimated these parameters using acoustic models or information known about closely related species or populations, obtaining direct measurements for a specific species and site would likely improve the estimates [63]. Most of these features can be estimated by reconstructing tracks from acoustic data. Group sizes can be estimated by identifying the number of individual tracks in an encounter. Detection ranges and probabilities can be estimated based on the positions of detected animals. Additionally, passive acoustic localization can provide valuable information about depths and durations of dives, foraging depths and behaviors, responses to anthropogenic sounds or other environmental stressors, and insights into potential harm mitigation strategies.

Passive acoustic localization of cetacean vocalizations using arrays of hydrophones has been used to reconstruct tracks of a number of cetacean species, like beaked whales, common dolphins (*Delphinus delphis*), and sperm whales (*Physeter macrocephalus*)([37, 11, 106, 69, 38, 10, 27, 95, 47, 40]. Different approaches to localization have been implemented for different configurations of hydrophones, and to observe different species or behaviors of interest. Many of these studies have used localization to reconstruct two-dimensional approximations of tracks, either horizontal tracks [110, 41] or depth and range to the instrument [11, 10]. Three-dimensional localizations have been obtained using an individual hydrophone when accurate three-dimensional travel-time models could be constructed from measurements of sound speed profiles and bathymetry data [96].

Time difference of arrival (TDOA) localization uses the times a signal arrived at various receivers to estimate the location of a source. When receivers have sufficient coverage, a received signal can be localized in three-dimensional space. TDOA has been used to localize a number of vocalizing animals, including birds [36, 89, 97] bats [53], terrestrial animals [73], and aquatic animals [71, 37, 6, 106].

Reflections off the surface or refractions due to ray bending, called "multipath arrivals", can be used in localization [11, 48, 55, 68, 94, 96, 102]. Often, multpaths can be used to improve localizations or estimate the range between a source and an array [11, 94]. In cases where accurate models of multipath propagation can be made and there is significant azimuthal variation on these propagation patterns, the measured times of arrival of each multipath can be matched to models to estimate source locations in 3 dimensions from a single hydrophone [68, 96].

*Zc* and common dolphins (*Delphinus delphis*) have been tracked in three dimensions using a small-aperture volumetric array [106]. The array contained four hydrophones in a tetrahedron configuration with $\approx 0.5$ m spacing between them. By measuring the TDOA between the hydrophones, the Direction Of Arrival (DOA) of the sound could be estimated as an azimuth and elevation angle to the animal. The most likely DOA was determined by minimizing the least squares error between model TDOAs and calculated TDOAs. By identifying differences in detection amplitude and azimuth angle, two individual *Zc* whales were tracked by assuming a constant dive speed.

Localization can be performed by combining both small-aperture and large-aperture TDOAs [66, 1, 37]. Gassmann *et al.*[37] demonstrated this embedded array approach by using two small-aperture volumetric arrays and three single-channel hydrophones to localize and track *Zc* offshore of Southern California. With these additional instruments, a total of 22 TDOAs could be used to estimate the location of a whale: six TDOAs each from two small-aperture arrays, and ten large-aperture TDOAs from five widely spaced instruments. This approach results in an overdetermined system which can improve estimation accuracy. However, uncertainty can be introduced due to ambiguous signal matching across widely spaced instruments. The difficulty increases as the number of sources increases, since the number of vocalizations arriving in the window of possible TDOAs also increases. To resolve this ambiguity, Gassmann *et al.*[37] plotted all possible TDOAs and manually identified the most likely correct TDOA from these sequences. They then used a maximum likelihood equation to determine the model location that best fit the measured TDOAs, successfully localizing a total of 11 individual beaked whales in groups of up to three individuals vocalizing concurrently.

Methods of associating sources automatically are necessary for accelerating the localization process. One method for source association is to temporally align sequences of clicks on widely spaced receivers [6]. If the same pattern of clicks exists in multiple hydrophones, then these patterns can be aligned to determine which clicks arrived from each source.

Automated tracking methods are emerging which use advanced multi-target tracking algorithms to identify source associations, remove false detections, and estimate likely tracks using two volumetric arrays for encounters with simultaneous detections on both arrays. [47]. Due to the directional nature of many species' echolocation clicks [109, 37], simultaneous detections become increasingly uncommon as the distance between the instruments increases. Incorporating single-channel instruments, which are easier and cost less to deploy and recover, can increase the number of trackable encounters.

In this article, we provide a semi-automated method with opportunities for expert oversight to assist in the association of detections. We have developed a user-friendly MATLAB toolkit that builds on the methods of [106], [6], and [37] to assist researchers in obtaining tracks from acoustic datasets. To demonstrate the effectiveness of our toolkit, we used it to reconstruct $\approx 80$ *Zc* tracks from a four-month deployment in the Southern California Bight. We were able to reconstruct tracks for groups of up to five individuals vocalizing concurrently, a significant improvement over previous methods. We also addressed several challenges in preparing datasets for localization, including determining instrument locations and array orientations, synchronizing clocks, and calculating uncertainties. Overall, our toolkit provides an efficient tool for localizing beaked whales and other vocalizing animals and has the potential to significantly advance our understanding of their behavior and ecology.

# Methods

## Time Difference of Arrival Localization

TDOA localization is a technique that estimates the location of a single sound source by using the arrival times at which the sound is detected on multiple time-synchronized receivers. Typically the source origin time is unknown, but the difference in received times between receiver pairs can be used to determine possible source locations.

There are two forms of TDOA localization that are relevant to our process and are based on array sensor spacing: large-aperture and small-aperture. Large-aperture TDOA localization is used when the distance between the source and receivers is on the same order of magnitude as the distance between the receivers. On the other hand, small-aperture TDOA localization uses receivers that are much closer together than the distance to the source. In this case, the propagation of the signal through the arrays can be approximated as a plane wave.

### Large Aperture TDOA

The TDOA of a signal between two receivers is determined by the distances between the source and each receiver, as shown in Eq (1.1).

$$\begin{aligned} \mathrm{TDOA}_{i,j} = & \underbrace{\frac{\sqrt{(x_s-x_i)^2+(y_s-y_i)^2+(z_s-z_i)^2}}{c}}_{\text{travel time to instrument } i} \cdots \\ & - \underbrace{\frac{\sqrt{(x_s-x_j)^2+(y_s-y_j)^2+(z_s-z_j)^2}}{c}}_{\text{travel time to instrument } j}, \end{aligned} \tag{1.1}$$

where $x_s$, $y_s$, and $z_s$ are the Cartesian coordinates of the source location, $x_i$, $y_i$, $z_i$, $x_j$, $y_j$, and $z_j$ are the locations of the $i^{\text{th}}$ and $j^{\text{th}}$ receivers, and $c$ is the speed of sound between the source and receivers.

The TDOA from a single pair of receivers produces a hyperboloid of potential source locations, as shown in Fig. 1.1A. The hyperboloid has rotational symmetry about the axis formed by the two receivers. When a detection is received on multiple receiver pairs, the source location can be estimated by finding the intersection of the hyperboloids. However, this approach works best if the receiver pairs are not collinear or somewhat orthogonal to each other and the source is interior to the region defined by the receivers.

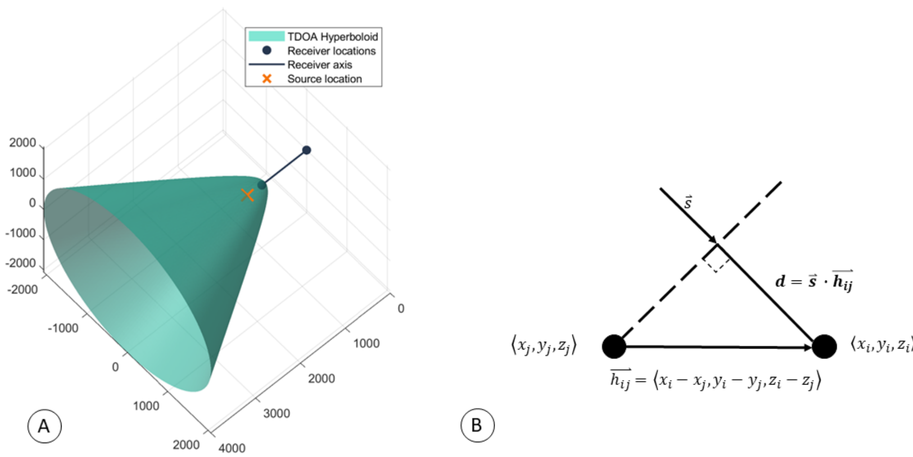


**Figure 1.1. Time Difference of Arrival.** Graphical representation of the TDOA for both large and small aperture separation between two sensors. A) Example of a hyperboloid of possible source locations when the TDOA between two widely spaced receivers is known. B) Small-aperture TDOA when the signal's propagation through the array is approximated as a plane wave. The dashed line represents the wave-front, and $\vec{s}$ is the unit vector normal to the wavefront.

### Small Aperture TDOA

When the distance between receivers is much smaller than the distance to the source, the calculation of the TDOA can be simplified as a plane wave propagating through the receiver array. The TDOA is the distance a plane wave travels between the receivers ($d$) divided by the speed of sound ($c$), which can be calculated as the dot product of the vector formed by the hydrophone pair ($\vec{h}_{i,j} = h_j - h_i$) and the unit vector pointing from the source to the receiver ($\vec{s}$). Fig. 1.1B and Eq. 1.2 below demonstrate this calculation.

$$\mathrm{TDOA_{i,j}} = \frac{d_{i,j}}{c} = \frac{\vec{s} \cdot \vec{h}_{i,j}}{c}, \tag{1.2}$$

For a pair of receivers, this gives a single angle of arrival estimate, resulting in a cone of potential source locations. The hyperboloid shown in Fig. 1.1(A) converges to the cone formed under the plane-wave approximation and introduces negligible error. When multiple small-aperture receiver pairs are combined, the resulting cones intersect along a single line referred to as the Direction of Arrival (DOA). The DOA can be estimated from the TDOAs by placing all hydrophone pairs $\vec{h}_{i,j}$ and their corresponding TDOAs into a system of linear equations, and solving for the unknown values of $\vec{s} = \langle s_x, s_y, s_z \rangle$.

Since the DOA is a unit vector, it can be more intuitively represented by two angles: azimuth and elevation. We define the azimuth (az) as the top-down counter-clockwise horizontal angle, where East is 0°, and North is 90°. The elevation (el) angle is the vertical angle, where 0° is directly down, 90° is horizontal, and 180° is upward toward the sea surface. We convert from $\vec{s}$ to az and el with Eqs. 1.3 and 1.4:

$$\mathrm{az} = \arctan2(-s_y, -s_x), \tag{1.3}$$

$$\mathrm{el} = 180^\circ - \arccos(-s_z), \tag{1.4}$$

where arctan2 is the 2-argument arctangent (`atan2d` in MATLAB). We display these values as pointing from the receiver to the source, which accounts for the negative signs on $s_x$, $s_y$, and $s_z$.

## *Where's Whaledo* software package

The *Where's Whaledo* MATLAB-based software package was designed to help analysts obtain as many animal tracks as possible by providing easy-to-use tools that allow detections to be annotated and tracks of detections to be reconstructed from localized acoustic recordings. This is done using a combination of automated processing and manual annotation of graphical data.

*Where's Whaledo* is specifically designed to accommodate deployments with two volumetric small-aperture arrays and a variable number of single-channel receivers. To perform TDOA localization, the package provides methods to detect signals of interest, determine the time differences of a signal on various receivers, and estimate the most likely source location associated with those time differences. The *Where's Whaledo* toolkit was built in a modular fashion, so each individual step can be adapted to obtain higher precision results or for different instrument configurations. The typical workflow is shown in Fig. 1.2.

### Detection

Detection steps can be tailored to different species different species using their acoustic parameters. For detecting *Zc* echolocation clicks, we used a fourth-order, zero-phase, high-pass elliptical filter with a cutoff frequency of 20 kHz, a peak-to-peak stop-band ripple of 0.1 dB and a minimum stop-band attenuation of 40 dB. After filtering, waveform sound pressure levels greater than approximately 68 dB re 1 $\mu$Pa$^2$ were identified. Peaks within a $\pm$5 ms window around a larger peak were removed to avoid multiple cycles within a single echolocation click from being counted as separate detections. The remaining peak times were retained as potential click detections.

For the 4-channel data, we cross-correlated the acoustic waveform around each detection across the other receivers in the array to determine the small-aperture TDOA. The TDOA was then converted to an azimuth and elevation using Eqs. 1.2, 1.3, and 1.4.

### Association with `brushDOA` tool

A major challenge in localizing multiple sources with widely-spaced instruments involves identifying the source from which a detection originated. To help analysts with this task, *Where's*

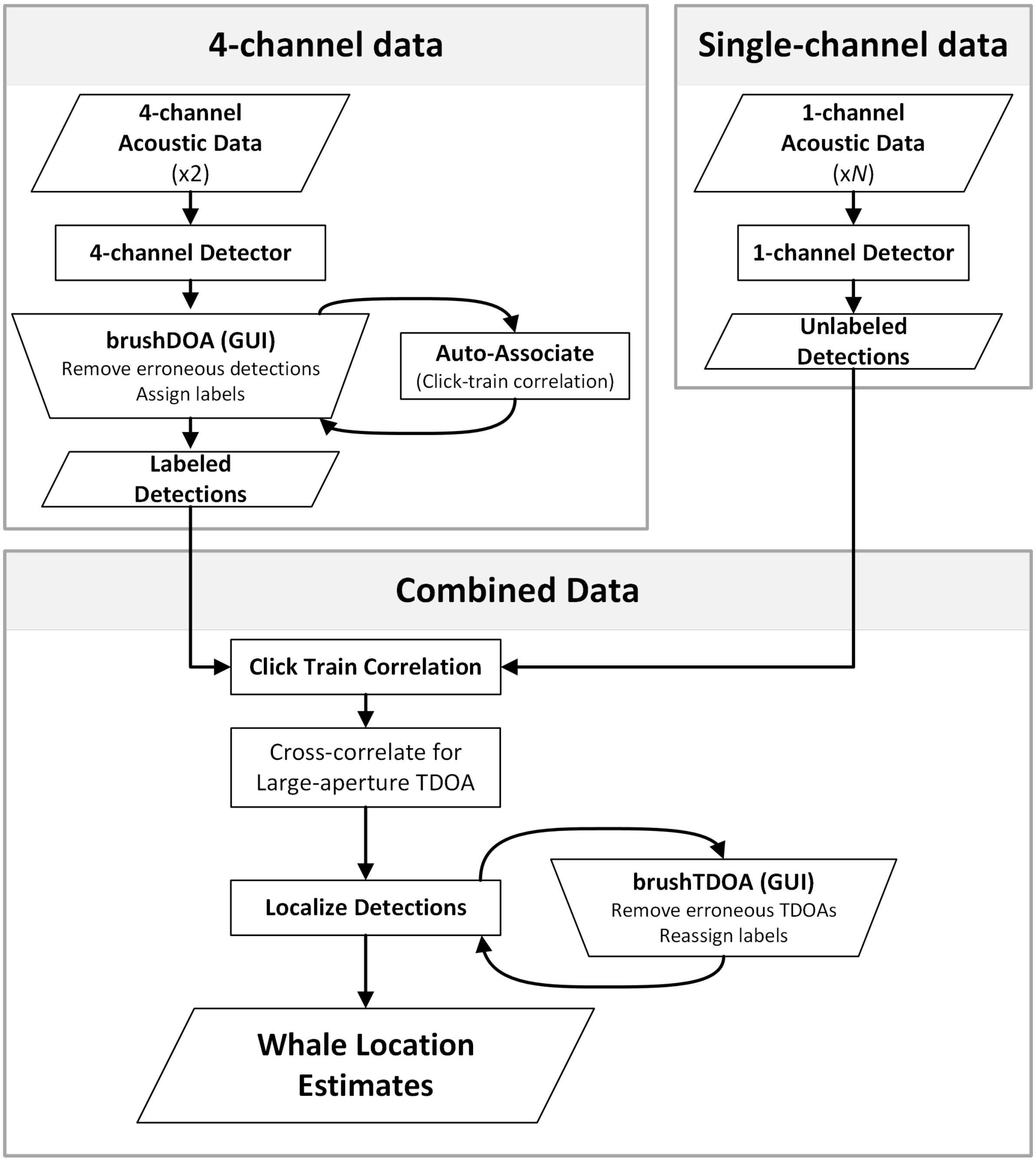


**Figure 1.2. The *Where's Whaledo* workflow.** The typical workflow used to estimate whale tracks via TDOA localization. The parallelograms indicate data inputs or outputs; the rectangles represent an automated process; the trapezoids indicate a graphical user interface (GUI).

*Whaledo* used an iterative process that combines automated association with analyst manual editing using graphical representations.

A graphical user interface (GUI) tool called `brushDOA` was designed specifically for the purpose of removing false detections, identifying the number of unique sources, and associating detections across the two small-aperture arrays. Using this interface, an analyst can select data points to remove them from the dataset or to assign labels. Collections of detections originating from a single source can be identified by observing the gradual changes in their azimuth and elevation. When azimuth angles from two sources are too similar to differentiate, their elevation angles often provide sufficient separation, and vice-versa. Analysts typically focus their efforts on labeling the array with the most detections and least ambiguity. For example, in Fig. 1.3, array 2 had more detections and clear separation between the various tracks, making it easier for the analyst to identify unique sources and assign labels.

### Association with *Click-Train Correlation* tool

After labeling one of the arrays, *Click-Train Correlation (CTC)* tool is used to associate detections across the two arrays. The CTC method identifies associations between detections from different instruments by searching for matching patterns [6]. This involves aligning a set of detected clicks in a window of time on different instruments to determine which ones originated from the same source. To accomplish this the method generates click-train vectors $k_i$ by setting a value of one at each detection time:

$$k_i(t) = \{ 1 \text{ if there is a detection at time } t \text{ on instrument } i, 0 \text{ otherwise.} \tag{1.5}$$

For recordings from instruments with labeled detections, different vectors of $k_{w,i}[n]$ are generated to include only the echolocation clicks associated with each unique label $w$. For unlabeled data, all detections within the window are used to create the click-train vector. Once the click-train vectors $x_{c,i}$ are generated for each instrument and each whale, they are convolved with a 20 ms wide Hanning window to give some width to the detections. This accounts for uncertainty in

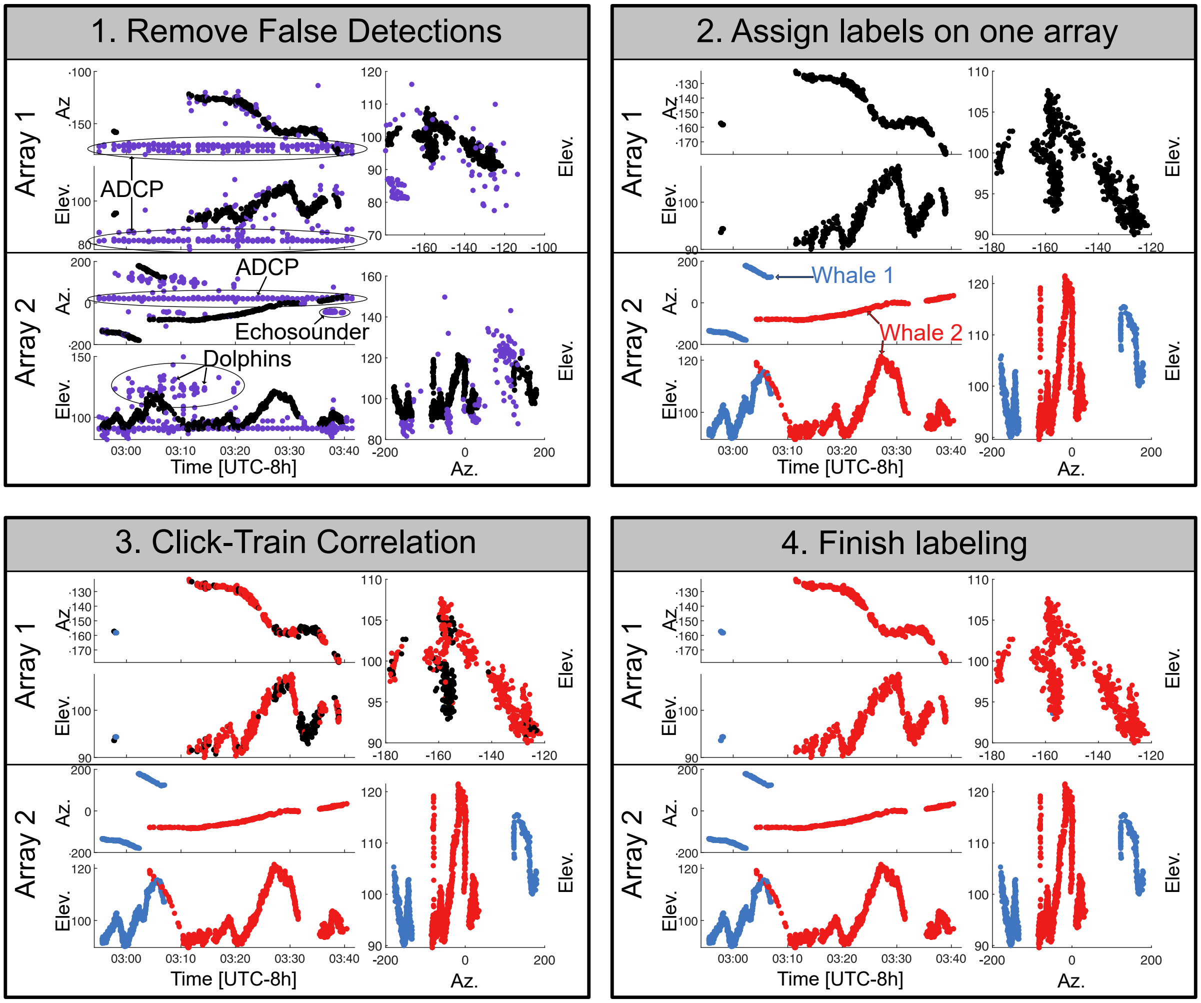


**Figure 1.3. The** `brushDOA` **user interface for editing detections on two 4-channel arrays.** The `brushDOA` user interface allows analysts to select detections, remove false detections, and assign color labels to the detections originating from the same source. The interface includes six plots: azimuth vs. time and elevation vs. time for both arrays, and the azimuth vs. elevation for both arrays. Each frame above shows the `brushDOA` interface during four stages of labeling encounters: 1. The analyst removes false detections caused by other nearby sound sources (e.g. ADCP pings, dolphins, instrument noise); 2. The analyst assigns labels on one array to each of the animals present in the encounter using a combination of spatial and temporal separation of detections; 3. Click-Train Correlation is used to automatically associate detections on the labeled array with their corresponding detections on the unlabeled array; and 4. The remaining detections are assigned labels.

the times of arrival and potential changes in the interval between clicks due to a non-stationary source. The resulting click trains are then cross-correlated, and the location of the peak of the cross-correlation between two click trains gives an estimate of the TDOA ($\tau_w$).

To determine which detections in the unlabeled array are associated with those in the labeled array, the unlabeled detections that align with the labeled detections after being delayed by $\tau_w$ are assumed to originate from the same source and are assigned labels accordingly. However, in cases where both instruments have inadequate detections from the same source, the resulting click-trains may not correlate strongly and may only produce small peaks with no clear dominant peak that can be used to estimate $\tau_w$. To address this, a condition is set to determine if the click-train correlation has failed due to insufficient detections arriving from the same source. Specifically, if the highest peak in the cross-correlation is not sufficiently higher than all other peaks, the click-train correlation is considered to have failed, and no detections in the window will be assigned labels. As a default parameter, if the second-highest peak is greater than 80% of the value of the highest peak, it is classified as too ambiguous. This percentage is adjustable by the user.

Once a sufficient number of detections are associated with CTC, the analyst uses them to determine which other detections are likely to have originated from the same source based on their azimuths and elevations. However, in some cases, there may be ambiguity in sources as the azimuths and elevations of two sources intersect. These sources can still be associated using CTC from the labeled detections on the other array. Once the labeling process is complete, the analyst can move on to the next phase of localization by incorporating the single-channel detections, as shown in the "Combined Data" box in Fig. 2.

The CTC function in *Where's Whaledo* allows adjustment of several parameters including:

- the length of the window used in the click-train correlation,
- the width of the Hanning window convolved with each click train,
- the minimum ratio of the highest peak to the second highest peak in the click-train correlation required to assume the clicks are associated with the same source.

All of these parameters can be adjusted according to the instrument locations, the species of

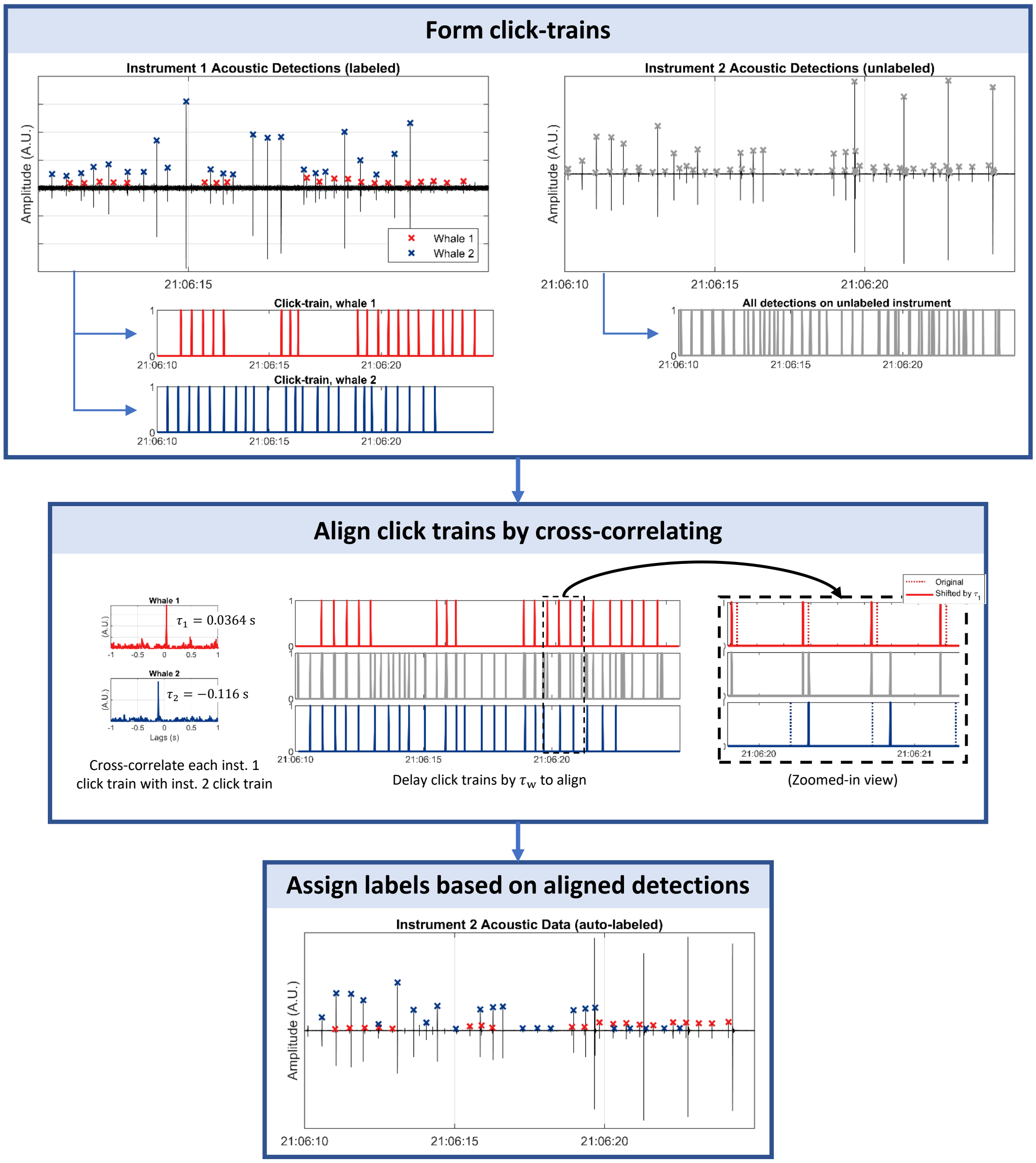


**Figure 1.4. Click-Train Correlation.** An example of click-train correlation (CTC) using a window of detections arriving from two sources. The labeled detections (left column) are separated into two click trains, and each is cross-correlated with the unlabeled click train. CTC is used to associate detections across instruments and determine the delay which would align the clicks.

interest, and other features of a deployment. After performing click-train correlation in a window around one detection, the algorithm steps forward to the next detection and repeats the process.

Once the CTC method is used to associate animals across instruments and estimate an approximate TDOA, a fine-scale TDOA measurement is calculated by cross-correlating the acoustic data. To accomplish this, the expected detection times are used to extract the acoustic data around each detection. If there is a mismatched sampling rate, the data are resampled, then filtered and cross-correlated. The time corresponding to the peak in the cross-correlation is used as the precise large-aperture TDOA measurement.

To ensure accuracy, analysts can use a final interactive view to facilitate the removal of erroneous TDOAs or reassign labels to detections that are misassociated in previous steps. This interface is similar to `brushDOA` and typically requires very few changes.

### Monte Carlo Bootstrap Localization

To improve localization accuracy, calculate confidence intervals, and combine multiple instrument pairs for each detection, a Monte Carlo Bootstrapping approach is implemented for each detection. First, small gaps in TDOAs are filled in by interpolating between recent detections. Interpolation is only performed when detections are no more than five minutes apart.

Locations are estimated using either one 4-channel array and one single-channel or two 4-channel arrays. For the first case, the intersection between the DOA of the 4-channel and the hyperboloid formed by the large-aperture TDOA between the two instruments is found by calculating the expected large-aperture TDOA at each range step along the DOA line, then taking the range where the error between the expected and measured TDOA is minimized. When localizing with two DOAs, the source location is estimated as the point along one DOA where the distance to any point along the second DOA line is minimized.

A Monte Carlo perturbation method is used to approximate the distribution of locations that can be estimated from each set of TDOAs. Random perturbations are added to the TDOAs using a normally distributed pseudo-random number generator (`randn` in MATLAB) with variances of $\sigma^2_{\mathrm{sml}}$ (Eq. 1.6) and $\sigma^2_{\mathrm{lrg}}$ (Eq. 1.7) for the small- and large-aperture TDOAs respectively. The process of deriving the variances is presented in the supplemental materials. DOAs are estimated using the perturbed small-aperture TDOAs, and source locations are estimated for each combination of DOA and large-aperture TDOA available and using both DOAs. This process is repeated 50 times using different random perturbations.

$$\sigma_{\text{sml}} = \sqrt{\left(\frac{\sigma_{H_{k,l}}}{c}\right)^2 + \left(\frac{||H_{k,l}||}{c}\right)^2 \left(\frac{1}{100^2}\sigma_{h_i}^2 + \sigma_{\text{ray}}^2\right) + \left(\frac{\text{TDOA}(k,l)_{\text{calc}}}{c}\right)^2 \sigma_c^2 + \sigma_{\text{xcorr}}^2}. \quad (1.6)$$

$$\sigma_{\text{lrg}} = \sqrt{\frac{\sigma_{h_i}^2 + \sigma_{h_j}^2}{c^2} + (\text{TDOA}(i,j)_{\text{calc}})^2 \frac{\sigma_c^2}{c^2} + \sigma_{\text{travel time}}^2 + \sigma_{\text{drift}}^2 + \sigma_{\text{xcorr}}^2}. \quad (1.7)$$

Each Monte Carlo location estimate is stored to produce a distribution of potential source locations for one detection. Location estimates are assigned a weight equal to the inverse of the variance of the location estimates using the same combination of instruments. A bootstrapping estimate of the weighted average is used to produce the final source location estimate [29, 33]. This involves randomly replacing location estimates with other estimates in the distribution and recalculating the weighted average source location estimate (resampling with replacement). Resampling is repeated 50 times, and the average of the resampled weighted average estimates is used as the final source location estimate. The 95% confidence intervals are estimated using a Studentized bootstrap method [29, 26].

**Alternative localization approach – DOA intersect**

For deployments localizing with two volumetric arrays and no single-channel instruments, the localization process can be linearized and performed much faster. The process is identical to the 4-channel data box in Fig. 1.2, but rather than incorporating the single-channels with click train correlation, the labeled detections from each 4-channel were localized by finding the closest point of intersection between the two DOA lines. This is done by solving the system of equations relating the source location to the directions of arrival,

$$\overrightarrow{s}_1 r_1 + h_1 = \overrightarrow{s}_2 r_2 + h_2 = g_{i,j,k}, \tag{1.8}$$

where $\overrightarrow{s}_n$ is the unit vector representing the DOA line for the $n^{\text{th}}$ array, $r_n$ is the range from the $n^{\text{th}}$ array to the source, and $h_n$ are the Cartesian coordinates of the $n^{\text{th}}$ array location (see Fig. 1.5 for a visualization). By finding the values for $r_1$ and $r_2$ which minimize $(\overrightarrow{s}_1 r_1 + h_1) - (\overrightarrow{s}_2 r_2 + h_2)$, we can estimate the point along each DOA line where the lines are closest to intersecting. To do this, a 2x3 matrix $\mathbf{S} = [\overrightarrow{s}_1; -\overrightarrow{s}_2]$ is constructed and $\mathbf{R} = [r_1; r_2]$ is solved for using MATLAB's "backslash" (or `mldivide`) function (Eq. 1.9). This results in two estimates: $g_1 = \overrightarrow{s}_1 r_1 + h_1$ and $g_2 = \overrightarrow{s}_2 r_2 + h_2$. The final source estimate is the average of $g_1$ and $g_2$.

$$\mathbf{R} = \mathbf{S} \backslash (h_2 - h_1). \tag{1.9}$$

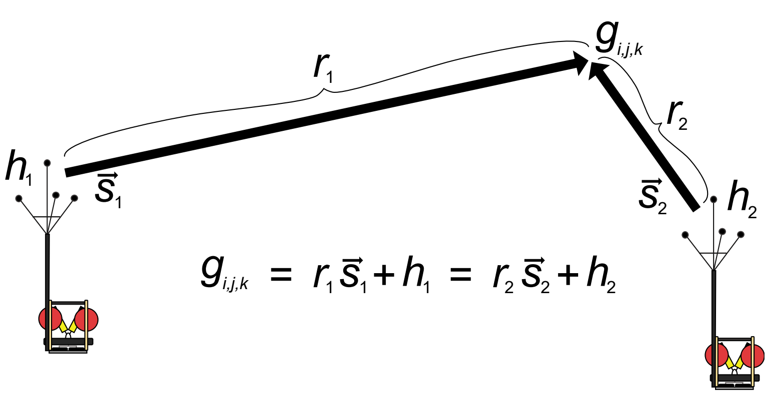


**Figure 1.5. Visualization of the DOA intersect localization method.** An alternative method of localization when detections are present on both 4-channel arrays is to find the intersection of the two DOA lines, $\overrightarrow{s_1}$ and $\overrightarrow{s_2}$. This is done by solving the Eq. 1.8 using MATLAB's `mldivide` function (Eq. 1.9).

The confidence intervals for this method of localization were obtained using the jackknife variance estimator [82]. One TDOA and its associated receiver pair is removed from the DOA estimation, and a new DOA is estimated using the remaining five TDOAs. A new whale location is estimated using the intersection point of the newly obtained DOA and the DOA of the other array using Eq. 1.9. This is repeated for each receiver pair, removing one TDOA and localizing with the remaining 11, until 12 different whale location estimates have been produced. The variance of these location estimates is determined and used in the inverse Student's T distribution to estimate the 95% confidence intervals.

## Case Study - Tanner Basin

Our demonstration of *Where's Whaledo* localizes *Ziphius cavirostris* (*Zc*, colloquially referred to as goose-beaked whale or Cuvier's beaked whale) using a dataset collected during a four-month deployment about 200 km southwest of Los Angeles, California, in the Tanner Basin, known for its *Zc* presence (Fig. 1.6). Four High-frequency Acoustic Recording Packages, or HARPs [106, 105] were deployed from March 16$^{\text{th}}$ to June 11$^{\text{th}}$, 2018. The north and south HARPs each had a single omnidirectional hydrophone with a sampling rate of 200 kHz moored approximately 10 m above the seafloor. The east and west HARPs each had volumetric arrays of four omnidirectional hydrophones in a tetrahedron configuration with $\approx 1$ m spacing between hydrophones. The 4-channel arrays had a sampling rate of 100 kHz and sat $\approx 6$ m above the seafloor on a rigid mast. The distance between each HARP was between 470 and 1075 m.

### Oceanographic conditions and Instrument Locations

TDOA localization requires knowledge of receiver locations and the properties of the medium of propagation that affect travel times. The speed of sound in water depends on various oceanographic conditions, such as temperature, pressure, and salinity, resulting in both temporal and spatial variation in sound speed[62, 19, 31]. However, to simplify computation, a constant sound speed was used for our case study. This approximation is generally acceptable at close ranges. To quantify the error introduced by the constant sound speed approximation, we estimated the variations in sound speed using a CTD (Conductivity, Temperature, Depth) profiler mounted

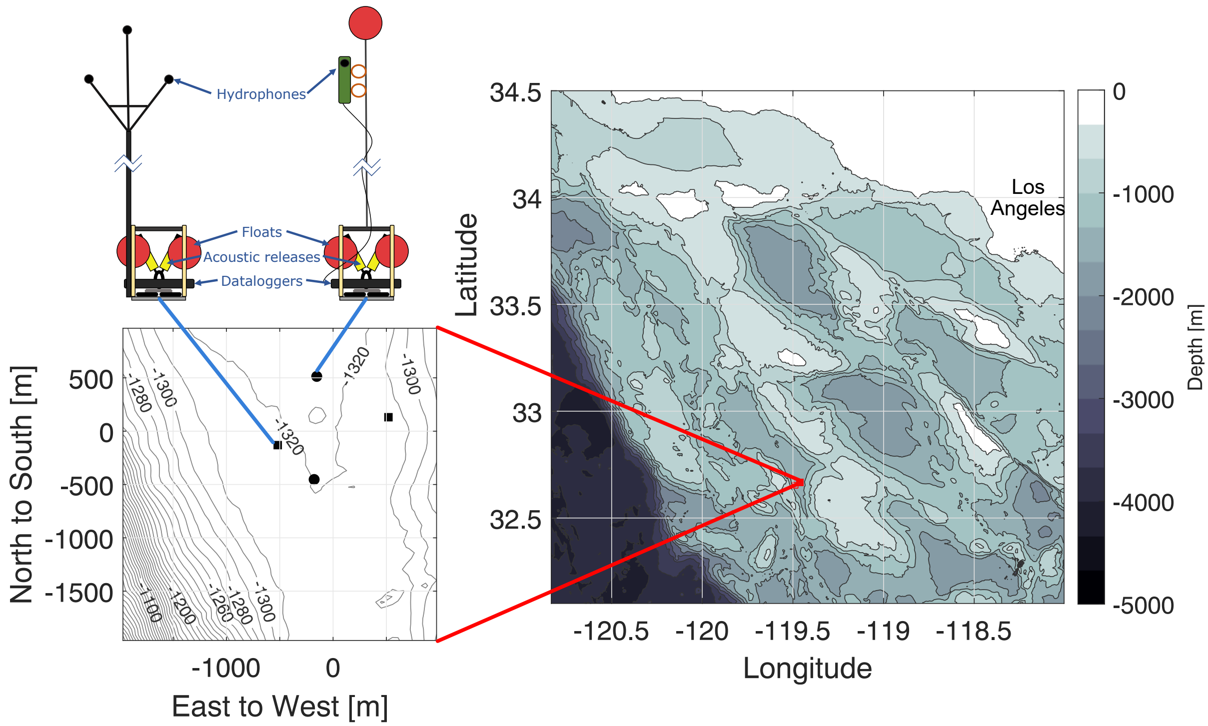


**Figure 1.6. Study site.** The case study site where *Zc* tracks were reconstructed using the *Where's Whaledo* MATLAB toolkit. Site is in Tanner Basin, ≈ 200 km southwest of Los Angeles, California. Two instrument types were used: single channel instruments (black circles on the left plot) and 4-channels (black squares).

at the study site. Empirical relationships between sound speed, temperature, salinity, and depth were used to estimate sound speed from the CTD measurements [62, 19, 31]. The uncertainty in the assumed sound speed is accounted for in the overall uncertainty of the localization estimates. Further details on the uncertainty calculations can be found in the supplemental materials.

Each instrument is equipped with an Edgetech acoustic release that can emit an acoustic ping in response to a ping received from a transducer on the ship. The two-way travel time of these acoustic signals from various ship locations is used to estimate the positions of the instruments. The uncertainty in instrument position is incorporated into the overall uncertainty and is discussed further in the supplemental materials.

To determine the relative positions of the hydrophones in the small-aperture arrays, we use the plane-wave approximation as shown in Eq. 1.2. Instead of relying on a narrow-band ping, we used the broadband engine noise emanating from the ship during the instrument localization period. The engine noise is bandpass filtered and cross-correlated to estimate the TDOA in one-second bins. The TDOA's and the ship location for each one-second bin (obtained from the ship's GPS system) are put into a system of equations using Eq. 1.2 to solve for the relative hydrophone positions within the array.

**Clock synchronization**

Ensuring clock synchronization is essential for combining data from various receivers used in localization. While all the receivers within each small aperture array were synchronized, the large aperture array required a two-step process to correct for clock drift. Initially, we synchronized the clocks using the pings transmitted by each instrument's acoustic release during instrument localization. Then, we used the pings from an Acoustic Doppler Current Profiler (ADCP) which was deployed concurrently with our instruments and transmitted a 75 kHz ping approximately every 60 seconds to synchronize the clocks for the remainder of the deployment. Well 75 kHz is above the Nyquist frequency of the 4-channel instruments (50 kHz), the pings were recorded as aliased signals of 25 kHz and could still be used for clock synchronization.

Each instrument's acoustic release was enabled only during the period when it was being localized. Instrument localization was performed over the course of seven hours, and each acoustic release was enabled for between one and two hours. The pings were detected with a narrowband filter and a threshold. Due to the consistency of the amplitude of the pings, a different threshold was used for each instrument which was well above the noise levels at this frequency but had a near-zero probability of missed detection. The TDOA was calculated by cross-correlating the pings detected on each instrument. False detections produced TDOAs that significantly deviated from the true TDOAs and were manually removed. The clock drifts were calculated as the values that minimized the errors between the expected TDOAs (based on instrument locations and sound speed) and the calculated TDOAs.

The ADCP pinged approximately every minute at 75 kHz. Since the 4-channel HARPs had a sampling rate of 100 kHz, the aliased frequency of 25 kHz was used to calculate the TDOA of the ADCP pings. The single-channel data were downsampled from 200 kHz to 100 kHz to deliberately alias the ADCP pings. The TDOA was then calculated by cross-correlating the detected ADCP pings for the entire deployment. The relative clock drifts between each instrument pair was then estimated as the change from the expected TDOA (based on the TDOA of the ADCP pings calculated during localization). A fifth-order polynomial fit was applied to the resulting clock drift estimates to simplify correcting for clock drift during localization.

# Results

In our case study dataset, we used a specialized beaked whale detector in tandem with DetEdit [87] to identify 600 separate time periods containing *Zc* detections. Of these initial periods with detections, 107 contained detections with a high enough SNR and were in close enough proximity to the instruments for analysts to identify unique individuals in the encounter using `brushDOA`. However, many of these individual tracks had too few detections to be reliably localized; encounters that lasted less than 5 minutes or contained fewer than 300 detected clicks were removed from analysis, and ultimately approximately 90 encounters contained a sufficient number of localized detections in succession to be considered usable tracks. These encounters contained between one and six uniquely identifiable individual animals.

We demonstrate our approach with three examples. The first example is the simplest case, where source association is unambiguous, and tracks can be obtained quickly and easily. The second example is an encounter with six whales where source association was more challenging due to the number of whales vocalizing simultaneously and their proximity to each other. In the last example, a large pod of vocalizing dolphins obscured the beaked whale vocalizations, but we were still able to obtain tracks of two individual *Zc* using DOA information and click-train correlation.

## Example 1 - Simple source association

In this example, two whales were observed that exhibited both spatial and temporal separation, facilitating a straightforward association of clicks to each source. The encounter occurred on June 11, 2018, as the whales both approached the acoustic array. The first whale swam to the northeast, passing just west of the array, while the second whale swam northward, moving directly into the center of the array (Fig. 1.7). The distinct spatial and temporal gap between the whales allowed for unambiguous source association. Click-train correlation performed well on both tracks, further ensuring accurate source associations. Additionally, sporadic detections of a possible third and fourth whale occurred during this time period, but they were insufficient to establish reliable track formations.

Both whales in this example exhibited a dive descent at the beginning of their tracks. The first whale was positioned more than 3000 m from the center of the array. Since errors in DOA angle estimates scale with range, this leads to larger confidence intervals when compared to the much closer second whale. During the dive phase of the second whale, detections were present only on the west 4-channel and one or both of the single channels. Once the whale reached foraging depth, all four instruments had a significant number of detections, allowing for optimal track reconstruction.

## Example 2 - Large group size

An encounter involving at least five *Zc* was identified on April 29, 2018 (Fig. 1.8). The whales were observed in two distinct clusters: a first group of three whales swimming from the south and east toward the center of the array at the beginning of the encounter (red, blue, and yellow), and a second pair following about 10 minutes behind from the same direction (purple and green).

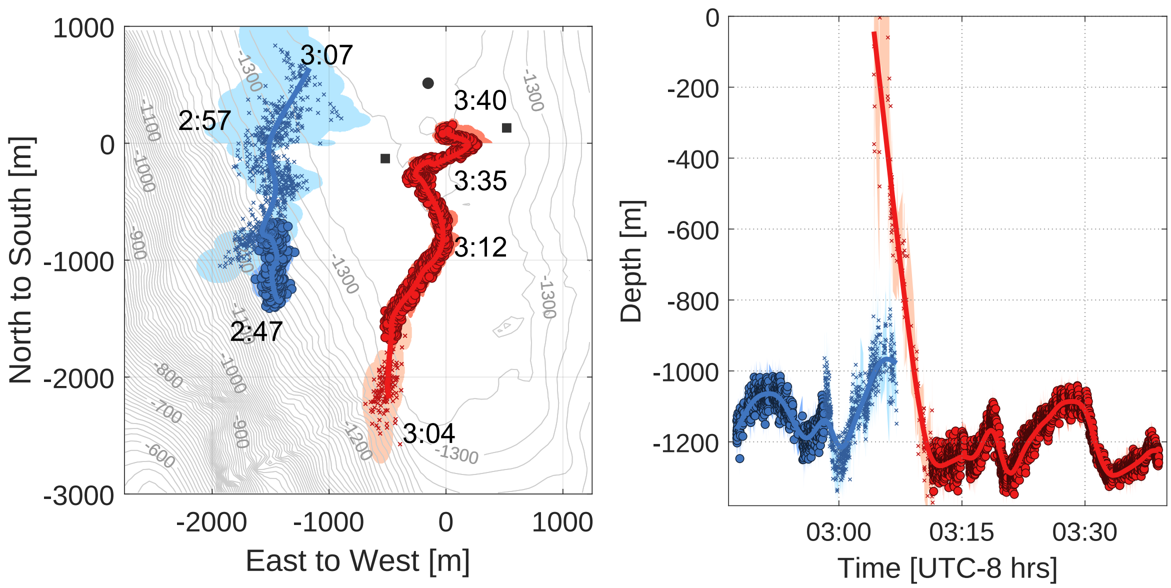


**Figure 1.7.** ***Zc*** **track reconstructions with clear source association.**
The left panel is a map view with time annotations along two separate animal tracks, and the right panel shows the animals' depth versus time. The colors represent different whales, and the semi-transparent shading represents their 95% confidence intervals. Points with circles are localized with two 4-channel instruments, whereas points with "x" were detected on only one 4-channel and one or two single-channels, Confidence intervals vary due to differences in the number of instruments used to localize, the position of the whale, or the precision and accuracy of the TDOAs.

## Example 3 - *Zc* co-occurance with dolphins

An encounter on April 22, 2018 consisted of a group of two *Zc* echolocating simultaneously with a large pod of dolphins (Fig. 1.9). The overlap in the frequencies of both dolphin and *Zc* clicks led to a high number of false detections. It is worth noting that dolphin dive depths are much shallower than *Zc*, resulting in the elevation angles of the dolphin detections being closer to 180° than the *Zc* detections. However, when the dolphin group sizes are large, as for this case, multiple individuals' clicks arrive within the allowed small-aperture TDOAs, and their cross-correlations frequently produce erroneous DOA estimates. Consequently, the resulting DOA plots appear cluttered with detections seemingly coming from all directions, including the seafloor.

Nevertheless, the *Zc* clicks produce reliable TDOA estimates, allowing for their visual identification in the DOA plots. Dolphin detections could also be identified by their periodicity, with clicks occurring in clusters that faded in and out every few minutes. This characteristic made them easier to identify and remove from the analysis.

In this instance, identifiable *Zc* tracks were present in array two, while they were less distinct in array one. Array two was therefore cleaned and labeled, followed by click-train correlation to determine the most likely *Zc* clicks on array one (Fig. 1.9). The resulting *Zc* tracks approach the array center from the southwest, apparently in a coordinated manner.

# Discussion

This study demonstrates the utility of *Where's Whaledo* as a tool for reconstructing tracks using passive acoustic localization. We were able to obtain 90 reliable tracks from a four-month deployment offshore of Southern California. The process has the potential to be applied to similar deployments, and further development of the software could expand its usefulness to other receiver configurations, environments, and species of interest.

Identifying potential tracks and removing erroneous or unreliable detections can be done with the `brushDOA` GUI, which allows analysts to efficiently identify and annotate detections arriving from the same source on a small aperture array. Automated source association between widely spaced receivers is performed with click-train correlation, which searches for patterns of clicks arriving from one source in the various receivers. Once detections are correctly associated, they can be cross-correlated to determine the fine-scale TDOA, then localized using maximum likelihood comparison with a TDOA model.

A primary localization challenge is categorizing clicks by individual animals. When the animals are far apart, individuals can be successfully identified in the Azimuth/elevation plots. This was occasionally challenging with *Zc*, but for most encounters, distinct tracks could be identified on at least one of the small-aperture arrays. Calculating the TDOA on the small-aperture arrays by cross-correlating a window of time around a detection assumes only one detection within the window. For species with more individuals or whose interval between clicks is shorter than the maximum possible TDOA like some dolphin species, this may not hold, and an alternative method for identifying sources would be necessary. Click-train correlation can be effective in finding patterns of clicks on separate instruments, but may not work for other species with less unique click patterns or where detections are too sparse for adequate correlation. In these cases, analysts may rely on identifying periods of simultaneous elevation change on both arrays or incorporate other methods to associate detections with sources.

In this study, simultaneous occurrences of *Zc* and delphinids presented challenges for tracking beaked whales. One solution would be to use a more sophisticated detector that better differentiated between each species' vocalizations, for instance using measurements of peak frequency and number of cycles within a click to separate species, or using a machine-learning based detector [76, 107]. However, due to identifiable patterns in the DOA plots, such as higher elevation angles, periodicity in vocalizations, and a high number of erroneous DOA estimates, dolphin detections were frequently able to be manually removed by analysts while *Zc* detections were retained.

The tracks obtained from our approach often contain spatial offsets in clusters of detections arriving from the same source, causing the path to appear bifurcated. This is generally due to different combinations of instruments detecting the echolocation pulses. The most reliable detections were those that were detected on both 4-channel instruments. Due to the distance between the two 4-channels in this deployment (1070 m) and the highly directional nature of *Zc* echolocation clicks, many detections were only present on one of the 4-channels. Placing the arrays closer together would increase the number of clicks detected on both 4-channels. However, this would decrease the range at which reliable localizations were possible. Therefore, finding the optimal balance between the distance between the arrays and the number of clicks detected on both 4-channel instruments is crucial. Click directionality also greatly influences the spatial distribution of tracks obtained, since an encounter is far more likely to be tracked when the animal is facing multiple instruments. This may introduce bias into the types of track obtained at a given site, and a thorough analysis of this spatial bias should be performed for each deployment.

*Where's Whaledo* was developed for and tested specifically on deployments with two 4-channel HARPs and a varying number of single-channel instruments. With some adaptations, *Where's Whaledo* could prove useful with varying instrument configurations, such as large-aperture only or linear arrays. As of publication, the detector and TDOA estimator included on the *Where's Whaledo* GitHub page were developed for *Zc*, but the software could be expanded to be used for localizing other sources, such as baleen whales or anthropogenic sounds.

To improve *Where's Whaledo*, a more advanced detector could be used to incorporate low SNR clicks without generating false detections. Jang *et al.*[47] implemented a Generalized Cross-correlation detector on the same dataset, which was effective in removing most false detections caused by repeated instrument sounds. Additionally, Jang et al [47] used a multi-target tracking (MTT) algorithm to reconstruct *Zc* tracks using the two small aperture volumetric arrays. Components of this algorithm could be incorporated into *Where's Whaledo* to automate the removal of false TDOA measurements and improve source association. By incorporating estimates of an animal's swim speed into localizations, the reliability of track reconstructions could be further enhanced [47, 11].

# Conclusion

Passive acoustic localization is a powerful way to track animal movement, which can provide valuable insights into animal behavior and the parameters needed for density and distribution measurements. Several previous studies have demonstrated the capability of using TDOA localization of cetacean vocalizations to reconstruct their tracks. Some common challenges may limit the number of tracks obtained, including efficiently identifying potential tracks in large datasets, identifying the number of sources, and associating detections to the appropriate source. The *Where's Whaledo* toolkit provides an efficient and reliable workflow for TDOA localization of odontocete echolocation clicks. The toolkit is designed for deployments of hydrophones containing a combination of small-aperture volumetric arrays and single-channel instruments. *Where's Whaledo* includes a number of functions and GUIs to aid in the process of identifying separate sources, associating detections to each source, removing erroneous or unreliable detections, and estimating the most likely whale position from the TDOAs.

We demonstrate the utility of *Where's Whaledo* by localizing *Zc* echolocation clicks in the Tanner Basin. In the four-month dataset, tracks were reconstructed for $\approx 90$ individual whales, with group sizes ranging from one to six individuals. Track reconstructions were successfully performed in the presence of significant masking due to dolphin echolocation clicks and in situations where animals were in close proximity. With some adaptations, *Where's Whaledo* could be configured to work with a variety of receiver configurations, environments, and species of interest.

# Acknowledgments

Funding provided by the Office of Naval Research Young Investigator Program, Office of Naval Research Task Force Ocean, and the Pacific Fleet. We thank Robert Headrick and Chip Johnson for their support. Special thanks to: Bruce Cornuelle for providing expertise and assistance with code implementation and matrix inversions; Junsu Jang for testing Kalman and particle filter implementations and general feedback; Bayleigh Coleman, Alma Leon, and Ryan Parkes for beta-testing earlier versions of *Where's Whaledo* software. Ana Mae Shickich, Grace Randall, and Lauren Baggett for testing the current version of the dataset and providing valuable feedback. *Where's Whaledo* naming credit goes to Margaret Morris.

Chapter 1, in full, is a reprint of the material as it appears in: Snyder, E. R., Solsona-Berga, A., Baumann-Pickering, S., Frasier, K. E., Wiggins, S. M., & Hildebrand, J. A. (2023). Where's Whaledo: A software toolkit for array localization of animal vocalizations. bioRxiv,

2023-08.

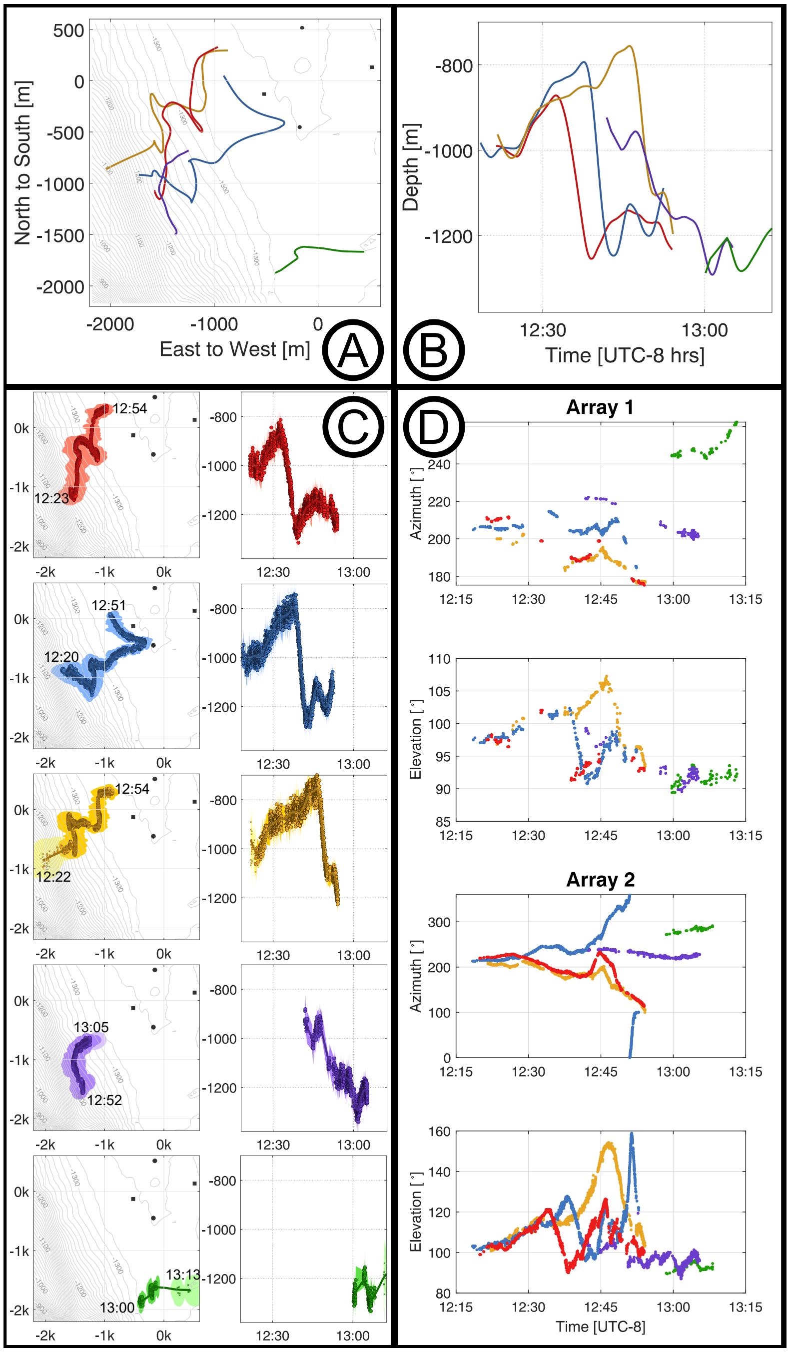


**Figure 1.8.** ***Zc*** **tracks with large group sizes.**
An encounter with five whales vocalizing concurrently. Panels A and B show the map view and the depth vs. time of the track estimates of all five animals, where the colors correspond to the same detections shown in the other panels. Panel C shows the map view and depth vs. time views for each individual separately, where the different colors represent different whales and the semi-transparent shading represents their 95% confidence intervals. Panel D shows the labeled azimuths and elevation angles of each of the animals in the encounter.

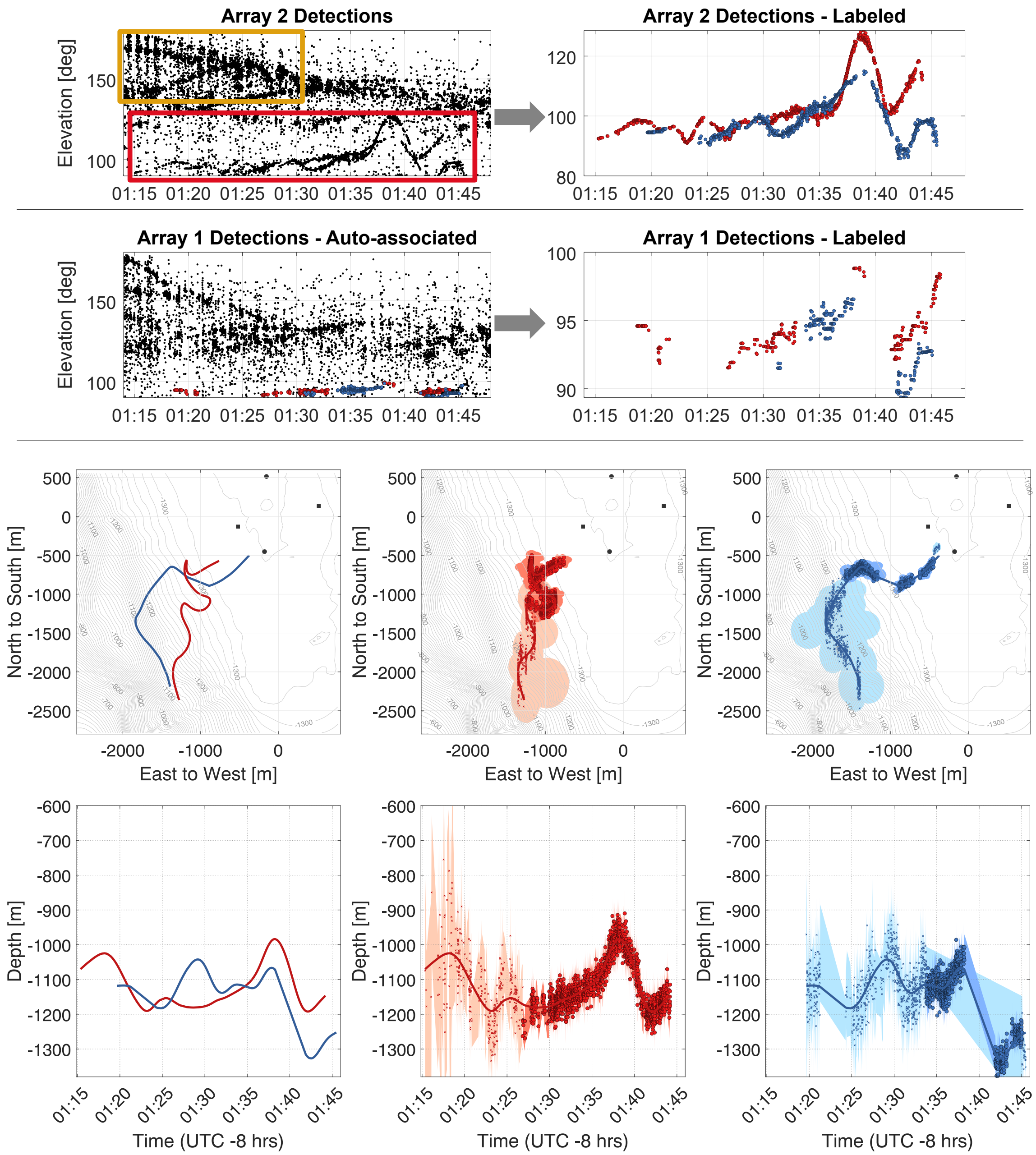


**Figure 1.9. Reconstructing *Zc* tracks in the presence of false-detections.**
Top left panel shows array-two detections, including: (yellow box) echolocating dolphins and (red box) two echolocating *Zc*. Upper right panel illustrates removal of dolphin detections, due to their higher elevation angles, periodicity (where detections fade in and out on an $\approx 1$ min cycle), and ”fuzziness” (where multiple dolphin clicks present in one window gave erroneous DOAs). Middle panels show array-one detections (left) before and (right) after dolphin echolocation removal. Lower panels show maps with tracks of (left) both *Zc* and (middle and right) individual animals.

# Chapter 2

# *Ziphius cavirostris* diving behavior in the Tanner Basin

## 2.1 Introduction

*Ziphius cavirostris* (*Zc*) is an odontocete species found in temperate waters throughout the ocean [24, 44]. *Zc* have the broadest distribution of the 24 known beaked whale species and have both the deepest and longest documented dives of any mammal [81]. They are a species of interest due to their sensitivity to anthropogenic noise, particularly Mid-Frequency Active Sonar (MFAS), which has been linked to several mass-stranding events [13, 22, 25, 32, 84, 85]. Better understanding *Zc* behavior and distribution would allow for more informed policy implementation for their protection and could contribute to a better understanding of their role and impacts in ecosystems.

Like other odontocetes, *Zc* emit regular echolocation clicks for foraging and navigation [109]. The regularity of these clicks makes them excellent candidates for passive acoustic studies [12]. *Zc* clicks were first described in scientific literature as early as 2002 [35], and a number of studies since have improved upon these measurements [12, 109, 50]. *Zc* regularly dive below 1000 m and the median dive duration is approximately one hour [72, 81, 91].

*Zc* diving behavior has been observed in a number of studies, both with tagging and passive acoustics. Animals have been recorded regularly diving to depths of over 1000 m [6, 7, 37, 72, 81, 83, 99], with some dives approaching 3000 m [81, 83]. Data from tags outfitted with acoustic recording devices indicate that animals begin echolocating during the dive phase at a few hundred meters depth, continue echolocating during the entirety of the foraging phase, and cease vocalizations while ascending [99, 3]. L. Baggett reconstructed 162 *Zc* tracks from three different deployments at a site in the Southern California Bight [7] using the intersection of two direction of arrival (DOA) estimates to two volumetric arrays with the *Where's Whaledo* software package described in chapter 1 [86]. Baggett categorized the localized portions of the dive into one of three behaviors: initial descent, consistent trajectory, and variable trajectory. Since *Zc* do not vocalize during the ascent phase, these portions of the tracks could not be localized.

*Zc* have been observed both as solitary individuals and in small groups of two to eight animals [3, 8, 20, 65]. In recent years, efforts have been made to understand the synchronicity and cooperative nature of beaked whale diving behavior. Simultaneously tagged *Zc* in the Ligurian Sea arm of the Meditteranean Sea were observed exhibiting synchronous diving behavior, but seemed to diverge during foraging [3]. Similarly, tagged whales in the Hatteras Canyon in the Atlantic also exhibited synchronous diving behavior, and some groups contained multiple adult males [20]. It is hypothesized that group cohesion near the surface is a predation avoidance technique, but once the animals are at depth they may forage apart to avoid contending with each other's echolocation signals [3, 20]. Passive acoustic localization using two small-aperture volumetric arrays can provide additional insight into group sizes and the synchronicity of diving and foraging behavior [7, 37].

*Zc* have a highly directional echolocation beam, meaning the intensity of the echolocation click measured in front of the animal is significantly higher than a click measured off-axis [109, 37, 23]. Click directionality affects the probability of detection, range of detectability, and probability of missed detection, all of which have implications for density estimation from passive acoustics [64, 46]. A single oscillating piston model has been proposed as an approximation of the directivity of odontocete echolocation signals [5].

Some attempts have been made to measure the acoustic beam pattern of a *Zc*, comparing the results to the piston model [109, 37]. Zimmer, *et al.* [109] reconstructed the dives of two

*Zc* simultaneously using DTAGs, which are outfitted with accelerometers, magnetometers, and pressure sensors as well as acoustic recording devices [51]. The estimated relative orientations between the two animals and calculated the Apparent Source Level (ASL) with relative heading angle using the vocalizations of one animal recorded on the other animal's DTAG. The study found that a piston model with a peak intensity at 15° off-axis best fit the data [109]. Gassman, *et al.* [37] reconstructed the dives of *Zc* by localizing echolocation clicks using an array of bottom-mounted hydrophones. For one of the reconstructed tracks, the animal turned past a range of angles in relation to three of the hydrophones used. The Source Levels (SL) of each click were estimated using spherical spreading, and the relative angle of the whale vs SL was plotted for each detected click. The authors observed a number of high SL detections at an off-axis angle of 30° and proposed a piston model fit centered around this angle [37].

Here, we reconstructed 143 individual dives using the intersection of the Direction of Arrival (DOA) estimates to two 4-channel volumetric arrays [86]. The instruments were deployed from March to July of 2018 at a site in the Tanner Basin, located approximately 200 km west of San Diego, California. The Tanner Basin has a known *Zc* presence and is approximately 60 km due south of the US Navy-controlled San Nicolas Island, exposing *Zc* to MFAS in this region [74]. From these track reconstructions, we estimated a number of features, including group sizes, spatial distributions, and dive depths. We selected 12 tracks to use in estimating echolocation click source levels with heading angle and compared the results to the piston model.

## 2.2 Methods

### 2.2.1 Data Collection and Parameter Calculation

To reconstruct *Zc* behavior through passive acoustic localization, we deployed four HARPs – two 4-channel arrays and two single-channel moorings (Figure 2.1, Table 2.1).

Instrument locations were determined by transmitting a ping from a ship-board transducer. An EdgeTech Acoustic Release mounted on the instruments received the ping and transmitted

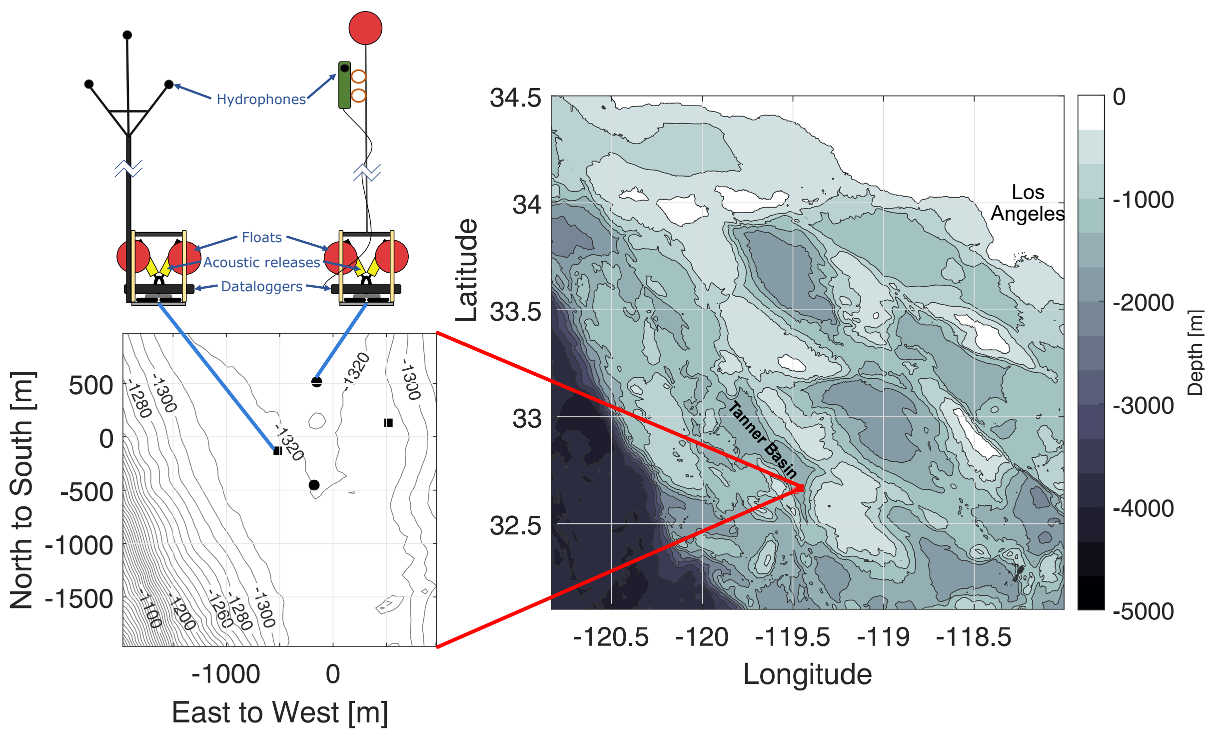


**Figure 2.1. Study Site.** The case study site where *Z. cavirostris* tracks were reconstructed using the *Where's Whaledo* MATLAB toolkit [86]. The study site is in the Tanner Basin, $\approx 200$ km southwest of Los Angeles, California. Two instrument types were used: single-channel instruments (circles on the left plot) and four-channels (squares).

one. The two-way travel time (minus the turn-around time) was used to estimate the range to the instrument. This was repeated for a variety of ship locations, as the ship encircled each instrument and performed a transect directly above the instrument. The ship locations were recorded by the ship's navigational system, an the instrument locations were estimated using MATLAB's `fmincon`. Precise receiver positions within a four-channel array were estimated by cross-correlating one second bins of bandpass filtered acoustic data of the ship's engine noise during the localization circle and transect (100 Hz and 10 kHz 4th order elliptical filter with, with 0.1 dB peak-to-peak passband ripples and 40 dB stopband attenuation). The time corresponding to the peak of the cross-correlation between two hydrophones was used as the TDOA of the ship engine sound between those two instruments. By placing all TDOAs and ship locations into a linear equation, precise hydrophone locations were estimated by matrix inversion.

**Table 2.1.** Instrument locations and details.

| | East | West | North | South |
|---|---|---|---|---|
| Latitude | 32° 39.528′ N | 32° 39.381′ N | 32° 39.732′ N | 32° 39.210′ N |
| Longitude | 119° 28.624′ W | 119° 29.230′ W | 119° 29.053′ W | 119° 29.069′ W |
| Depth | 1337 m | 1338 m | 1344 m | 1350 m |
| No. of Channels | 4 | 4 | 1 | 1 |
| Sampling Freq. | 100 kHz | 100 kHz | 200 kHz | 200 kHz |

Periods with *Zc* presence were identified on the southern HARP using a specialized beaked whale detector in tandem with DetEdit [12, 87]. For each of these periods, the localization process was performed, as described in Chapter 1 [86]. Initially, $>$ 600 *Zc* encounters were identified. Encounters with no tracks that could be visually identified with the `brushDOA` interface were omitted. This could be due to an insufficient number of detections, unreliable or uncertain source associations, masking due to the presence of dolphins, or excessive distance to the sensors. 145 encounters were deemed reliable enough to be used for track reconstructions. When possible, the intersection of the DOA lines was used for track reconstructions. This method produces more robust location estimates. However, a significant number of tracks had few or no detections on one of the four-channel instruments, meaning localization could only be performed by incorporating the single-channel instruments. The subsequent analyses were performed on the tracks obtained using the DOA intersect. A piece-wise cubic spline fit was applied to the localizations for final track estimates.

### 2.2.2 Diving Behavior

Group sizes were estimated using two methods: 1) the number of individual whales identified within a 60-minute period; and 2) the maximum number of whales vocalizing concurrently in a 60-minute period. The 60 minute period is approximately the median dive duration of a *Zc* observed by Quick, *et al.* [72]. These measures were obtained by counting the number of unique labels assigned during an encounter rather than the number of tracks obtained in the azimuth and elevation plots since a significant portion of animals were only identified on one of the two arrays.

L. Baggett proposed grouping observed diving behaviors into one of three categories [7]:

1. Initial decent, where the animal started shallower than 800 m and the change in depth exceeded 350 m;

2. Consistent trajectory, where the animal remained deeper than 800 m, and its trajectory remained relatively constant (varied less than 100 m in any direction from the straight path);

3. Variable trajectory, where the animal varied more than 100 m from the straight path in any direction.

These categories could serve as a hypothesis for three phases of a dive: the initial dive, the "transiting" portion while the animal searches for a foraging ground, and the foraging portion. A fourth phase, when the whale rises to the surface, was not included because the *Zc* cease vocalizing during this phase and therefore cannot be localized. The precise values used in the categorization could be potentially refined with further analysis and may vary at different sites [7].

### 2.2.3 Source level estimation

To analyze the directionality of *Zc* echolocation clicks, nine track segments were selected where the track estimate turned past a distribution of angles close to on-axis to both of the single-channel instruments and had a high number of detections on both four-channels during the turn. For each localized detection, the whale's heading was calculated. The heading relative to each single-channel instrument was calculated as the difference between the absolute heading of the whale and the angle between the whale and the receivers. Broadband peak-to-peak source levels were estimated by correcting the acoustic data for hydrophone sensitivity and assuming spherical spreading between the estimated whale position and each single-channel hydrophone.

A broadband piston model beam pattern was used as a comparison to the measured beam patterns [5, 37, 109]. The source level $B$ as a function of angle $\theta$ of a flat circular piston is given by:

$$B(\theta) = \frac{\int_{-\infty}^{\infty} P^2(\theta, f) W^2(f) df}{\int_{-\infty}^{\infty} W^2(f) df}, \tag{2.1}$$

where $P$ is the source level as a function of frequency $f$ and angle $\theta$ and $W$ is the variation in source level with frequency. $W(f)$ was calculated by averaging the spectra of $\approx 14,000$ clicks from the 9 tracks selected for beam pattern analysis. The frequencies between 20 and 100 kHz were used in these calculations. The 4-channel instruments were omitted from SL calculations since the Nyquist frequency of 50 kHz was too low to capture the full spectrum of a Cuvier's click. The frequency-dependent source level is given by:

$$P(x) = P_0 \frac{2J_1(x)}{x}, \tag{2.2}$$

where $P_0$ is the on-axis source level (217 dB re $1\,\mu\text{Pa}^2$), $J_1$ is a Bessel function of the first kind. $x$ is given by:

$$x = \frac{2\pi f a \sin\theta}{c}, \tag{2.3}$$

where $a$ is the piston radius and $c$ is the speed of sound. Zimmer *et al.*[109] and Gassmann *et al.*[37] used a piston radius of 20 cm and 25 cm respectively. In this analysis, a sound speed of $c = 1488.4\,\frac{\text{m}}{\text{s}}$ and a reference intensity of $P_0 = 217$ dB re $1\,\mu\text{Pa}^2$ were used. Eq. 2.1 creates a beam pattern centered around a peak angle of 0°. Zimmer *et al.*[109] used an off-axis peak angle of 15° and Gassmann *et al.*[37] used an off-axis peak angle of 30°, both done by shifting $\theta$ by the offset.

**Table 2.2.** Track Categorizations

| | No. of tracks | Max. duration (min) | Min. duration (min) | Average duration (min) |
|---|---|---|---|---|
| Type 1 (Initial Descent) | 12 | 46.8 | 8.9 | 30.2 |
| Type 2 (Consistent trajectory) | 8 | 10.7 | 2.1 | 4.3 |
| Type 3 (Variable trajectory) | 123 | 40.8 | 2.5 | 20.6 |

## 2.3 Results

During the study period, we successfully obtained a total of 143 individual reconstructions of *Zc* encounters. Tracks were located mostly along the steep canyon wall west of the arraysFigure 2.2 shows the lateral positions of all tracks. Figure 2.3 shows the number of detections localized to each grid location in *x* and *y* using a 100x100 m grid. The majority of detections come from the west side of the array system, with a peak in detections in between the south and west instruments. Similarly, the polar histograms of azimuths in Figure 2.4 indicate the majority of detections arriving from the west of the array system.

Figure 2.6 shows all the tracks categorized into the three dive categories proposed by Baggett *et al.* [7] (see Table 2.2). The majority of tracks fell into Type 3 (variable trajectory). Type 2 (consistent trajectory) had the fewest tracks and the shortest durations. Encounters of less than two minutes were removed from the analysis.

Figure 2.7 shows nine track segments selected for SL analysis. The maximum SL observed was 221.3 dB re 1$\mu$Pa @ 1 m, and the mean SL was 185.3 dB with a standard deviation of 7.9 dB re 1$\mu$Pa @ 1 m. Figs. 2.8 and 2.10 show the SL vs horizontal angle of the animals in relation to each array. Figs. 2.9 and 2.11 show the same estimates using a 3-D estimate of the whale's heading.

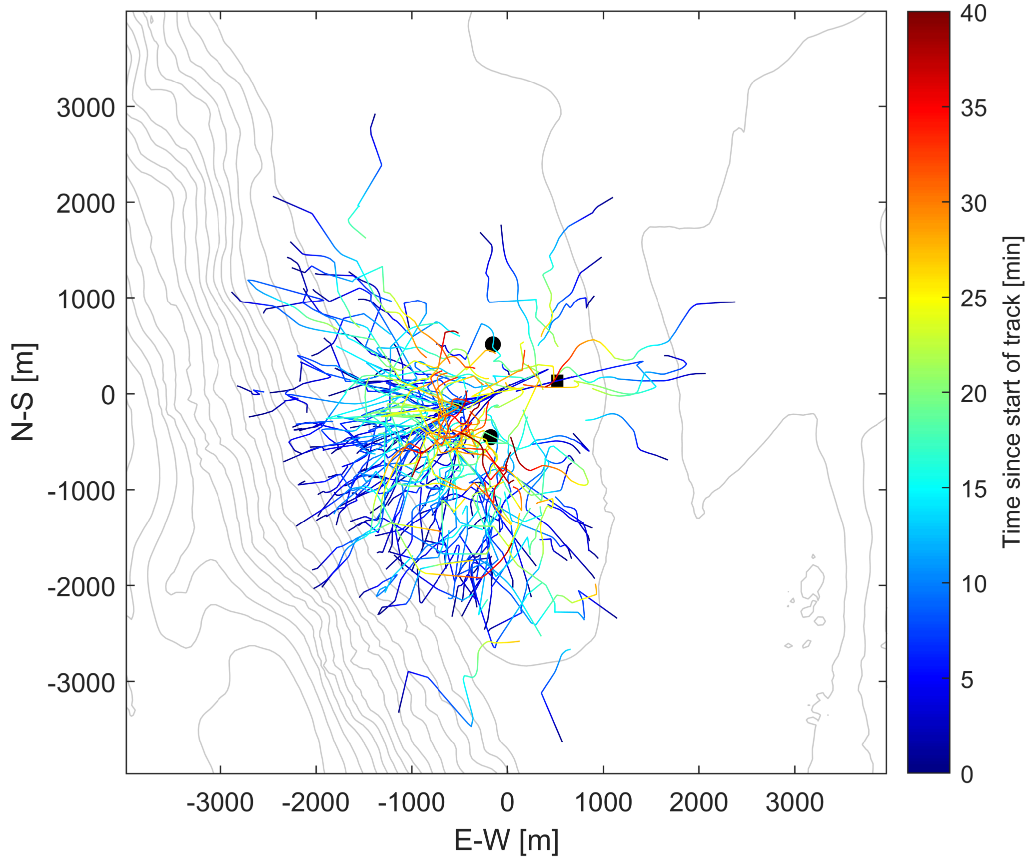


**Figure 2.2. All *Zc* tracks.** The lateral position of all 143 tracks reconstructed from passive acoustic localization using two four-channel arrays. The color represents the time since the first localized detection. Black squares represent the 4-channel arrays and black circles represent the single-channel instruments. Bathymetric data obtained from the Global Multi-Resolution Topography database [78]

## 2.4 Discussion

### 2.4.1 Preference for Slope in Foraging

Throughout the deployment, the whales demonstrated a clear preference for the western side of the arrays, potentially using the steep slope in their foraging strategies (Figure 2.2). It is

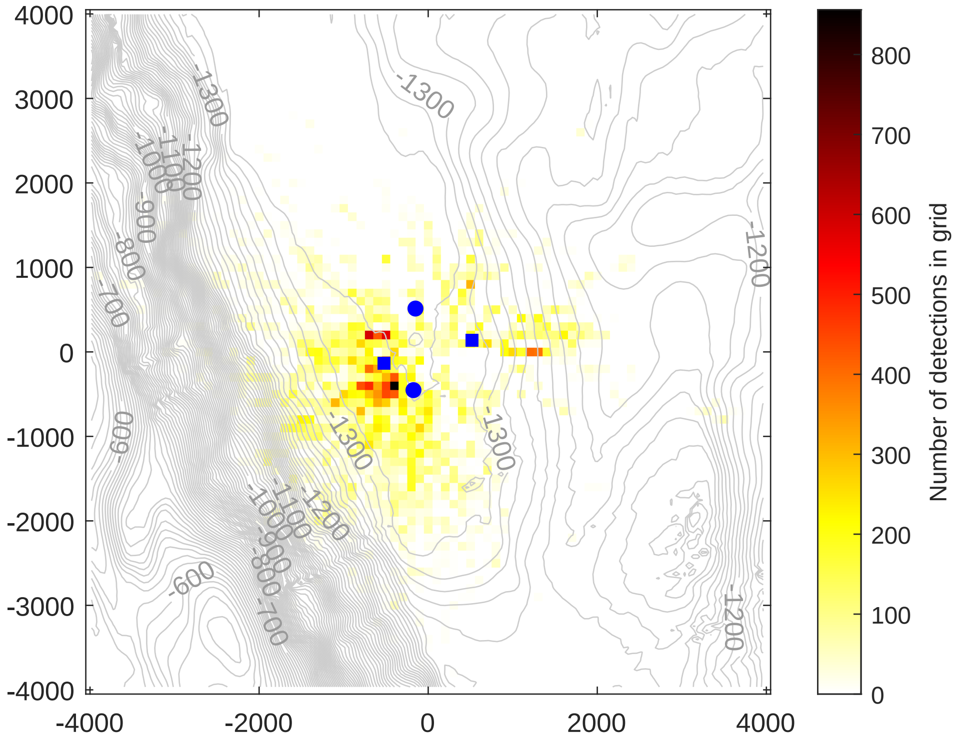


**Figure 2.3. Detection locations.** A heat map of 100x100 m grid locations in which an animal was localized at any depth. The instruments are plotted in blue.

important to note that the instrument geometry introduces some biases in the spatial distribution of obtainable tracks. The first bias is due to the fact that the South instrument was used to identify potential *Zc* encounters, causing animals that passed closer to the South instrument to have a higher likelihood of being detected and tracked. The second bias is due to click directionality – since a click is more likely to be detected by both four-channel instruments when the whale is facing both arrays, a bias is introduced when the whales are more aligned with the axis formed by both arrays. When histograms of the azimuths of all labeled detections on both 4-channel instruments are plotted, the majority of detections are slope-ward rather than towards the south instrument (Figure 2.4, top). By overlaying these histograms onto the map, it becomes clear that the detections on the East instrument demonstrate a bias towards the South instrument; however, the West instrument still shows a significantly higher presence towards the slope on the west despite the South instrument being to the south-east (Figure 2.4, bottom).

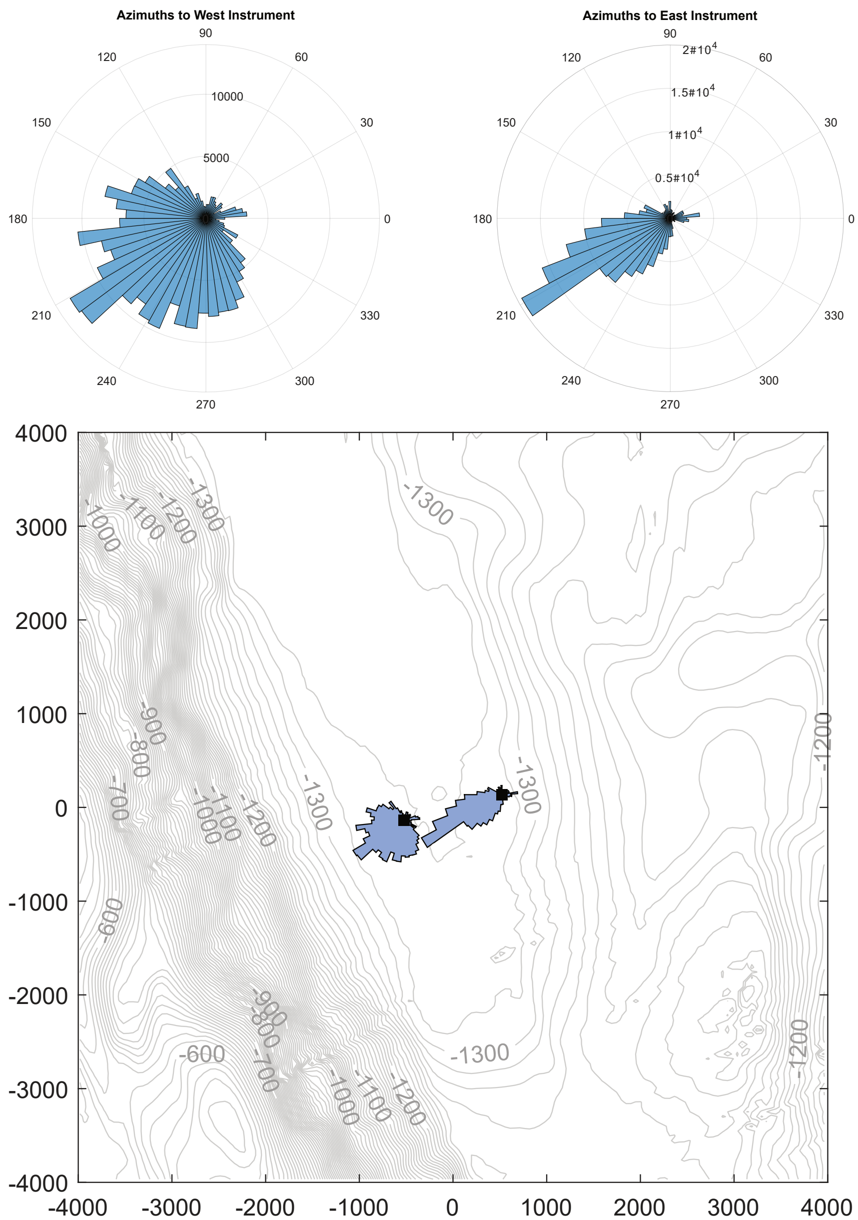


**Figure 2.4. Detection Angles.** TOP: Polar histograms of the estimated azimuths all detections retained on the West (left) and East (right) four-channel instruments after manual brushing using `brushDOA`. BOTTOM: The same polar histograms overlaid on the map, indicating a significantly higher detection rate of *Zc* towards the slope.

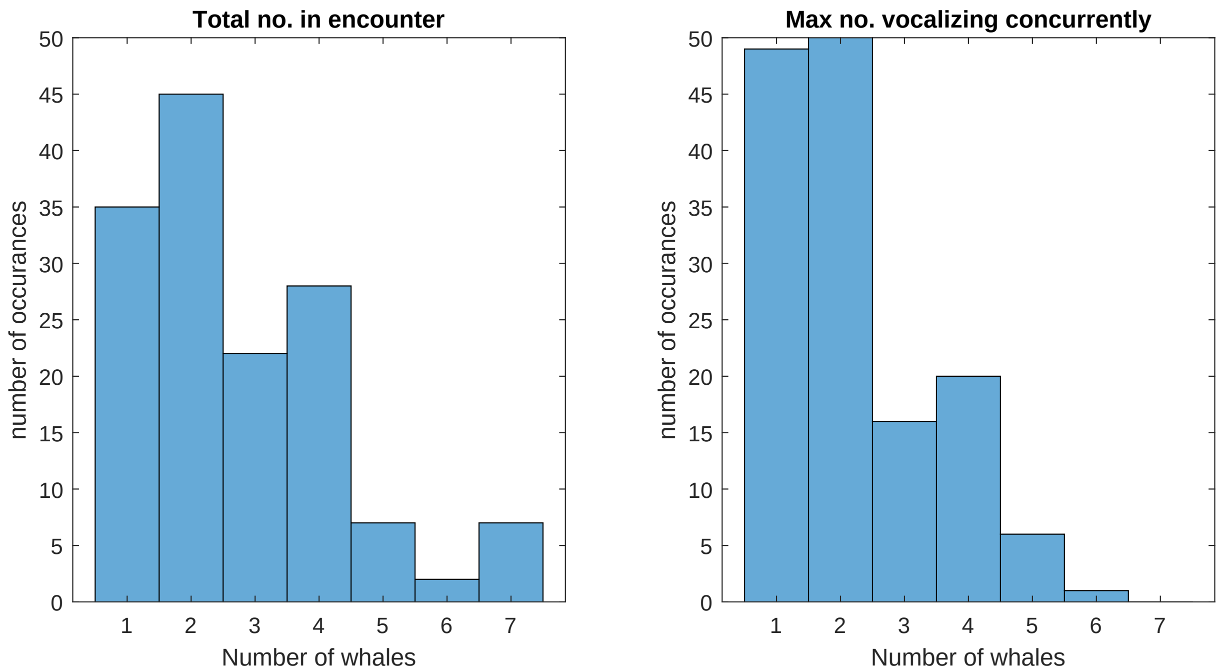


**Figure 2.5. Group Sizes.** Distributions of group sizes, counted both as the number of uniquely identified tracks within a 60-minute period (left) and the maximum number of animals vocalizing concurrently in a 60-minute period (right). Mean group sizes were $2.6 \pm 1.7$ and $2.1 \pm 1.3$ animals for each method respectively.

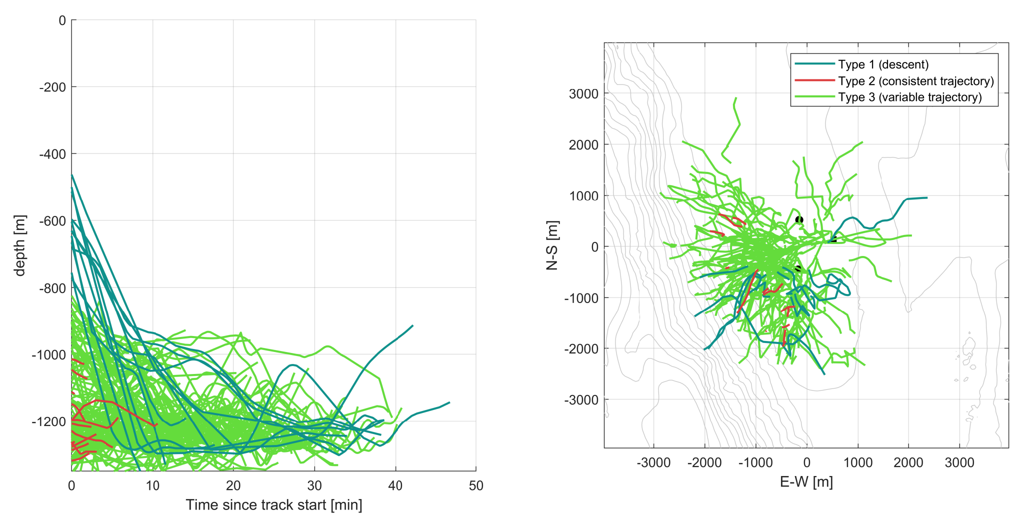


**Figure 2.6. Tracks by type.** Tracks as depth vs time (left) and lateral position (right) colored according to dive type.

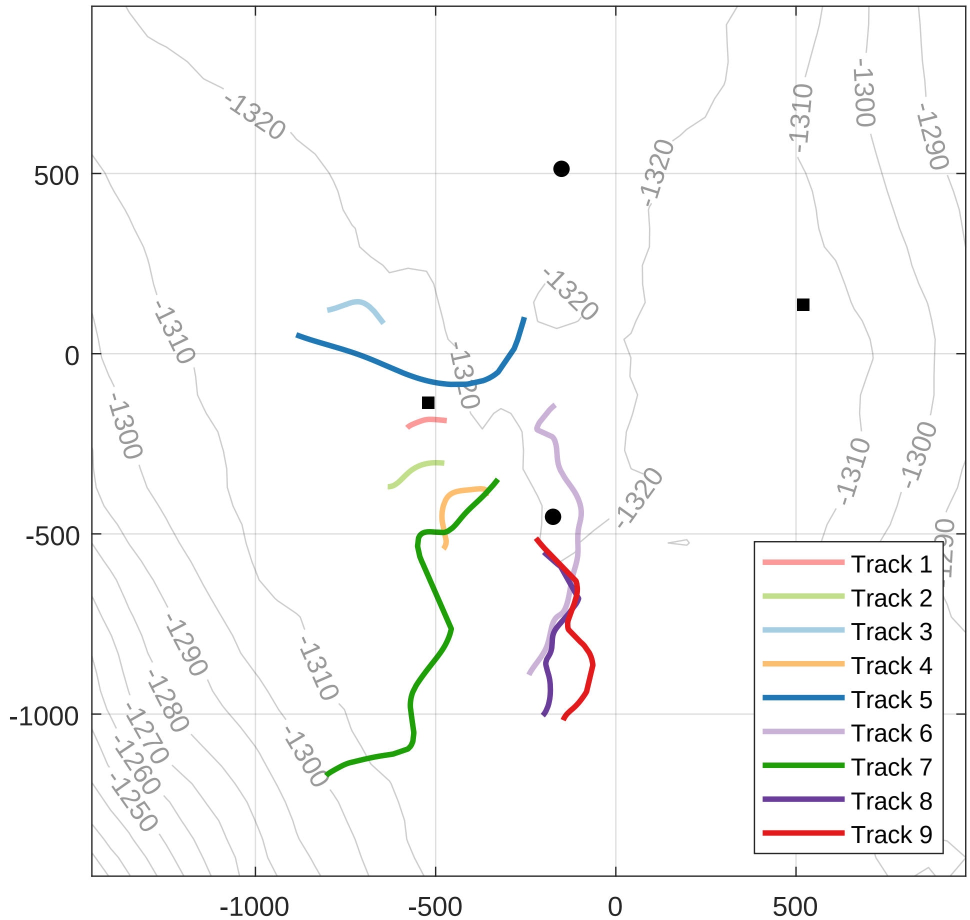


**Figure 2.7. Track segments for SL calculation.** Lateral positions of track segments used in source level calculations. An elevation of $-90°$ represents the whale being directly above the instrument, and $0°$ represents the whale being on the same horizontal plane as the instrument. The roll of the animal could not be estimated and is assumed to be $0°$.

### 2.4.2 Acoustic Diving behaviors

The low number and short durations of the type 2 (consistent trajectory) tracks most likely indicate their complete absence from the dataset. The few tracks of this type that were observed are more likely to be type 3 (variable trajectory) tracks that were too short to observe the spatial variability necessary to be categorized as such. The lack of type 2 tracks could have a number of explanations, some of which are outlined below.

- This site may have fallen within a suitable foraging ground making transiting behavior unnecessary.

- Due to bathymetric features, transiting whales still varied their trajectory enough to be categorized as type 3 tracks even if they weren't actively foraging.
- Transiting behavior happened primarily in a region of the map where detections were unlikely to be localized.

.

The array configuration likely prevented a significant number of initial descents (type 1 tracks) from being localized. Some encounters contained nearly linearly decreasing elevation angles indicative of the descent phase, but detections were only present on one of the four-channel instruments. We attempted to localize some of these dives using one four-channel and one single-channel instrument but found the depth estimates to be unreliable. Placing the four-channel instruments closer together could improve the number of localized dives. It would also likely be beneficial to have the arrays offset vertically by placing two four-channel volumetric arrays several hundred meters apart on the same mooring. This configuration presents some additional signal processing challenges to account for array rotation and tilt, but would likely improve depth resolution and the total number of trackable dives.

### 2.4.3 Click directionality

The source level estimates in Figures 2.8 and 2.10 confirm strong click-directionality. These figures indicate a range of angles between $\pm 30°$ where the highest intensity signal can be detected. This is likely due to limits in the precision of angle and animal position estimates rather than physiological features. This localization method is unable to capture small variations in animal positions, so it is unclear how much the animal's true heading varies compared to the estimated heading from the track reconstructions. The animal's roll cannot be measured and is assumed to be 0° (i.e. the whale is not tilting).

Source level estimates may also contain some inaccuracies due to the proximity to the instruments and hydrophone sensitivity; at the ranges between the animals and hydrophones, an on-axis click may likely have been clipped in the acoustic data. Tracks at greater ranges would not have been as subject to clipping but would have had less precision in angle and range estimates. This could be accounted for in future studies either by placing a hydrophone further from the four-channel arrays or by using hydrophones with higher clipping levels. Incorporating more track segments into future analyses of source levels with angle may help determine directionality and beampattern asymmetry with more precision.

### 2.4.4 Future Work

The configuration of instruments used in localization could be altered to improve localization tracking results. There is a tradeoff when localizing with two volumetric arrays: if the arrays are placed further apart many encounters become untrackable due to insufficient detections on both arrays, but if the instruments are placed closer together the region over which track reconstructions are possible is greatly reduced. The distance between the arrays (1076 m) in this deployment caused a significant number of encounters to be removed from the analysis. This is largely due to click-directionality since the animal must either be on-axis or in close proximity to be detected. This problem could be alleviated by deploying more volumetric arrays. For example, replacing the single-channel instruments with volumetric arrays in this deployment would have significantly increased the number of tracks localized and allowed for more straightforward evaluation of probability and range of detection needed for density estimates. In this specific case, single-channels were deployed because the 100 kHz sampling rate of the four-channels cannot capture the full bandwidth of a *Zc* echolocation click, making single-channels necessary for SL estimates and other acoustic analyses. However, improved CPU speeds have allowed for the development of 200 kHz sampling rates for four-channel HARPs.

Another potentially valuable configuration is two volumetric arrays deployed on a long-line mooring. Many of the *Zc* dives were only captured on one of the arrays, but placing both arrays in vertical alignment with a separation of 700-800 m would likely increase the number of simultaneous detections during the dive phase and also improve the precision of these localizations. Array tilt and rotation would add complications during the data processing, but by incorporating compass measurements and aligning azimuths of detection on both instruments, it is likely these factors would not add much uncertainty. While this configuration would reduce the horizontal range over which localizations were possible, it would be valuable for improving vertical resolution. The horizontal range could be improved by deploying multiple array moorings.

## 2.5 Conclusions

Passive acoustic localization provides several valuable insights into beaked whale diving and echolocation behavior. We reconstructed a total of 143 *Zc* tracks using TDOA localization on two four-channel volumetric arrays, ranging in duration from 2.1 to 46.8 minutes. 12 of these contained behavior consistent with the descent phase. The vast majority of tracks were present West of the arrays, where the bathymetric data indicated a steep slope. Since it is unlikely this slope preference was due to a bias in the localization algorithm or array configuration, it is most likely a preference exhibited by the animals themselves, possibly a strategy to aid in foraging.

*Zc* have a highly directional echolocation click, which has a significant effect on ranges of detection and acoustic density estimates. Some previous studies have attempted to characterize the beam pattern of a click by estimating the SL as a function of the angle of the animal in relation to a receiver [37, 109]. Both of these studies estimated the highest intensity signal to arrive at an angle other than 0° (*i.e.* directly in front of the animal), which may be the result of *Zc* skull asymmetry [23]. However, by analyzing 9 track segments ideal for beam angle and source level estimation, we found a range of angles between ±30° at which the highest intensity signal may be found. This range is likely due to precision in track reconstructions rather than a physiological feature, and further research is required to more adequately characterize the beam pattern.

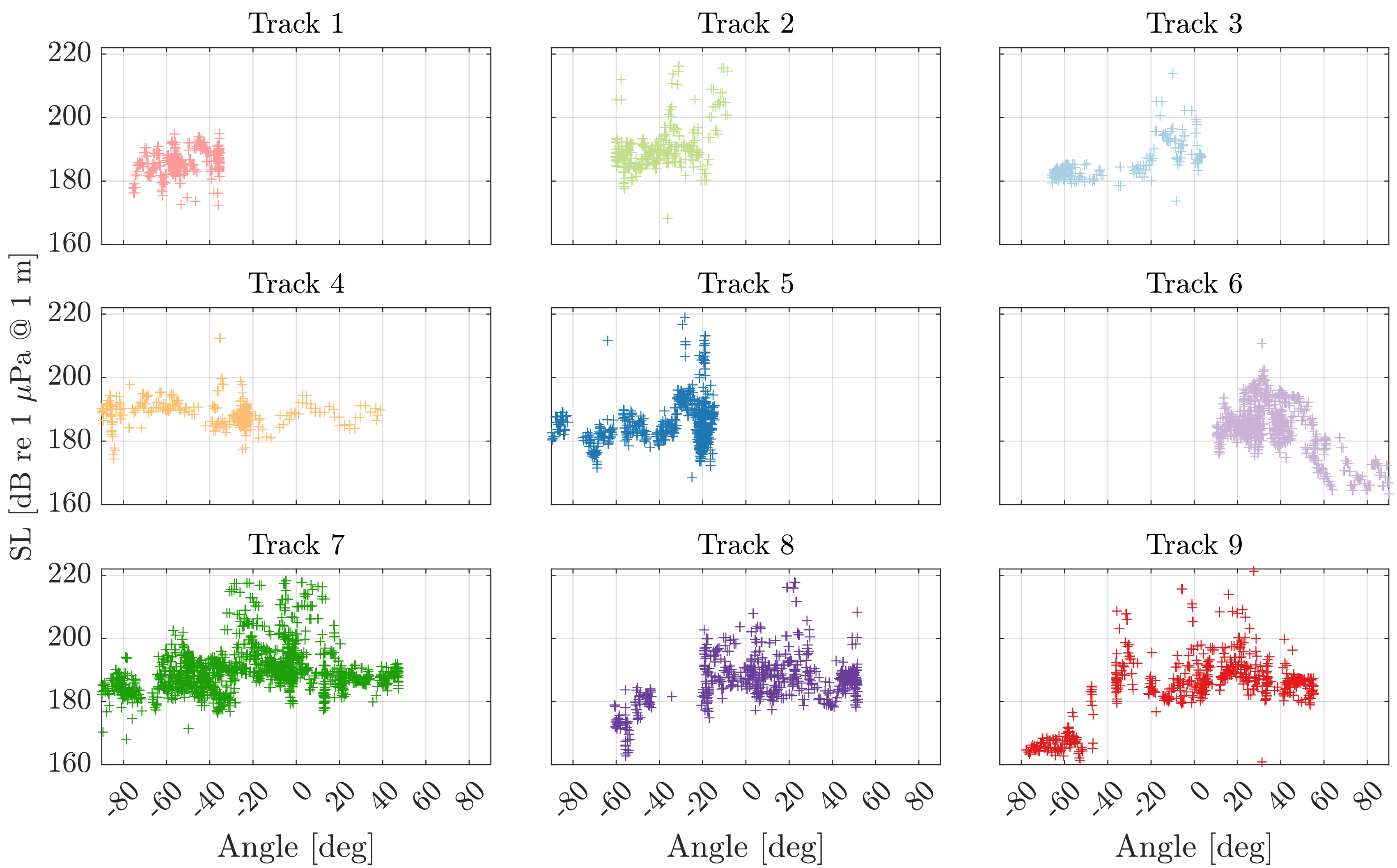


**Figure 2.8. Source Level vs. Beam Angle**. Source level vs beam angle of each track segment. The beam angles represent the heading of the whale in relation to the hydrophone, where a hydrophone directly in front of the whale would measure the SL at 0°, and a hydrophone on the whale's right would measure the +90° SL, etc. The icons represent the instrument used for SL estimation, where "x" represents detections on the North instrument and "+" represents detections on the South instrument. The marker colors correspond to the track colors in Figure 2.7.

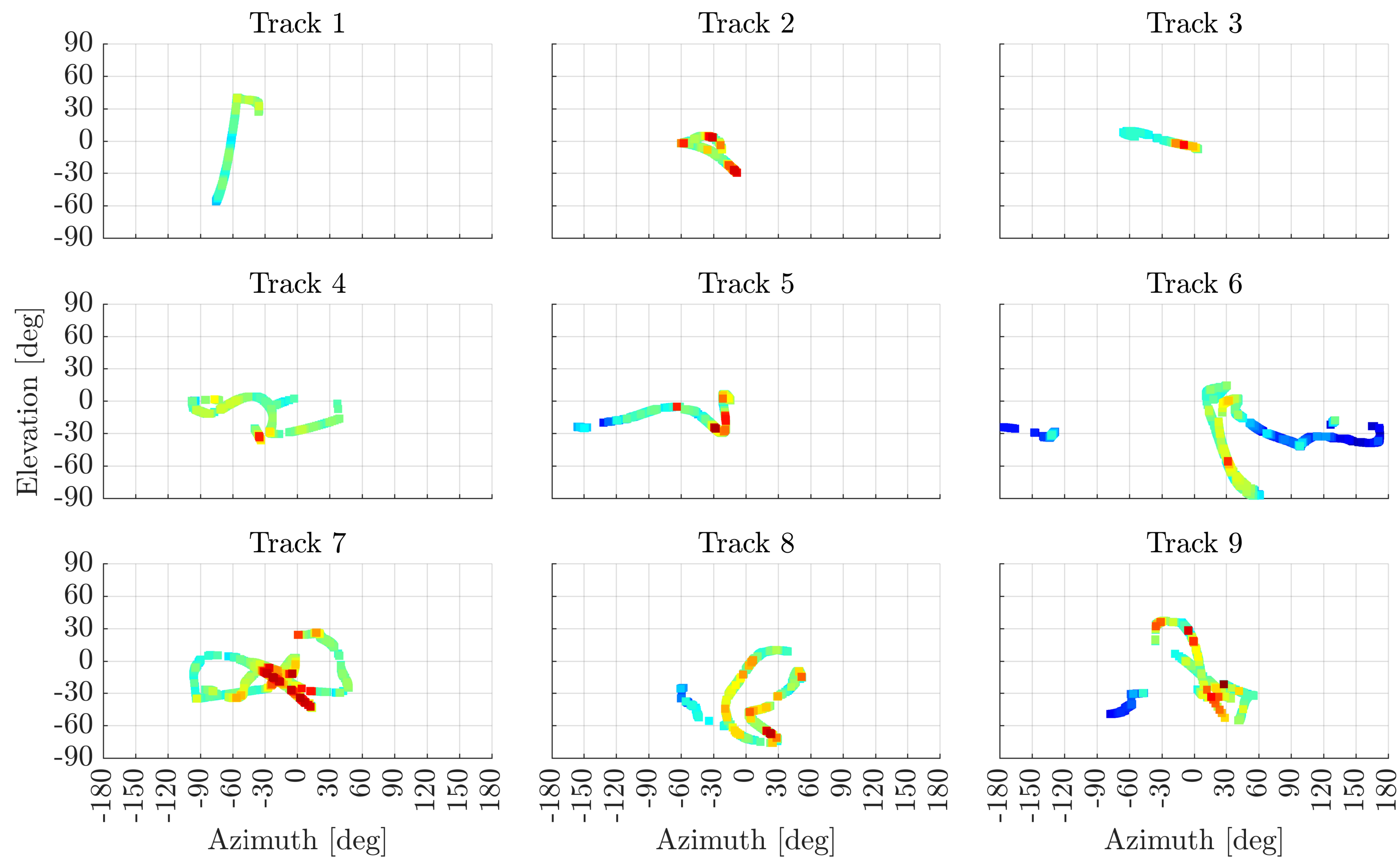


**Figure 2.9. Source Level vs. 3-D Beam Angle of each track segments**. The source level vs. beam angle in 3-D estimated from each track in Figure 2.8. Figures contain the same data as in Fig. 2.8, but three-dimensional orientation of the whales have been estimated.

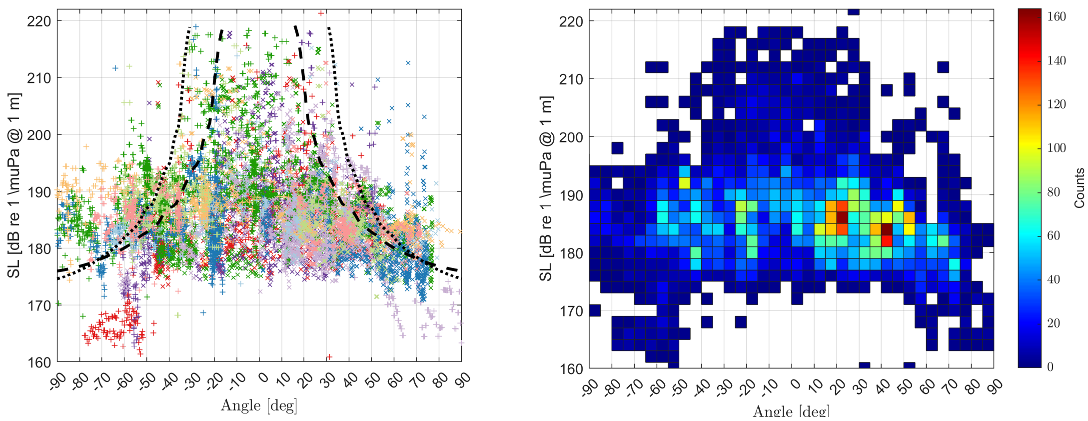


**Figure 2.10. Source Level vs. Beam Angle of all track segments**. The estimated source level vs. beam angle of all detections in Figure 2.8 combined onto one scatter plot (Left) and as a two-dimensional histogram (right). On the left plot, the piston model described in Eq. 2.1 is plotted as the black line, where the negative and positive angles of the piston model have been shifted by $+30°$ and $-30°$, respectively. Axes, icons, and colors are the same as described in 2.8. The dashed line represents the piston model used by Zimmer, *et al.*[109] with a radius of 20 cm and an offset of $\pm 15°$. The dotted lines show the piston model used by Gassmann *et al.*[37] with a radius of 25 cm and an offset of $\pm 30°$. In both piston models, the positive angles have been shifted so the peak is at +15 or +30 degrees and the negative angles have been shifted so the peak is at -15 or -30 degrees.

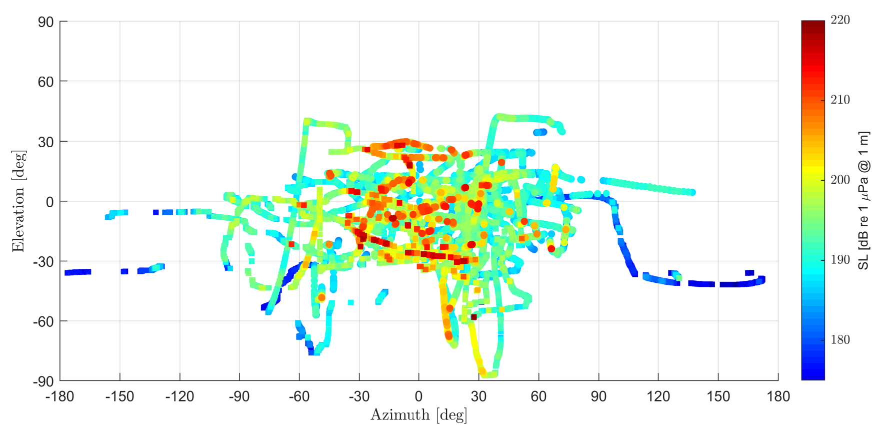


**Figure 2.11. Source Level vs. 3-D Beam Angle of all track segments combined**. The source level vs. beam angle in 3-D estimated from all tracks in Figure 2.8 displayed on the same axes.

# Chapter 3

# Echoes Across the Gulf: Challenges of long-range localization of broadband sources in the Gulf of Mexico

## 3.1 Introduction

Time-difference of arrival (TDOA) localization, in its simplest form, assumes that a signal propagates in a direct path and at a constant velocity between the source and receivers. This simplification is sufficient for ocean acoustic localization problems at close ranges and when sound speeds are relatively constant. At greater distances, the complexity of the environment must be accounted for to accurately estimate a source location from passive acoustic recordings. Surface reflections, refraction in the water column due to sound speed gradients, and interactions with sediment and bathymetry all add complications to using long-range signals in TDOA localization problems [49, 100]. To account for these complications, a thorough understanding of how ocean and bathymetric properties affect acoustic travel times is required.

### 3.1.1 Airguns

Seismic surveys are regularly performed in the Gulf of Mexico (GOM) to identify potential oil deposits beneath the ocean floor. These surveys use airguns, a high-intensity, impulse-like source to make observations of the reflectivity of different layers in the seafloor. A single airgun injects a high-pressure air bubble into the water, which rapidly expands and collapses causing an acoustic pressure wave to radiate outward. This process creates an initial pulse and several subsequent pulses at decreasing amplitudes as the bubble volume repeatedly expands and collapses [79]. An ideal seismic source is a single impulse to avoid complications in separating reflections from the various pulses. Various methods have been implemented to reduce the bubble ringing. These include: injecting a second burst of bubbles from the airgun to distort the structure of the ringing [67]; using a screen to destroy the bubble immediately after the first bubble collapse [54]; and firing arrays of airguns with varying bubble volumes simultaneously so the ringing pulses occur at differing intervals, thereby allowing the initial pulses to be amplified by summing without substantially amplifying the ringing pulses [101, 30].

In offshore environments, the high intensity of airgun noise can have a significant impact on ocean soundscapes extending hundreds of kilometers [45]. The soundscape of the Gulf of Mexico is dominated by the noise of airguns at frequencies $< 100$ Hz with levels $> 90$ dB re $1\mu\text{Pa}^2/\text{Hz}$ at $< 40$ Hz [104].

### 3.1.2 Propagation modeling

There is widespread interest in estimating the propagation of an airgun array at long ranges to assess the impacts of seismic surveys on local marine fauna. Often, transmission loss is assumed to be spherical in deep water and at close ranges, and cylindrical in shallow water and at long ranges. However, sound speed profiles, bathymetry, and sediment properties all have a significant impact on the transmission loss with range. Numerous studies and assessments have instead used propagation models to estimate the transmission loss of airgun signals across long ranges. Often, these models are implemented using freely available software that runs on 2-dimensional range slices, like RAM Parabolic Equation (PE) modeling [21, 28, 42, 60, 59, 61, 93]. Additionally, the complexity of the Gulf of Mexico's current system and bathymetry likely causes significant 3-dimensional propagation effects that cannot be captured by 2-dimensional propagation models [57].

DeRuiter *et al.* used both the ray tracing software RAY [15] and PE modeling software

RAM [21] to model travel times of airgun pulses in the Gulf of Mexico and compared the results to measurements obtained by hydrophones in DTAGs attached to two sperm whales [28]. Ray tracing produces straightforward travel time estimates by integrating along the ray path. PE modeling computes a complex frequency-domain estimate of the wave field and must be converted to a time-domain signal to estimate travel times. DeRuiter *et al.*used Fourier pulse synthesis, where the 2-D PE propagation model output is multiplied by the frequency spectrum of a source signal before the inverse Fourier transform is computed [49]. While they found good agreement between the two model types, they noted some significant mismatch between the modeled and measured travel times. The mismatch was attributed to imprecise model parameters, like inaccurate bathymetry and sound speed profile estimates and not accounting for source directionality [28].

The 2-D approximation is convenient and widely used in ocean acoustic propagation modeling as it greatly reduces computation time. While for many applications and environments this approximation suffices, there are numerous scenarios in which 3-D should not be ignored [18, 17, 80, 98]. Many seismic surveys are performed on continental shelves, where sloped bathymetry causes effects akin to acoustic propagation in a wedge [18, 43, 52]. In more recent years, 3-D PE modeling was developed and applied to airgun propagation in the Gulf of Mexico [57, 58]. The study modeled a 50 Hz signal on a $\approx 30$ km$^2$ section of the Gulf using both 3-D PE and a series of 2-D PE range slices to compare the effects of out-of-the-vertical-plane refections. They found differences of $> 10$ dB in portions of the modeled region where 3-D effects were most prominent [57]. We found no papers using 3-D propagation models to estimate the travel times of airgun signals.

### 3.1.3 This contribution

Here, we analyzed a 110-minute period on January 2, 2015 where five ships were performing a coordinated seismic survey in the GOM. Time-difference of arrival localization of the airgun sounds recorded on five widely spaced hydrophones was used to both estimate the ship locations and determine five average sound speeds between the airguns and each of the five hydrophones. We used both ray trace and PE 2-D propagation models to estimate the travel times between one ship and receiver. The modeled data are compared to the real data. Using a series of simplified 2-D and 3-D ray trace models we provide potential explanations for patterns seen in real data and for the mismatch between data and model outputs.

## 3.2 Methods

The acoustic data presented here were collected from five locations in the northern and eastern GOM instrumented with High-frequency Acoustic Recording Packages (Fig. 3.1.). For these deployments, the instrumentation package was located at or near the seafloor with the hydrophone sensor tethered to the instrument and buoyed approximately 10 m above the seafloor. All acoustic data were converted to sound pressure levels based on hydrophone and electronic system calibrations. Three of the recording sites (Mississippi Canyon - MC, Green Canyon - GC, and Dry Tortugas - DT) were located in deepwater (at 980, 1100, and 1300 m respectively). Two sites (Main Pass - MP and DeSoto Canyon - DC) were located on the continental shelf (at 86, and 268 m respectively).

A 110-minute period on January 2, 2015, from 02:40 to 04:30 UTC was selected for analysis due to its significant airgun presence. Publicly available AIS data were used to identify the MMSI ships with airgun-towing capacity in the area during the analysis period. Five of these ships were performing synchronized transects consistent with seismic surveying. The latitudinal and longitudinal positions of the ships during the 110-minute analysis period are shown in (3.2).

### 3.2.1 Associating received signals to sources

Software was developed to separate sequences of airgun pulses into those from a single source ship. The code is applied to *wav* format audio files from a single acoustic recorder. The code starts by running a peak detector with a specified threshold on a short segment of data (typically 5 minutes). Within the 5-minute window typically 10-30 airgun peaks are detected.

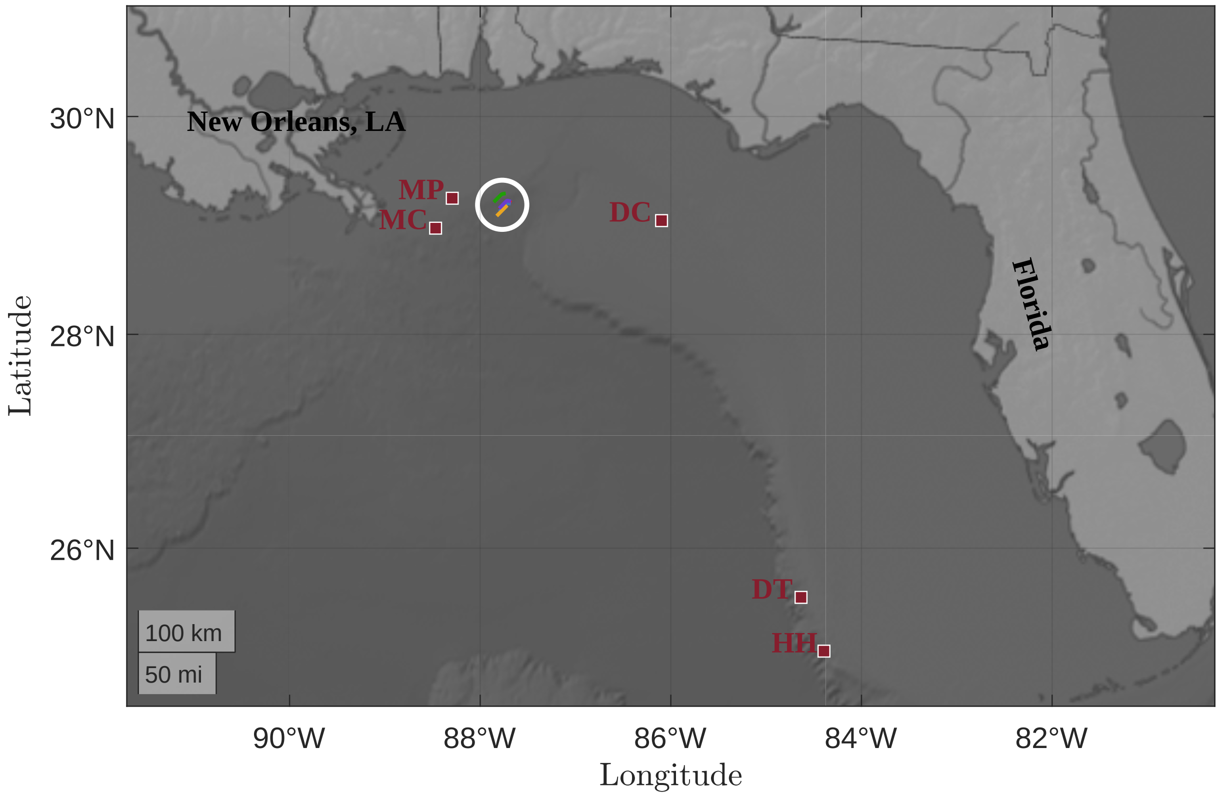


**Figure 3.1. Map of ship locations and sites.** All HARP locations used for TDOA localization of airgun arrivals are plotted as red and white squares. The ship locations from the AIS data during the study period are shown as the colored lines inside the white circle. A more zoomed-in view can be seen in Fig. 3.2

The cross-covariances of the detected peaks are then examined, and groups of peaks with both high covariance and approximately (+/- 1 s) consistent inter-pulse-interval are designated as potentially originating from the same source. The 5-minute time series is then displayed with each arrival marked in a color associated with its presumed source. Manual editing is allowed to correct for errors in identification and the process is repeated on another data segment, advanced by only one-half the data window to allow the already identified pulses to act as a guide for successive identifications. In this way, a process of discovery can occur to recognize the number of separate sources represented in the data. It is presumed that differences in both the source signature and the propagation path result in differences in the received waveform.

Once separated into individual sources, additional steps are involved in fine-scale tem-

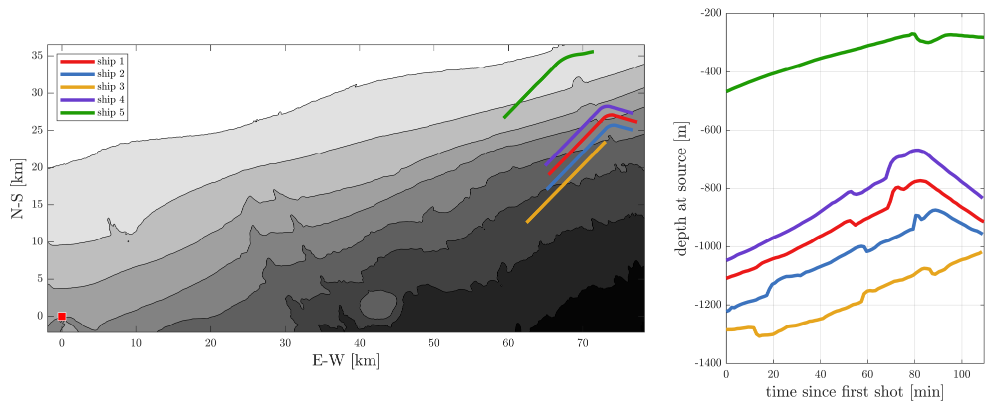


**Figure 3.2. Map of ship locations and site MC, and plot of depths at ship locations.**
LEFT: A map of the ship locations (color lines, indicated by the legend in the top left) relative to site MC (red square in the bottom left).
RIGHT: The corresponding depths at each location (right). The time axis on the depths vs time plot is in minutes since the first received time for each ship. The colors correspond to the same ships on the left plot.

poral alignment of pulse sequences, and the ability to time-align sequences from two or more sources. Timing of the airgun shot firing is not regular in time at the source vessel but is instead constantly adjusted to adapt to the speed of the source vessel (producing a consistent spacing over ground) and also adjusted to deconflict the arrival of each source array at the various receivers. This results in an irregular shot interval for each airgun array source. Once the details of the shot timing have been determined for a single receiver, they become useful to find the shots from that source same vessel on other receivers, greatly facilitating subsequent analysis.

### 3.2.2 Environmental characterization

A range of environmental parameters are needed to model the interaction of sound with the marine environment. Primarily, it is important to consider the sound speed and its variation with depth. For this work we obtained sound speed profile estimates from the MIT Generalized Circulation Model (MITgcm) [2], which contain daily estimates of temperature, salinity, and depth at approximately 5 km lateral resolution. These values were converted to sound speed estimates using Mackenzie [62], since it uses depth as an input rather than pressure and the

MITgcm estimates specify estimates of salinity and pressure with depth. Bathymetric data for the Gulf of Mexico were obtained from the Global Multi-Resolution Topography Data Synthesis (www.gmrt.org), selected for latitudes 24-30 N and longitudes 92-80 W, with a resolution of 0.0005 degrees for both dimensions. A sediment profile was appended beneath the bathymetric data, based on core measurements from OPD Leg 308 core 1324 ( see Figure 38 of Flemings, *et al.* [34]) for the top 200 m beneath the seafloor, and assuming a linear sound speed gradient between 200 - 1000 m to arrive at a speed of 2000 m/s at 1000 m below the seafloor. Basement rocks are assumed to occur at 1000 m below the seafloor and are assigned a sound speed of 3000 m/s at the top of an infinite half-space. In practice, the sound paths of interest are found to be reflections between the sea-surface and the water-sediment interface, or rays that turn within the upper portion of the sediment. Little or no long-range sound propagation is found to interact with the basement rocks.

All ranges between source and receiver and along the bathymetric profiles were calculated using the WGS-84 reference ellipsoid as implemented by the MATLAB function *DISTANCE* which computes geodesic arc length and azimuth assuming that the points lie on the reference ellipsoid.

### 3.2.3 Propagation modeling between sources and receivers

We used two methods to model underwater acoustic propagation between source and receiver locations: ray trace and parabolic equation.

#### Ray tracing

Ray trace models were generated for a variety of simplified environments by way of demonstrating principles of acoustics necessary for interpreting the data. These models were generated using ZRAY, a MATLAB-based ocean acoustic ray-tracing package adapted from RAY [15, 39]. To demonstrate the effect of 3-D propagation in a wedge, Bellhop 3-D was run for a perfect wedge environment [70].

In ray theory, the arrival patterns in an environment can be characterized using the horizontal velocities of various paths of propagation, referred to herein as the group velocity $v_{g,m}$:

$$v_{g,m} = \frac{T_m}{r}, \tag{3.1}$$

where $T_m$ is the travel time of the $m^{\text{th}}$ ray and $r$ represents the range between the source and receiver. We can also define the phase velocity, $v_{p,m}$, given as the additional travel time required for a particular ray path to travel to the receiver from two adjacent source positions:

$$v_{p,m} = \frac{\Delta T_m}{\Delta r}, \tag{3.2}$$

where $\Delta T_m = T_m(r) - T_m(r-1)$ is the additional travel time of the $m^{\text{th}}$ arrival and $\Delta r$ is the change in range due to the moving source. In the simplest environment, where the sound speed is constant and both the surface and bottom are perfectly reflecting, the group and phase speeds are a function of the launch angle ($\theta$) and sound speed ($c$): $v_{g,m} = c\cos\theta$, and $v_{p,m} = \frac{c}{\cos\theta}$. This also gives the relationship $c = \sqrt{v_{g,m}v_{p,m}}$ for all $m$ rays. $v_{g,m}$ can be easily obtained from a ray trace model using the calculated travel time and range for each ray. To calculate $v_{p,m}$, a second model is calculated with the source position moved by a small amount (100 m in these examples). Ray paths between the two models can be matched by identifying the ray in the second model which has the smallest difference in launch angle from a given ray in the first model and also has the same number of surface and bottom reflections or turning points. The difference in travel time of the matching rays is then used in Eq. 3.2 to calculate $v_{p,m}$ (see Fig. 3.3 and Fig. 3.4). In cases where rays are refracted away from the surface or bottom, the points where the ray reaches a local maximum or minimum depth (the upper and lower turning points) are used to identify matching rays between two source positions.

Some complexity can be added to the models and the phase and group speeds can still be calculated by matching rays between two models, as long as the models are similar enough

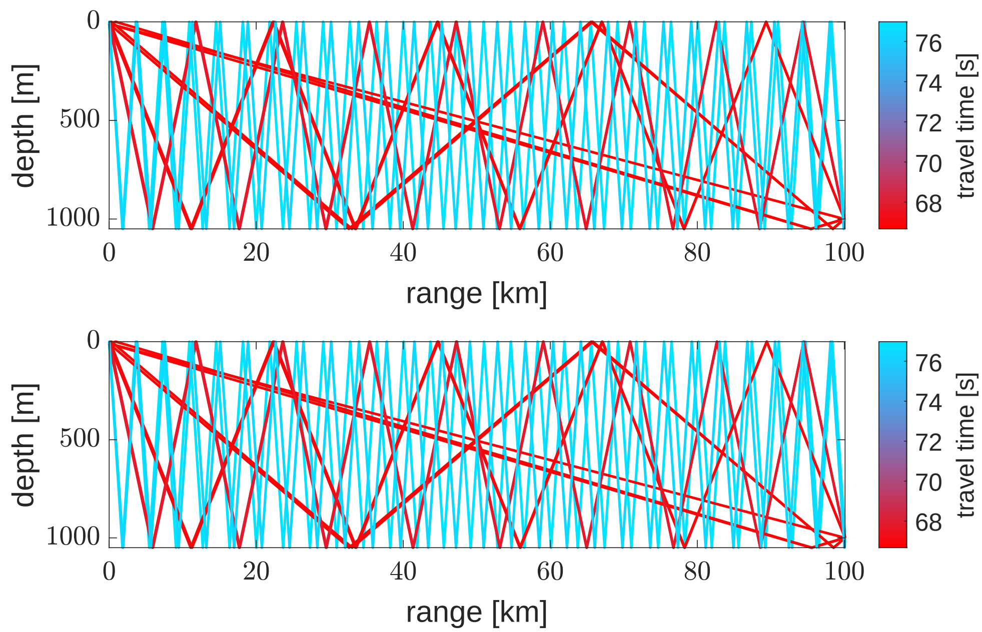


**Figure 3.3. Isovelocity ray plots.** A selection of eigenrays for an isovelocity environment with perfectly reflecting boundaries. The top plot represents a range between source and receiver of 100 km and the bottom plot represents a range of 100.1 km. The source is at a depth of 10 m, the receiver at 1000 m, and the rigid bottom is 1050 m.

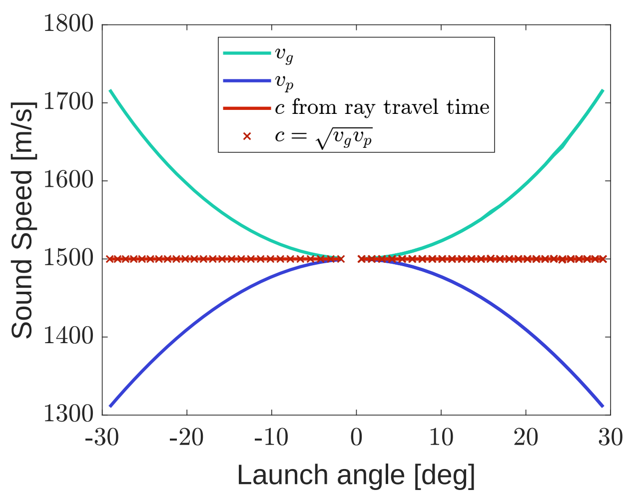


**Figure 3.4. Group and phase speeds for an isovelocity environment.** By matching rays between the two ray trace models in Fig. 3.3, the phase and group speeds were calculated for the various rays in the isovelocity environment. The x-axis represents the angle from the horizontal at which the ray was launched.

to produce matching ray paths. The models were run using a Munk sound speed profile, which is often used as an approximation of ocean sound speeds with depth, and a linearly increasing sound speed beneath the Munk profile as an approximation of a sediment layer rather than a rigid bottom (Fig. 3.5). The eigenrays calculated using this environment for both a range of 100 and 100.1 km (Fig. 3.6). The ray plots at both source were ranges exhibit a high level of similarity, allowing us to calculate the phase and group speeds of each ray by matching rays with the same number of bounces and similar launch angles (Fig. 3.7). Since rays launched at steeper angles penetrate deeper into the sediment layer, the average instantaneous velocity $c$ for the rays increases with the absolute value of the launch angles. Despite this, the relationship of $c = \sqrt{v_g v_p}$ still holds, where $c$ now represents the average velocity along the ray path rather than a constant water velocity.

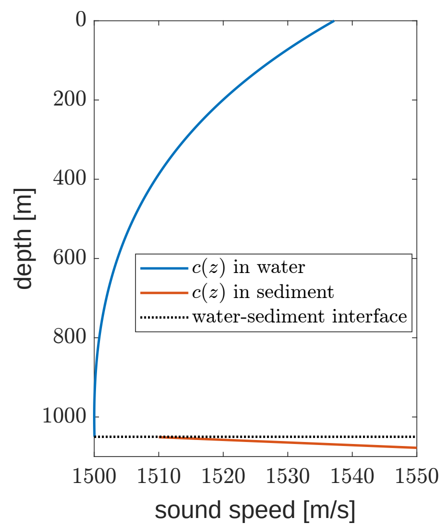


**Figure 3.5. Munk sound speed profile with sediment layer.** The sound speed with depth, $c(z)$, of a Munk sound speed profile with an upward refracting sediment layer. The sediment layer is linearly increasing from 1550 m/s at 1050 m depth to 3000 m/s at 2050 m depth.

When the environment has a slope, however, the relationship between the phase and group speeds begins to change, and the average instantaneous speed can no longer be estimated using $c = \sqrt{v_g v_p}$. Fig. 3.8 demonstrates the effect of a sloped bottom on a ray, whereupon each reflection the ray's trajectory becomes closer to horizontal. When the bottom slopes in the other direction, it has the opposite effect and the rays become more vertical. In the ray paths shown in Fig. 3.9, the slope is much more subtle and the effect is smaller, but the slope still causes

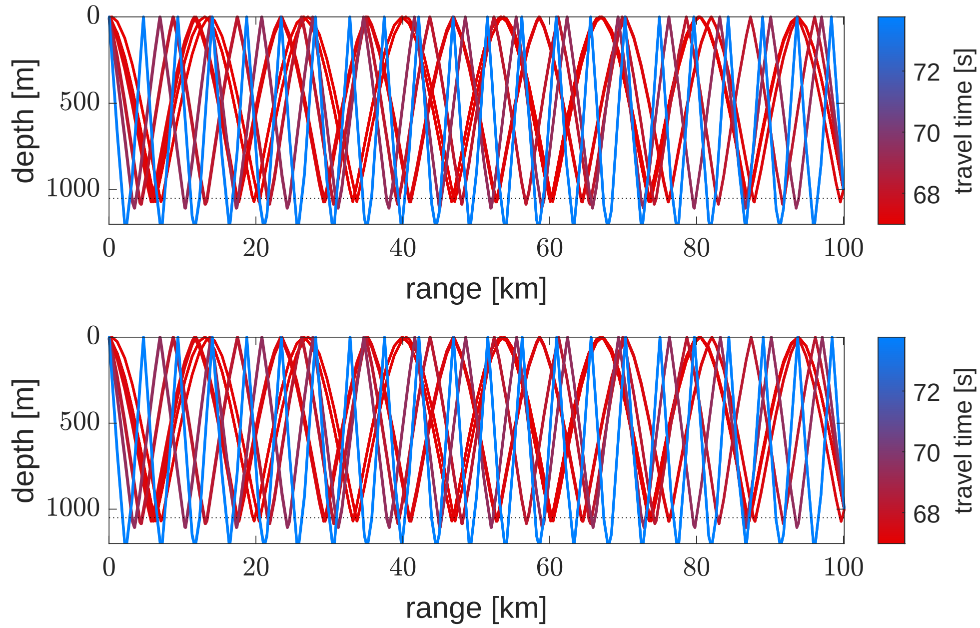


**Figure 3.6. Ray plot for Munk SSP with sediment layer.** A selection of eigenrays for an environment with depth-dependent sound speed and a refracting sediment layer, shown in Fig. 3.5. The top plot represents a range between source and receiver of 100 km and the bottom plot represents a range of 100.1 km. The source is at a depth of 10 m, the receiver at 1000 m, and the sediment layer is shown as the black dotted line.

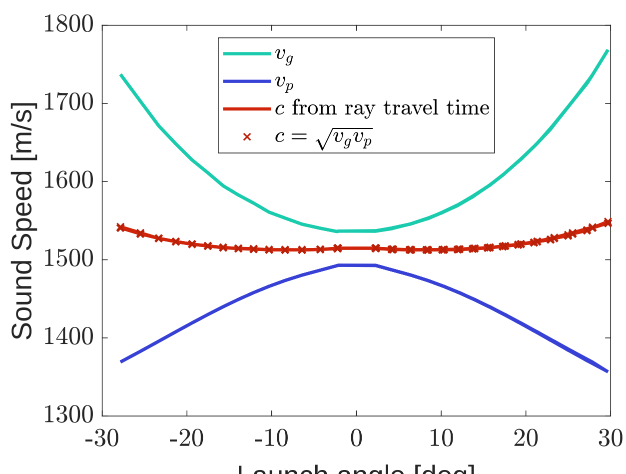


**Figure 3.7. Group and phase speeds for a Munk SSP with sediment layer.** By matching rays between the two ray trace models in Fig. 3.6, the phase and group speeds were calculated for the various rays. The x-axis represents the angle from the horizontal at which the ray was launched.

the phase speeds and group speeds to diverge at different rates (Fig. 3.10). In this example, the estimated water velocity is increasingly underestimating the actual water velocity using

$c = \sqrt{v_g v_p}$ since the rays are more horizontal at the source than at the receiver, and therefore have a lower phase speed than a flat bottom would produce. (Note that since in both the models and the real data, we move the source rather than the receiver to estimate phase speeds, we are in actuality measuring the phase speed at the source). Fig. 3.11 demonstrates the inverse, when the depth at the receiver is greater than at the source. Fig. 3.12 shows group and phase speeds calculated from a range of sloped bathymetries.

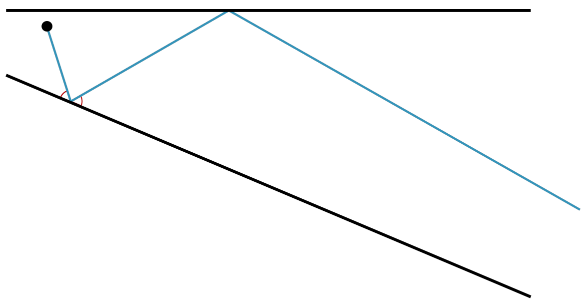

**Figure 3.8. A ray reflecting off a sloped bottom.** An example of a ray's trajectory becoming more horizontal, and therefore its phase speed decreasing, as it reflects off of a sloped bathymetry.

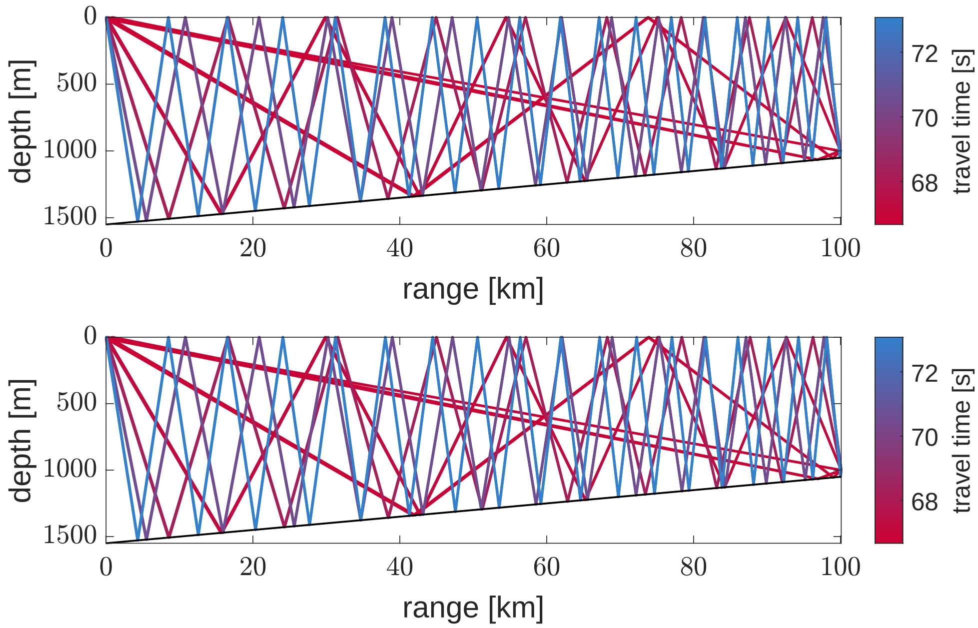


**Figure 3.9. Ray plot for a sloped bathymetry.** A selection of eigenrays for an environment with sloped rigid bathymetry, and constant sound speed. The top plot represents a range between source and receiver of 100 km and the bottom plot represents a range of 100.1 km. The source is at a depth of 10 m, the receiver at 1000 m, and the bathymetry is shown as the black line.

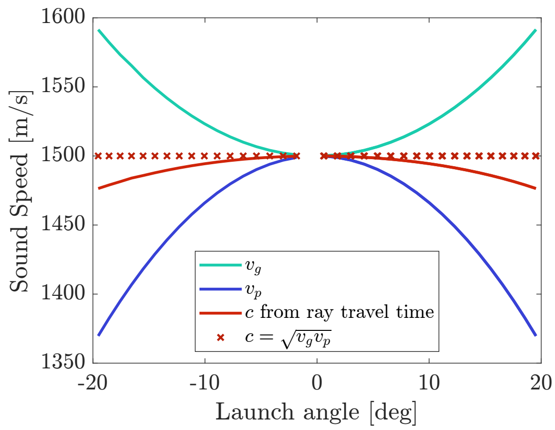


**Figure 3.10. Group and phase speeds for an upward-sloped bathymetry.** The phase and group speed estimates for ray trace models with a slope of $-5 \times 10^{-3}$ degrees.

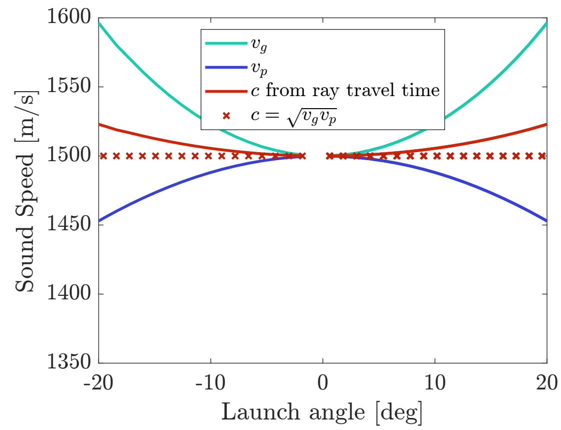


**Figure 3.11. Group and phase speeds for a downward-sloped bathymetry.** The phase and group speed estimates for ray trace models with a slope of $5 \times 10^{-3}$ degrees.

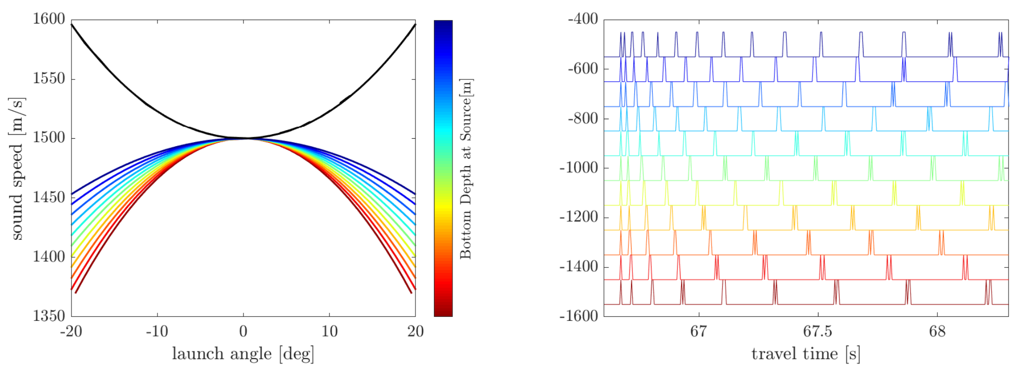


**Figure 3.12. Dispersion patterns for various sloped bathymetries (isovelocity and perfectly reflecting boundaries).**
LEFT: The phase and group speed estimates for ray trace models with sloped bathymetries. The depth at the receiver was fixed at 1050 m and the depth at the source ranged from 550 to 1550 m. The phase speed (black line) is always the same since the x-axis of the plot are the ray launch angles from the source and the phase speed is calculated at the source.
RIGHT: A synthetic waterfall plot of the arrivals for the various sloped bathymetries. As the source moves to shallower water, the various rays arrive in closer temporal proximity.

Ray matching between models becomes more difficult as models get more complex, particularly when range-dependent bathymetry is added. Small changes in the launch angle can lead to significantly different ray paths when the bathymetry is rough. Group speeds can still be coarsely estimated using ray travel times. However, phase speeds cannot be estimated by ray matching since the number of surface and bottom bounces/turning points does not necessarily indicate a similar ray path. For ray models using more realistic environments, only group speeds are reported.

In the previous models, the environments are run on a 2-D range slice, and any 3-D propagation effects are ignored. Fig. 3.13 shows that when rays are launched in a sloped bathymetry, 3-D effects cannot be ignored. In the figure, rays that are launched upslope eventually reflect back downslope. Every time a ray reflects off the seafloor, its azimuth angle shifts slightly more down-slope. The effect is that the rays appear to curve as they enter shallow water. The amount of curvature depends on both the azimuth and inclination of the launched ray, as more vertically launched rays will have more bottom reflections and undergo more downslope curving.

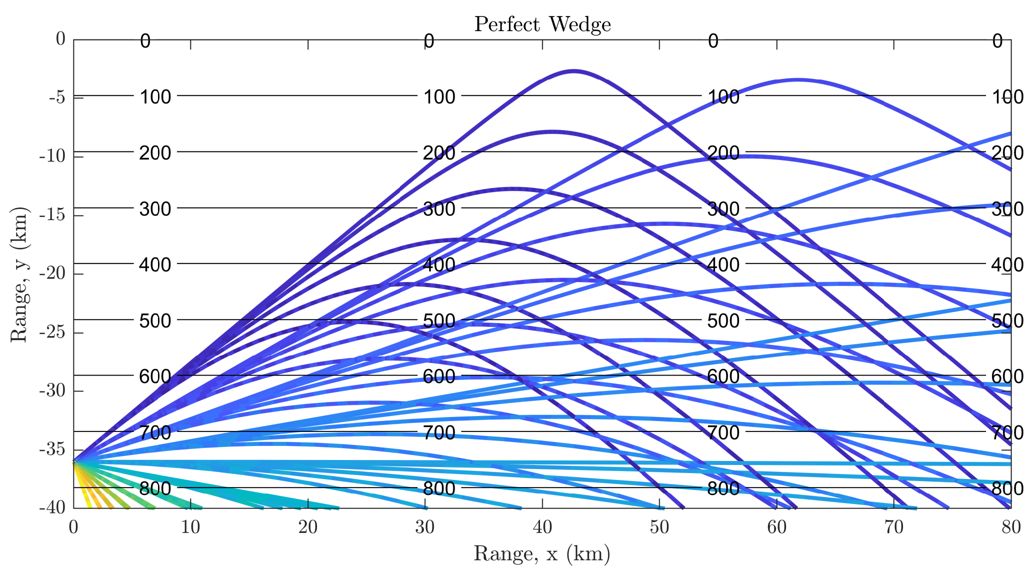


**Figure 3.13. 3-D rays in a wedge.** An example of the ray patterns in a wedge-shaped ocean run in Bellhop 3D [70]. The surface and bottom were modeled as perfectly reflecting and the water sound speed was a constant 1500 m/s. The horizontal contour lines show the depth changing in the y-direction. The coloring of the rays is related to the launch angle and was applied to allow more visual separation of the various ray paths.

### Parabolic Equation Modeling

Parabolic Equation (PE) models were first applied to ocean acoustics in the 1970s, and have since become a popular method for modeling range-dependent propagation [49, 56, 92]. PE estimates the acoustic pressure field for an individual frequency by assuming azimuthal symmetry and approximating a solution to the 2-dimensional Helmholtz equation as a function of range $r$ and depth $z$ [21, 49, 92]. More recently, PE has been extended to 3-dimensional modeling [58], however, the 2-dimensional PE modeling software RAM was used for modeling the acoustic propagation between source and receiver locations [21]. Parabolic equation (PE) models were run on a version of RAM adapted for MATLAB by Matthew Dzieciuch (SIO, pers. comm). PE models were run on frequencies from 1 to 99 Hz with a spacing of 0.03125 Hz. The time-domain signal at the receiver was estimated by mirroring the complex conjugate of the model output above the Nyquist frequency of 100 Hz and taking the inverse Fourier transform.

## 3.3 Results

During the 110-minute analysis period, each ship was increasing its distance to receiver MC. The ships were traversing upslope for the majority of the analysis period. Ships 1,2, and 4 began turning and heading into deeper water around the 82, 88, and 80-minute marks, respectively (Fig. 3.2). Ship 3 did not turn during this period and continuously moved into shallower water. Ship 5 turned slightly at the 80-minute mark and remained at a relatively constant depth thereafter. Fig. 3.14 shows the received data of the five separate sources on receiver MC as waterfall plots sorted by time. Each of the time-series plots shows a pattern of arrivals that changes throughout the analysis period. The time-differences between arrivals are shortest for each ship when the depth at the source is shallowest. This resembles the pattern observed in the simplified ray trace models, where, by varying the source depth along a sloped bathymetry, the time-differences between arrivals decrease as the source depth decreases (Fig. 3.2).

The waterfall plot of the PE model for ship 1 to receiver MC also shows a similar dispersion pattern, where the time-differences between arrivals is directly related to the depth at the ship locations (Fig. 3.15). The PE model predicts a significantly longer duration signal than is exhibited by the real data. Comparing the real data and PE model spectrograms for the first shot in the dataset in Fig. 3.16 also reveals a significantly longer duration signal in the model. The model also is more attenuated at higher frequencies. When all the spectra are stacked and sorted by range, the data and model both exhibit striations in the frequencies (Fig. 3.17). The striations in the real data shift in frequency at a greater rate than those exhibited by the model.

The ray travel times for a more realistic environment were modeled in ZRAY and used to estimate group speeds as a function of ray launch angle for all ship positions of ship 1 to receiver MC (Fig. 3.18). The data are sloped downward as the launch angle moves further from the horizontal. There may be some pattern of group speeds increasing as the bathymetric depth at the ship location increases, although this is obscured by the noisiness of the group speed estimates.

The group speeds of the first arrival were calculated from the travel times in both the ray trace and PE models. The ray model on average had a higher estimated group speeds, although the estimated speeds were much noisier than the PE model group speed estimates. The sound speed between all ship locations and site MC estimated using the TDOAs was about 20 m/s slower than either model predicted (see Fig. 3.19).

## 3.4 Discussion

The ray trace examples with simplified slopes shown in Fig. 3.12 imply that as a source moves into shallower water, the time between each arrival will shorten. The group speeds for all slopes decrease as the launch angle gets less horizontal, but the rate at which it decreases is directly tied to the slope: as the bottom depth at the source location decreases, the group speeds for all arrivals get closer together, which causes the time between the various arrivals to decrease. This pattern can also be seen in the real data for site MC (Figs. 3.14 and 3.2): as each ship travels into shallower water, the time between arrivals shortens, and when the ships turn and move back into deeper water the arrivals separate again. Each ship can be matched to its waterfall plot by identifying the time at which each ship is in the shallowest water and matching that to time when the waterfall plot shows the shortest time between arrivals.

Attempting to replicate the dispersion as a function of depth at the source on a more realistic model environment in ZRAY does not as clearly exhibit this pattern (Fig. 3.18). This is likely due to the noisiness of the travel time estimates produced by ray tracing over long distances with rough bathymetry. The group speeds estimated by the PE model for the first arrival are less noisy, and follow the pattern of being inversely related to the depth at the source.

### 3.4.1 Comparison of Data and PE model outputs

In comparing the PE model output and the real data, four areas of mismatch become evident: the frequencies contained in the received signal, the duration of the time domain signal, the dispersion patterns, and the estimated group speeds of the first arrivals. While some of this mismatch may be inaccuracies in the model parameters (*e.g.* sediment depth and composition, water sound speeds, attenuation) or source signature (*e.g.* unknown spectrum of the individual airgun arrays, or the directionality of the arrays), the cause of much of this mismatch could also potentially be attributed to the 2-D approximation used in the model. The straight-line path between the source locations and site MC runs perpendicular to the slope of the bathymetry, likely causing some 3-D propagation effects comparable to propagation in a wedge-shaped ocean.

The frequency mismatch is most clearly seen in Fig. 3.16, where the real signal's bandwidth is from 5-75 Hz but the PE model shows is significantly more attenuated above 50 Hz. In attempting to reduce the duration of the signal in the model to better match the data, the attenuation coefficients in the sediment were increased. While this reduced the signals' duration, this caused higher frequencies to be over-attenuated due to the frequency dependence of attenuation. The PE model does not account for energy being refracted out of the 2-D range slice between the source and receiver due to the sloped bathymetry running nearly perpendicular to the range slice.

Although the model and real data's dispersion patterns share common traits, there are also some notable differences. The spectrograms in Fig. 3.16 both show some frequency dispersion in the lower frequencies consistent with modal dispersion. The lowest frequencies arrive slightly delayed in comparison with the higher frequencies. In the real data, this dispersion happens most clearly in the 5 to 12 Hz band, but in the model data, the dispersion is more evident in the 4 to 8 Hz band. The mismatch might be a result of 3-D propagation effects, where energy propagates upslope to different depths and refracts back downslope to the receiver. Since frequency dispersion is determined by the depth of the seafloor, the propagation paths that reach shallower water are likely to have different frequency dispersion patterns than the 2-D approximation predicts.

The group speeds of the first arrival from the PE and ray models may also be higher than the group speeds calculated from the TDOA inversion due to the wedge-effect. Fig. 3.13 shows some rays that propagate nearly horizontally, but these rays are the paths that have very few interactions with the seafloor. With the downward refracting sound speed in the real environment, every ray has interacted multiple times with the bathymetry before arriving at the receiver. This would have the effect of only up-slope propagating rays reaching the receiver after curving back down-slope. The paths are therefore longer than the distance between the source and receiver, causing the sound speed estimates to be lower than the 2-D approximation.

## 3.5 Conclusion

Understanding the complexities of these environments is crucial for addressing long-range ocean acoustic propagation problems. The dispersion patterns are affected by sound speed profiles, sediment properties, and bathymetries. 2-D ray trace modeling on simplified environments reveals that the time between arrivals is tied to the slope of the bottom between the source and receiver; as the water depth at the source decreases, the time between arrivals also decreases. 3-D ray trace demonstrates the effect of a sloped seafloor running perpendicular to the axis formed by the source and receiver. Rays may propagate up-slope and refract back down-slope towards the receiver. The extent of the refraction depends on both the azimuth and inclination of the ray's launch angle.

Five ships performing a coordinated seismic survey were identified in the Gulf of Mexico on January 2, 2015, from 02:40 to 04:30 UTC. Five HARPs were within recording distance of the survey during this period. The vessels were equipped with airgun arrays, which were deployed and discharged systematically. Each vessel sequentially discharged its array, with an interval of 10 seconds between successive discharges. The signals were detected in the acoustic data using a peak detector. Peaks originating from the same source were associated using a combination of cross-covariances between detections, expected intervals between pulses, and manual verification.

2-D Parabolic Equation (PE) models [21] were run for range slices between site MC and 96 positions of ship 1 during the same period obtained from public AIS data. The models were run using a broadband source of 1 to 99 Hz with a spacing of 0.03125 Hz. The time series were reconstructed by taking the inverse Fourier transform of the model output at the receiver location.

The dispersion patterns observed in the PE model data showed some similarities to the patterns observed in the real data. Primarily, the seafloor depth at the source location was directly tied to the time between arrivals, as predicted by the simplified ray models with sloped bathymetries. However, the PE model differed from the real data in some notable ways. The spectra of the real data were more broadband and exhibited a slightly different frequency dispersion pattern. The duration of the modeled data was significantly higher than that of the real data.

An average first-arrival group speed between all ship locations and each receiver were estimated iterative approach. First, ships were localized using TDOA grid-search localization with an approximate sound speed estimate. Then, using those ship positions and the measured

TDOAs, five sound speeds were estimated, one for each hydrophone. Using the new sound speed estimates, the ships were localized again and the process was repeated five times. The sound speeds estimated using the TDOA inversions were significantly lower than the sound speeds calculated by both the PE and ray models.

3-D propagation effects may explain much of the mismatch between the model outputs and observations. The slope of the bathymetry running nearly perpendicular to the path between the ship locations and receiver MC causes ray paths to travel up-slope and refract back down-slope to the receiver. Since the rays are traveling a further distance than would be expected by a 2-D approximation, the group velocities estimated from the real data are likely lower than the models would predict. Additionally, the rays propagate into shallower water, which could lead to different frequency dispersion patterns and help explain the mismatch between the real and modeled spectrograms. Thus, 3-D modeling is necessary for accurate travel-time estimates and dispersion characteristics. 3-D effects may have important implications for estimating and assessing the impacts of proposed sound-producing activities, like seismic surveys. Further development of 3-D modeling tools with experimental verification of these models would lead to a better understanding of these impacts and the situations where 3-D modeling may be required. Additional mismatch may be due to inaccuracies in the model parameters or source signature (since the directionality of the airgun signals was not accounted for).

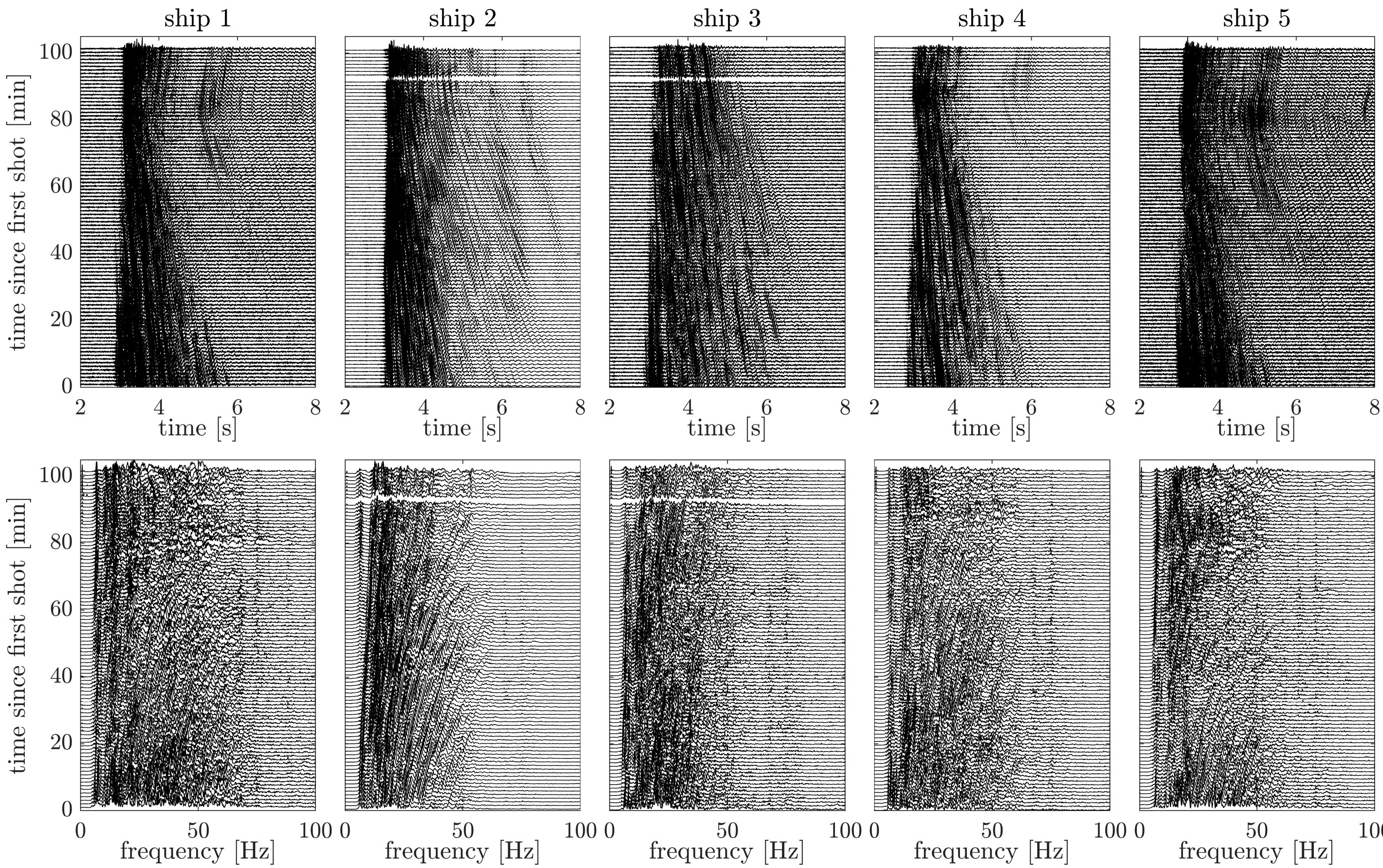


**Figure 3.14. Receiver 1 waterfall plot sorted by time.**
TOP: The time series of all shots sorted by individual ships as recorded by Receiver 1 (MC). Each shot is offset by the time in minutes of the first sample in the window. The x-axis represents seconds since the beginning of the time window for each arrival, and the y-axis represents time in minutes since the first arrival. The time series are aligned by a short 1 kHz ping transmitted approximately 1 second before firing each airgun.
BOTTOM: The waterfall plot of the spectra of each arrival associated with the same time series directly above.

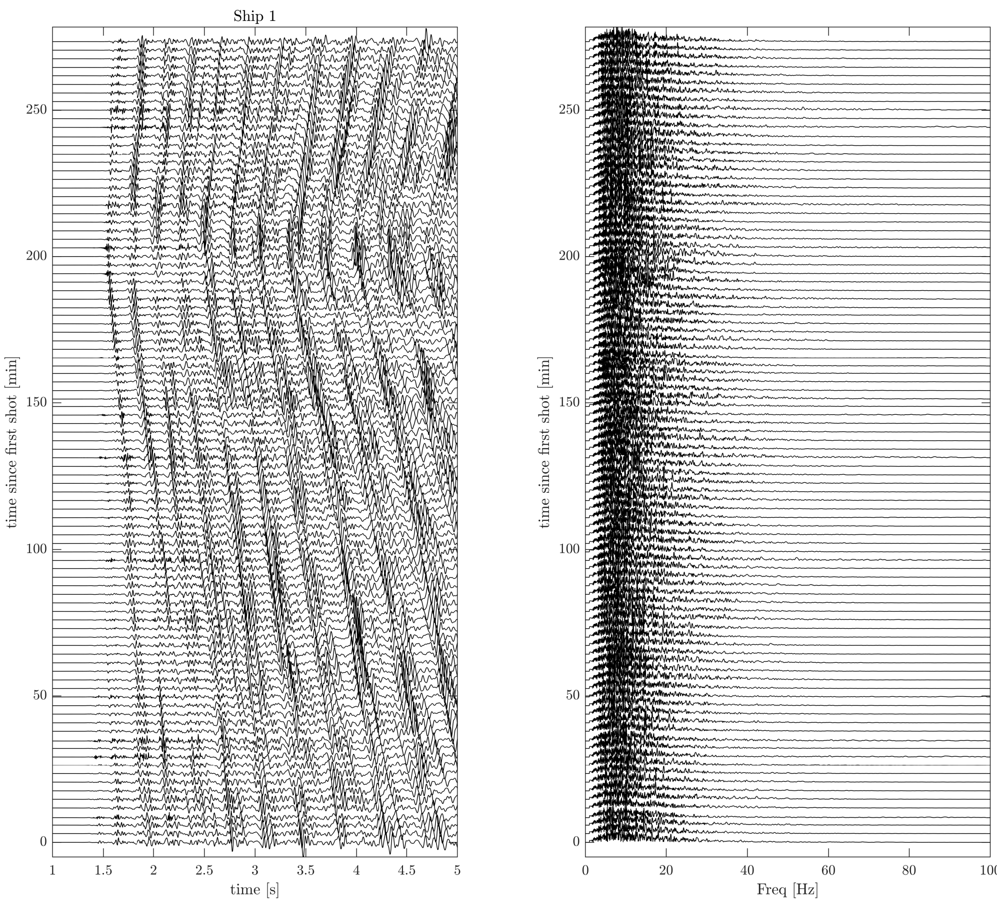


**Figure 3.15. PE Model waterfall plot of ship 1 to receiver MC.**
The time series (left) and spectra (right) of each shot were modeled using RAM Parabolic Equation method, and plotted as a waterfall plot.

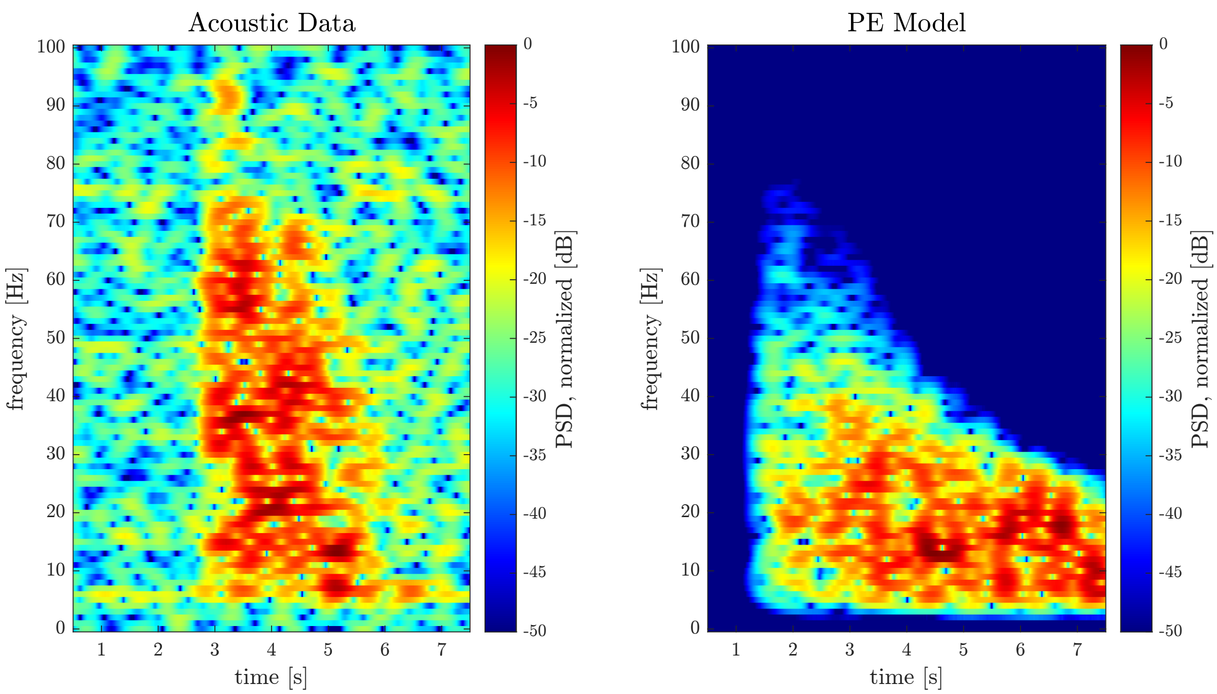


**Figure 3.16. Spectrograms of first shot from ship 1 to MC–PE model and real data.** The spectrograms of the acoustic data (left) and PE model (right) for the first shot from ship 1 to site MC. Spectrograms were calculated using a 200-point Kaiser-Bessel window with $\beta = 7.85$, 95% overlap. Prior to calculating the spectrogram, the real data were down-sampled from $fs = 2000$ Hz to $fs = 200$ Hz to match the sampling rate used in the PE model.

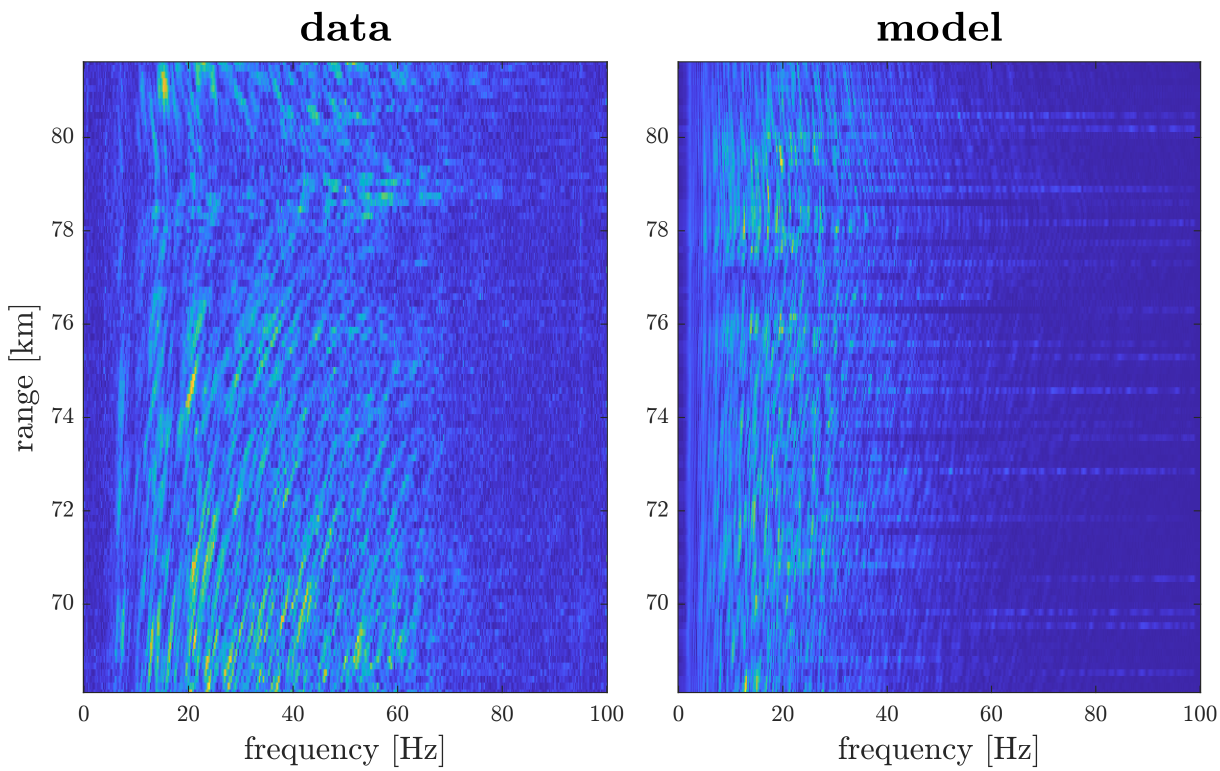


**Figure 3.17. Spectra of data from ship 1 to MC sorted by range–PE model and real data.** The spectra of the acoustic data (left) and PE model (right) from ship 1 to site MC, sorted by range between the ship and the receiver. The color scale represents the linear intensity of the spectra at each range slice, normalized by the maximum intensity in the entire track.

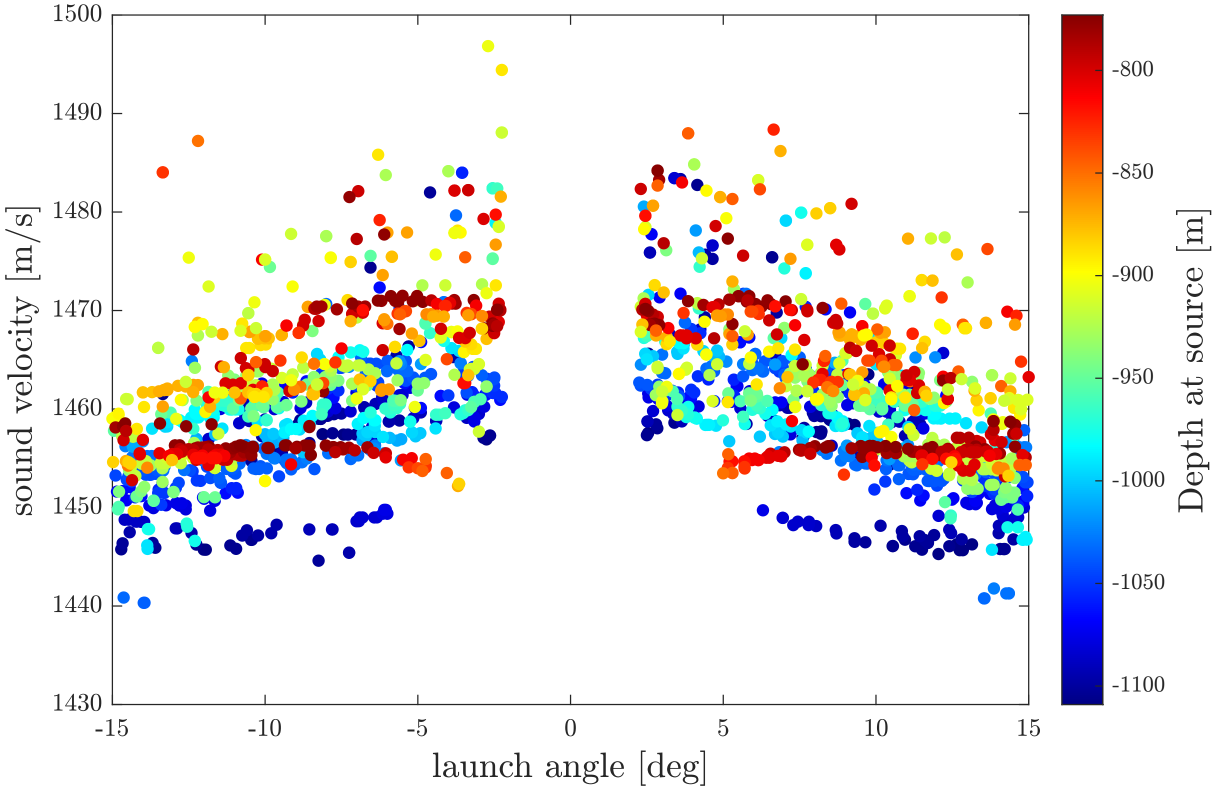


**Figure 3.18. Group speeds vs. launch angles estimated from ray trace on a realistic environment for all source positions of ship 1 to site MC.** The group speeds (color dots) estimated using more realistic bathymetry, sediment properties, and sound speed profiles in `ZRAY`. The color scale represents the depth of the bathymetry at the ship location.

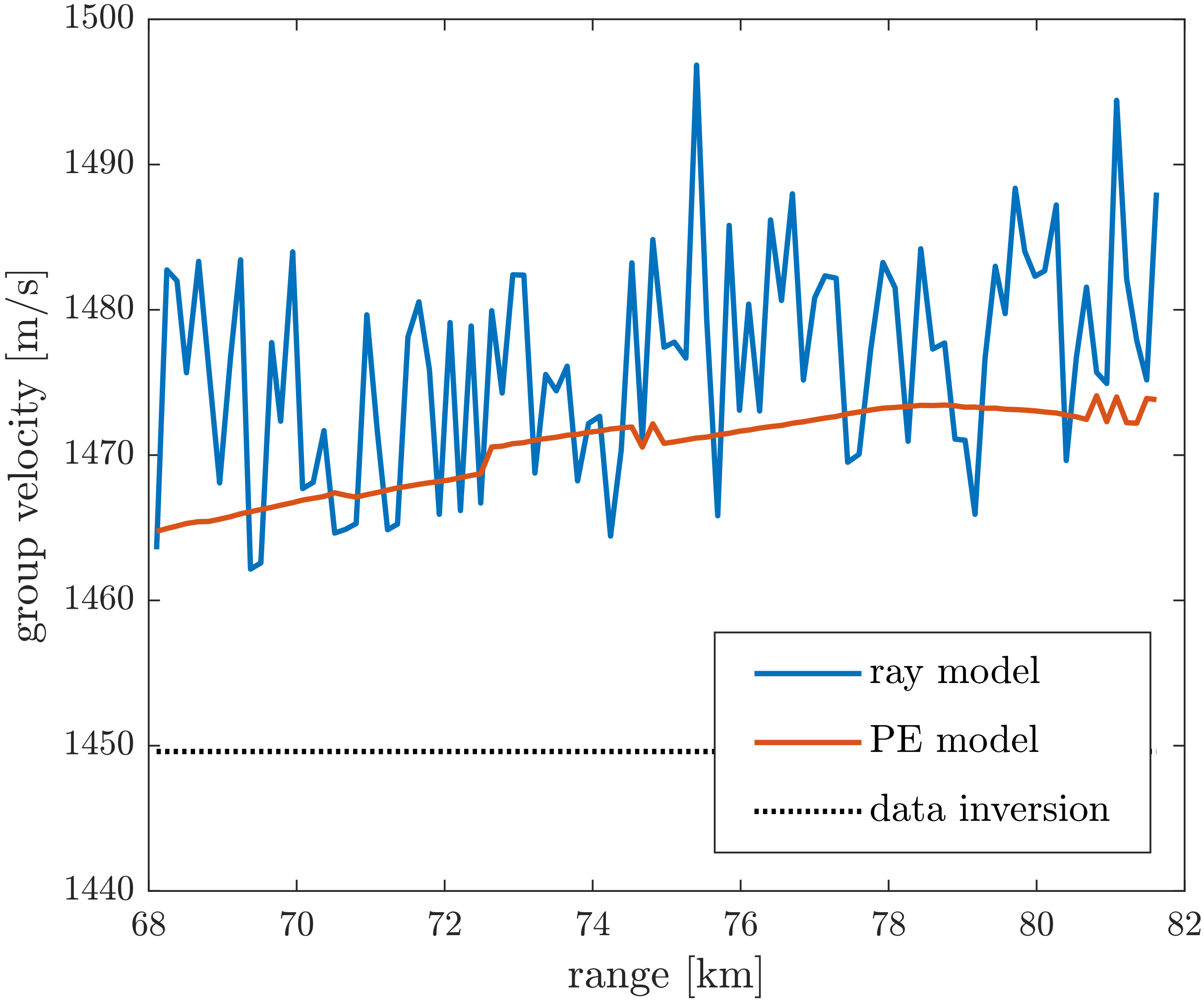


**Figure 3.19. Group speed estimates of first arrival, estimated from ray trace, PE, and TDOA inversion for ship 1, site MC.** A comparison of the estimated group velocities of the first arrival from both PE and ray models and compared with the estimated sound velocity between all the ship locations and site MC, obtained by iteratively localizing using the TDOAs of each shot to each receiver then solving for a single estimate of sound speed between all the ship locations and each receiver.

# Bibliography


[1] Omar Abdul-Latif, Peter Shepherd, and Stephen Pennock. Tdoa/aoa data fusion for enhancing positioning in an ultra wideband system. In *2007 IEEE International Conference on Signal Processing and Communications*, pages 1531–1534. IEEE, 2007.

[2] Alistair Adcroft, Chris Hill, Jean-Michel Campin, John Marshall, and Patrick Heimbach. Overview of the formulation and numerics of the mit gcm. In *Proceedings of the ECMWF seminar series on Numerical Methods, Recent developments in numerical methods for atmosphere and ocean modelling*, pages 139–149, 2004.

[3] Jesús Alcázar-Treviño, Mark Johnson, Patricia Arranz, Victoria E Warren, Carlos J Pérez-González, Tiago Marques, Peter T Madsen, and Natacha Aguilar de Soto. Deep-diving beaked whales dive together but forage apart. *Proceedings of the Royal Society B*, 288(1942):20201905, 2021.

[4] Patricia Arranz, Kelly J Benoit-Bird, Ari S Friedlaender, Elliott L Hazen, Jeremy A Goldbogen, Alison K Stimpert, Stacy L DeRuiter, John Calambokidis, Brandon L Southall, Andreas Fahlman, et al. Diving behavior and fine-scale kinematics of free-ranging risso's dolphins foraging in shallow and deep-water habitats. *Frontiers in Ecology and Evolution*, 7:53, 2019.

[5] Whitlow WL Au and Whitlow WL Au. Characteristics of dolphin sonar signals. *The sonar of dolphins*, pages 115–139, 1993.

[6] Paul M. Baggenstoss. Processing advances for localization of beaked whales using time difference of arrival. *The Journal of the Acoustical Society of America*, 133(6):4065–4076, 2013.

[7] Lauren M. Baggett, Simone Baumann-Pickerng, Kaitlin Frasier, and John Hildebrand. Long-term monitoring of cuvier's beaked whale diving behavior in southern california using 3d tracking from fixed hydrophone arrays, 2023. Master's Thesis.

[8] Robin W Baird. Behavior and ecology of not-so-social odontocetes: Cuvier's and blainville's beaked whales. *Ethology and behavioral ecology of odontocetes*, pages 305–329, 2019.

[9] Robin W Baird, J Fabrizio Borsani, M Bradley Hanson, and Peter L Tyack. Diving and night-time behavior of long-finned pilot whales in the ligurian sea. *Marine Ecology Progress Series*, 237:301–305, 2002.

[10] Yvonne M Barkley, Eva-Marie Nosal, and Erin M Oleson. Model-based localization of deep-diving cetaceans using towed line array acoustic data. *The Journal of the Acoustical Society of America*, 150(2):1120–1132, 2021.

[11] Jay Barlow, Emily T. Griffiths, Holger Klinck, and Danielle V. Harris. Diving behavior of Cuvier's beaked whales inferred from three-dimensional acoustic localization and tracking using a nested array of drifting hydrophone recorders. *The Journal of the Acoustical Society of America*, 144(4):2030–2041, 2018.

[12] Simone Baumann-Pickering, Mark A. McDonald, Anne E. Simonis, Alba Solsona Berga, Karlina P. B. Merkens, Erin M. Oleson, Marie A. Roch, Sean M. Wiggins, Shannon Rankin, Tina M. Yack, and John A. Hildebrand. Species-specific beaked whale echolocation signals. *The Journal of the Acoustical Society of America*, 134(3):2293–2301, 2013.

[13] Y Bernaldo de Quirós, A Fernandez, RW Baird, RL Brownell Jr, N Aguilar de Soto, D Allen, M Arbelo, M Arregui, A Costidis, A Fahlman, et al. Advances in research on the impacts of anti-submarine sonar on beaked whales. *Proceedings of the Royal Society B*, 286(1895):20182533, 2019.

[14] Daniel T Blumstein, Daniel J Mennill, Patrick Clemins, Lewis Girod, Kung Yao, Gail Patricelli, Jill L Deppe, Alan H Krakauer, Christopher Clark, Kathryn A Cortopassi, et al. Acoustic monitoring in terrestrial environments using microphone arrays: applications, technological considerations and prospectus. *Journal of Applied Ecology*, 48(3):758–767, 2011.

[15] JB Bowlin, JL Spiesberger, TF Duda, and LF Freitag. Ocean acoustical ray-tracing software ray, rep. Technical report, WHOI-93-10. Woods Hole Oceanograpic Institution, Woods Hole, MA, 1992.

[16] Ella Browning, Rory Gibb, Paul Glover-Kapfer, and Kate E Jones. Passive acoustic monitoring in ecology and conservation. *Report*, 2017.

[17] Michael J Buckingham. Theory of acoustic propagation around a conical seamount. *The journal of the acoustical society of America*, 80(1):265–277, 1986.

[18] Michael J Buckingham. Theory of three-dimensional acoustic propagation in a wedgelike ocean with a penetrable bottom. *The Journal of the Acoustical Society of America*, 82(1):198–210, 1987.

[19] Chen-Tung Chen and Frank J. Millero. Speed of sound in seawater at high pressures. *The Journal of the Acoustical Society of America*, 62(5):1129–1135, 1977.

[20] William R Cioffi, Nicola J Quick, Heather J Foley, Danielle M Waples, Zachary T Swaim, Jeanne M Shearer, Daniel L Webster, Ari S Friedlaender, Brandon L Southall, Robin W Baird, et al. Adult male cuvier's beaked whales (ziphius cavirostris) engage in prolonged bouts of synchronous diving. *Marine Mammal Science*, 37(3):1085–1100, 2021.

[21] Michael D Collins. A split-step padé solution for the parabolic equation method. *The Journal of the Acoustical Society of America*, 93(4):1736–1742, 1993.

[22] T. M. Cox, T. J. Ragen, A. J. Read, E. Vos, R. W. Baird, K. Balcomb, J. Barlow, J. Caldwell, T. Cranford, L. Crum, A. D'Amico, G. D'Spain, A. Fernandez, J. Finneran, R. Gentry, W. Gerth, F. Gulland, J. Hildebrand, D. Houser, T. Hullar, P. D. Jepson, D. Ketten, C. D. MacLeod, P. Miller, S. Moore, D. C. Mountain, D. Palka, P. Ponganis, S. Rommel, T. Rowles, B. Taylor, P. Tyack, D. Warzok, R. Gisiner, J. Mead, and L. Benner. Understanding the impacts of anthropogenic sound on beaked whales, 2006. Section: Technical Reports.

[23] Ted W Cranford, Petr Krysl, and John A Hildebrand. Acoustic pathways revealed: Simulated sound transmission and reception in cuvier's beaked whale (ziphius cavirostris). *Bioinspiration & Biomimetics*, 3(1):016001, 2008.

[24] ML Dalebout, CS Baker, JG Mead, VG Cockcroft, and TK Yamada. A comprehensive and validated molecular taxonomy of beaked whales, family ziphiidae. *Journal of Heredity*, 95(6):459–473, 2004.

[25] Angela D'amico and Richard Pittenger. A brief history of active sonar. *Aquatic Mammals*, 35(4), 2009.

[26] HE Daniels and GA Young. Saddlepoint approximation for the studentized mean, with an application to the bootstrap. *Biometrika*, 78(1):169–179, 1991.

[27] Annamaria Izzi DeAngelis, Robert Valtierra, Sofie M Van Parijs, and Danielle Cholewiak. Using multipath reflections to obtain dive depths of beaked whales from a towed hydrophone array. *The Journal of the Acoustical Society of America*, 142(2):1078–1087, 2017.

[28] Stacy L DeRuiter, Peter L Tyack, Ying-Tsong Lin, Arthur E Newhall, James F Lynch, and Patrick JO Miller. Modeling acoustic propagation of airgun array pulses recorded on tagged sperm whales (physeter macrocephalus). *The Journal of the Acoustical Society of America*, 120(6):4100–4114, 2006.

[29] Thomas J DiCiccio and Bradley Efron. Bootstrap confidence intervals. *Statistical science*, 11(3):189–228, 1996.

[30] Bill Dragoset. Introduction to air guns and air-gun arrays. *The Leading Edge*, 19(8):892–897, 2000.

[31] Brian D. Dushaw, Peter F. Worcester, and Bruce D. Cornuelle. On equations for the speed of sound in seawater. *The Journal of the Acoustical Society of America*, 93.1:255–275, 1992.

[32] Angela D'Amico, Robert C Gisiner, Darlene R Ketten, Jennifer A Hammock, Chip Johnson, Peter L Tyack, and James Mead. Beaked whale strandings and naval exercises. *Aquatic Mammals*, 35(4):452–472, 2009.

[33] Bradley Efron. *The jackknife, the bootstrap and other resampling plans*. SIAM, 1982.

[34] PB Flemings, C John, and Jan Behrmann. Expedition 308 synthesis: Overpressure, consolidation, and slope stability on the continental slope of the gulf of mexico. In *Proceedings of the Integrated Ocean Drilling Program*, volume 308, pages 1–19. Ocean Drilling Program, 2012.

[35] Alexandros Frantzis, John C Goold, Emmanuel K Skarsoulis, Michael I Taroudakis, and Varvara Kandia. Clicks from cuvier's beaked whales, ziphius cavirostris (l). *The Journal of the Acoustical Society of America*, 112(1):34–37, 2002.

[36] Karl-Heinz Frommolt and Klaus-Henry Tauchert. Applying bioacoustic methods for long-term monitoring of a nocturnal wetland bird. *Ecological Informatics*, 21:4–12, 2014.

[37] Martin Gassmann, Sean M. Wiggins, and John A. Hildebrand. Three-dimensional tracking of Cuvier's beaked whales' echolocation sounds using nested hydrophone arrays. *The Journal of the Acoustical Society of America*, 138(4):2483–2494, 2015.

[38] Douglas Gillespie, David K Mellinger, Jonathan Gordon, David McLaren, Paul Redmond, Ronald McHugh, Philip Trinder, Xiao-Yan Deng, and Aaron Thode. Pamguard: Semiautomated, open source software for real-time acoustic detection and localization of cetaceans. *The Journal of the Acoustical Society of America*, 125(4):2547–2547, 2009.

[39] Cristian Graupe, Lora J Van Uffelen, Peter F Worcester, Matthew A Dzieciuch, and Bruce M Howe. An automated framework for long-range acoustic positioning of autonomous underwater vehicles. *The Journal of the Acoustical Society of America*, 152(3):1615–1626, 2022.

[40] Pina Gruden, Eva-Marie Nosal, and Erin Oleson. Tracking time differences of arrivals of multiple sound sources in the presence of clutter and missed detections. *The Journal of the Acoustical Society of America*, 150(5):3399–3416, 2021.

[41] Regina A Guazzo, Tyler A Helble, Gerald L D'Spain, David W Weller, Sean M Wiggins, and John A Hildebrand. Migratory behavior of eastern north pacific gray whales tracked using a hydrophone array. *PLoS One*, 12(10):e0185585, 2017.

[42] Kevin D Heaney and Richard L Campbell. Parabolic equation modeling of a seismic airgun array. *IEEE Journal of Oceanic Engineering*, 44(3):621–632, 2019.

[43] Kevin D Heaney and James J Murray. Measurements of three-dimensional propagation in a continental shelf environment. *The Journal of the Acoustical Society of America*, 125(3):1394–1402, 2009.

[44] John E Heyning and James G Mead. Cuvier's beaked whale: Ziphius cavirostris. In *Encyclopedia of marine mammals*, pages 294–295. Elsevier, 2009.

[45] John A Hildebrand. Impacts of anthropogenic sound. *Marine mammal research: conservation beyond crisis*, pages 101–124, 2005.

[46] John A. Hildebrand, Simone Baumann-Pickering, Kaitlin E. Frasier, Jennifer S. Trickey, Karlina P. Merkens, Sean M. Wiggins, Mark A. McDonald, Lance P. Garrison, Danielle Harris, Tiago A. Marques, and Len Thomas. Passive acoustic monitoring of beaked whale densities in the Gulf of Mexico. *Scientific Reports*, 5(1):16343, 2015.

[47] Junsu Jang, Florian Meyer, Eric R. Snyder, Sean M. Wiggins, Simone Baumann-Pickering, and John A. Hildebrand. Bayesian detection and tracking of odontocetes in 3-d from their echolocation clicks. *The Journal of the Acoustical Society of America*, 153(5):2690–, 2023. _eprint: https://pubs.aip.org/asa/jasa/article-pdf/153/5/2690/17275427/2690_1_10.0017888.pdf.

[48] Susan M Jarvis, Ronald P Morrissey, David J Moretti, Nancy A DiMarzio, and Jessica A Shaffer. Marine mammal monitoring on navy ranges (m3r): A toolset for automated detection, localization, and monitoring of marine mammals in open ocean environments. *Marine Technology Society Journal*, 48(1):5–20, 2014.

[49] Finn B. Jensen, William A. Kuperman, Michael B. Porter, and Henrik Schmidt. *Computational Ocean Acoustics*. Springer New York, 2011.

[50] Mark Johnson, Peter T Madsen, Walter MX Zimmer, Natacha Aguilar de Soto, and Peter L Tyack. Beaked whales echolocate on prey. *Proceedings of the Royal Society of London. Series B: Biological Sciences*, 271(suppl_6):S383–S386, 2004.

[51] Mark P Johnson and Peter L Tyack. A digital acoustic recording tag for measuring the response of wild marine mammals to sound. *IEEE journal of oceanic engineering*, 28(1):3–12, 2003.

[52] Jared Kluesner, Patrick Hart, George Snyder, and Peter Triezenberg. National archive of marine seismic surveys web portal provides public access to us exclusive economic zone marine seismic surveys, 2024.

[53] Jens C Koblitz. Arrayvolution: using microphone arrays to study bats in the field. *Canadian Journal of Zoology*, 96(9):933–938, 2018.

[54] Jan Langhammer, Martin Landro, James Martin, and Eivind Berg. Air-gun bubble damping by a screen. *Geophysics*, 60(6):1765–1772, 1995.

[55] Christophe Laplanche, Olivier Adam, Maciej Lopatka, and Jean-François Motsch. Male sperm whale acoustic behavior observed from multipaths at a single hydrophone. *The Journal of the Acoustical Society of America*, 118(4):2677–2687, 2005.

[56] Ding Lee, Allan D Pierce, and Er-Chang Shang. Parabolic equation development in the twentieth century. *Journal of Computational Acoustics*, 8(04):527–637, 2000.

[57] Ying-Tsong Lin. Three-dimensional propagation of seismic airgun signals in the mississippi canyon area of the gulf of mexico. *JASA Express Letters*, 1(2), 2021.

[58] Ying-Tsong Lin, Timothy F Duda, and Arthur E Newhall. Three-dimensional sound propagation models using the parabolic-equation approximation and the split-step fourier method. *Journal of Computational Acoustics*, 21(01):1250018, 2013.

[59] Alexander MacGillivray. Modeling underwater sound propagation from an airgun array using the parabolic equation method. *The Journal of the Acoustical Society of America*, 122(5_Supplement):2942–2943, 2007.

[60] Alexander O MacGillivray and N Ross Chapman. Modeling underwater sound propagation from an airgun array using the parabolic equation method. *Canadian Acoustics*, 40(1):19–25, 2012.

[61] Alexander Orion MacGillivray. Acoustic modelling study of seismic airgun noise in queen charlotte basin, 2006. PhD Thesis.

[62] Kenneth V Mackenzie. Nine-term equation for sound speed in the oceans. *The Journal of the Acoustical Society of America*, 70(3):807–812, 1981.

[63] Tiago A Marques, Len Thomas, Stephen W Martin, David K Mellinger, Jessica A Ward, David J Moretti, Danielle Harris, and Peter L Tyack. Estimating animal population densities using passive acoustics. *Biological Reviews*, 2013.

[64] Tiago A Marques, Len Thomas, Jessica Ward, Nancy DiMarzio, and Peter L Tyack. Estimating cetacean population density using fixed passive acoustic sensors: An example with blainville's beaked whales. *The Journal of the Acoustical Society of America*, 125(4):1982–1994, 2009.

[65] Daniel J McSweeney, Robin W Baird, and Sabre D Mahaffy. Site fidelity, associations, and movements of cuvier's (ziphius cavirostris) and blainville's (mesoplodon densirostris) beaked whales off the island of hawai 'i. *Marine Mammal Science*, 23(3):666–687, 2007.

[66] Alex Mikhalev and Richard Ormondroyd. Passive emitter geolocation using agent-based data fusion of aoa, tdoa and fdoa measurements. In *2007 10th International Conference on Information Fusion*, pages 1–6. IEEE, 2007.

[67] Lewis Morton Mott-Smith. Air operated underwater seismic source, 1970. US Patent 3,525,416.

[68] Eva-Marie Nosal. Single sensor and compact array localization methods. Technical report, Office of Naval Research; Ocean, Atmosphere and Space Research Division, 2020.

[69] Eva-Marie Nosal and L. Neil Frazer. Sperm whale three-dimensional track, swim orientation, beam pattern, and click levels observed on bottom-mounted hydrophones. *The Journal of the Acoustical Society of America*, 122(4):1969–1978, 2007.

[70] Michael B Porter. Beam tracing for two-and three-dimensional problems in ocean acoustics. *The Journal of the Acoustical Society of America*, 146(3):2016–2029, 2019.

[71] Rosalyn Putland, Alayna Mackiewicz, and Allen F Mensinger. Using passive acoustics to localize vocalizing oyster toadfish (opsanus tau). *The Journal of the Acoustical Society of America*, 144(3):1692–1692, 2018.

[72] Nicola J Quick, William R Cioffi, Jeanne M Shearer, Andreas Fahlman, and Andrew J Read. Extreme diving in mammals: first estimates of behavioural aerobic dive limits in cuvier's beaked whales. *Journal of Experimental Biology*, 223(18):jeb222109, 2020.

[73] Tessa A Rhinehart, Lauren M Chronister, Trieste Devlin, and Justin Kitzes. Acoustic localization of terrestrial wildlife: Current practices and future opportunities. *Ecology and Evolution*, 10(13):6794–6818, 2020.

[74] Ally C Rice, Macey Rafter, Jennifer S Trickey, Sean M Wiggins, Simone Baumann-Pickering, and John A Hildebrand. Passive acoustic monitoring for marine mammals in the socal range complex july 2018-may 2019. Technical report, Technical report, Scripps Institution of Oceanography, 2020.

[75] W John Richardson, Charles R Greene Jr, Charles I Malme, and Denis H Thomson. *Marine mammals and noise*. Academic press, 2013.

[76] Marie A Roch, Holger Klinck, Simone Baumann-Pickering, David K Mellinger, Simon Qui, Melissa S Soldevilla, and John A Hildebrand. Classification of echolocation clicks from odontocetes in the southern california bight. *The Journal of the Acoustical Society of America*, 129(1):467–475, 2011.

[77] Samuel RP-J Ross, Darren P O'Connell, Jessica L Deichmann, Camille Desjonquères, Amandine Gasc, Jennifer N Phillips, Sarab S Sethi, Connor M Wood, and Zuzana Burivalova. Passive acoustic monitoring provides a fresh perspective on fundamental ecological questions. *Functional Ecology*, 2023.

[78] William BF Ryan, Suzanne M Carbotte, Justin O Coplan, Suzanne O'Hara, Andrew Melkonian, Robert Arko, Rose Anne Weissel, Vicki Ferrini, Andrew Goodwillie, Frank Nitsche, et al. Global multi-resolution topography synthesis. *Geochemistry, Geophysics, Geosystems*, 10(3), 2009.

[79] MH Safar. The radiation of acoustic waves from an air-gun. *Geophysical Prospecting*, 24(4):756–772, 1976.

[80] Henrik Schmidt and Finn B Jensen. Computational ocean acoustics: Advances in 3d ocean acoustic modeling. In *AIP Conference Proceedings*, volume 1495, pages 3–15. American Institute of Physics, 2012.

[81] Gregory S. Schorr, Erin A. Falcone, David J. Moretti, and Russel D. Andrews. First Long-Term Behavioral Records from Cuvier's Beaked Whales (Ziphius cavirostris) Reveal Record-Breaking Dives. *PLOS ONE*, 9(3):e92633, 2014.

[82] Jun Shao and CF Jeff Wu. A general theory for jackknife variance estimation. *The annals of Statistics*, pages 1176–1197, 1989.

[83] Jeanne M Shearer, Nicola J Quick, William R Cioffi, Robin W Baird, Daniel L Webster, Heather J Foley, Zachary T Swaim, Danielle M Waples, Joel T Bell, and Andrew J Read. Diving behaviour of cuvier's beaked whales (ziphius cavirostris) off cape hatteras, north carolina. *Royal Society Open Science*, 6(2):181728, 2019.

[84] MP Simmonds and LF Lopez-Jurado. Whales and the military. *Nature*, 351(6326):448–448, 1991.

[85] Anne E Simonis, Robert L Brownell Jr, Bruce J Thayre, Jennifer S Trickey, Erin M Oleson, Roderick Huntington, and Simone Baumann-Pickering. Co-occurrence of beaked whale strandings and naval sonar in the mariana islands, western pacific. *Proceedings of the Royal Society B*, 287(1921):20200070, 2020.

[86] Eric R Snyder, Alba Solsona-Berga, Simone Baumann-Pickering, Kait E Frasier, Sean M Wiggins, and John A Hildebrand. Where's whaledo: A software toolkit for array localization of animal vocalizations. *bioRxiv*, pages 2023–08, 2023.

[87] Alba Solsona-Berga, Kaitlin E. Frasier, Simone Baumann-Pickering, Sean M. Wiggins, and John A. Hildebrand. DetEdit: A graphical user interface for annotating and editing events detected in long-term acoustic monitoring data. *PLOS Computational Biology*, 16(1):e1007598, 2020.

[88] Alba Solsona-Berga, Natalie Posdaljian, John A. Hildebrand, and Simone Baumann-Pickering. Echolocation repetition rate as a proxy to monitor population structure and dynamics of sperm whales. *Remote Sensing in Ecology and Conservation*, 8(6):827–840, 2022.

[89] Phillip M Stepanian, Kyle G Horton, David C Hille, Charlotte E Wainwright, Phillip B Chilson, and Jeffrey F Kelly. Extending bioacoustic monitoring of birds aloft through flight call localization with a three-dimensional microphone array. *Ecology and Evolution*, 6(19):7039–7046, 2016.

[90] Larissa Sayuri Moreira Sugai, Thiago Sanna Freire Silva, José Wagner Ribeiro Jr, and Diego Llusia. Terrestrial passive acoustic monitoring: review and perspectives. *BioScience*, 69(1):15–25, 2019.

[91] David A Sweeney, Gregory S Schorr, Erin A Falcone, Brenda K Rone, Russel D Andrews, Shannon N Coates, Stephanie L Watwood, Stacy L DeRuiter, Mark P Johnson, and David J Moretti. Cuvier's beaked whale foraging dives identified via machine learning using depth and triaxial acceleration. *Marine Ecology Progress Series*, 692:195–208, 2022.

[92] FD Tappert. 'selected applications of the parabolic-equation method in underwater acoustics. In *International Workshop on Low-Frequency Propagation and Noise*, pages 155–194, 1977.

[93] Arslan M Tashmukhambetov, Natalia A Sidorovskaia, George E Ioup, Juliette W Ioup, Joal J Newcomb, Christopher D Walker, Ben Brock, and Grayson H Rayborn. 3-d airgun

source characterization and propagation modeling. In *SEG International Exposition and Annual Meeting*, pages SEG–2006. SEG, 2006.

[94] Ludovic Tenorio-Hallé, Aaron M Thode, Jit Sarkar, Christopher Verlinden, Jeffrey Tippmann, William S Hodgkiss, and William A Kuperman. A double-difference method for high-resolution acoustic tracking using a deep-water vertical array. *The Journal of the Acoustical Society of America*, 142(6):3474–3485, 2017.

[95] Aaron M Thode, Katherine H Kim, Susanna B Blackwell, Charles R Greene Jr, Christopher S Nations, Trent L McDonald, and A Michael Macrander. Automated detection and localization of bowhead whale sounds in the presence of seismic airgun surveys. *The Journal of the Acoustical Society of America*, 131(5):3726–3747, 2012.

[96] Christopher O Tiemann, Aaron M Thode, Janice Straley, Victoria O'Connell, and Kendall Folkert. Three-dimensional localization of sperm whales using a single hydrophone. *The Journal of the Acoustical Society of America*, 120(4):2355–2365, 2006.

[97] Irina Tolkova and Holger Klinck. Source separation with an acoustic vector sensor for terrestrial bioacoustics. *The Journal of the Acoustical Society of America*, 152(2):1123–1134, 2022.

[98] A Tolstoy. 3-d propagation issues and models. *Journal of Computational Acoustics*, 4(03):243–271, 1996.

[99] Peter L. Tyack, Mark Johnson, Natacha Aguilar Soto, Albert Sturlese, and Peter T. Madsen. Extreme diving of beaked whales. *Journal of Experimental Biology*, 209(21):4238–4253, 2006.

[100] Robert J Urick. *Principles of Underwater Sound*. McGraw-Hill, 1975.

[101] B Ursin. Attenuation of coherent noise in marine seismic exploration using very long arrays. *Geophysical Prospecting*, 26(4):722–749, 1978.

[102] Robert Daniel Valtierra. Source localization of narrow band signals in multipath environments, with application to marine mammals, 2013.

[103] Stephanie L Watwood, Patrick JO Miller, Mark Johnson, Peter T Madsen, and Peter L Tyack. Deep-diving foraging behaviour of sperm whales (physeter macrocephalus). *Journal of Animal Ecology*, 75(3):814–825, 2006.

[104] Sean M Wiggins, Jesse M Hall, Bruce J Thayre, and John A Hildebrand. Gulf of mexico low-frequency ocean soundscape impacted by airguns. *The Journal of the Acoustical Society of America*, 140(1):176–183, 2016.

[105] Sean M. Wiggins and John A. Hildebrand. High-frequency Acoustic Recording Package (HARP) for broad-band, long-term marine mammal monitoring. In *2007 Symposium on Underwater Technology and Workshop on Scientific Use of Submarine Cables and Related Technologies*, pages 551–557, 2007.

[106] Sean M. Wiggins, Mark A. McDonald, and John A. Hildebrand. Beaked whale and dolphin tracking using a multichannel autonomous acoustic recorder. *The Journal of the Acoustical Society of America*, 131(1):156–163, 2012.

[107] Morgan A Ziegenhorn, Kaitlin E Frasier, John A Hildebrand, Erin M Oleson, Robin W Baird, Sean M Wiggins, and Simone Baumann-Pickering. Discriminating and classifying odontocete echolocation clicks in the hawaiian islands using machine learning methods. *Plos one*, 17(4):e0266424, 2022.

[108] Walter M. X. Zimmer. *Passive Acoustic Monitoring of Cetaceans*. Cambridge University Press, 2014.

[109] Walter MX Zimmer, Mark P Johnson, Peter T Madsen, and Peter L Tyack. Echolocation clicks of free-ranging cuvier's beaked whales (ziphius cavirostris). *The Journal of the Acoustical Society of America*, 117(6):3919–3927, 2005.

[110] Ana Širović, John A. Hildebrand, and Sean M. Wiggins. Blue and fin whale call source levels and propagation range in the Southern Ocean. *The Journal of the Acoustical Society of America*, 122(2):1208–1215, 08 2007.